EGG-NTAP-5984

August 1982

NRC Research and/or Technical Assistance Rept

TRAC-BD1 COMPUTER CODE ASSESSMENT CALCULATIONS OF GENERAL ELECTRIC TLTA DBA AND SMALL BREAK TESTS

M. A. Bolander

U.S. Department of Energy
Idaho Operations Office • Idaho National Engineering Laboratory

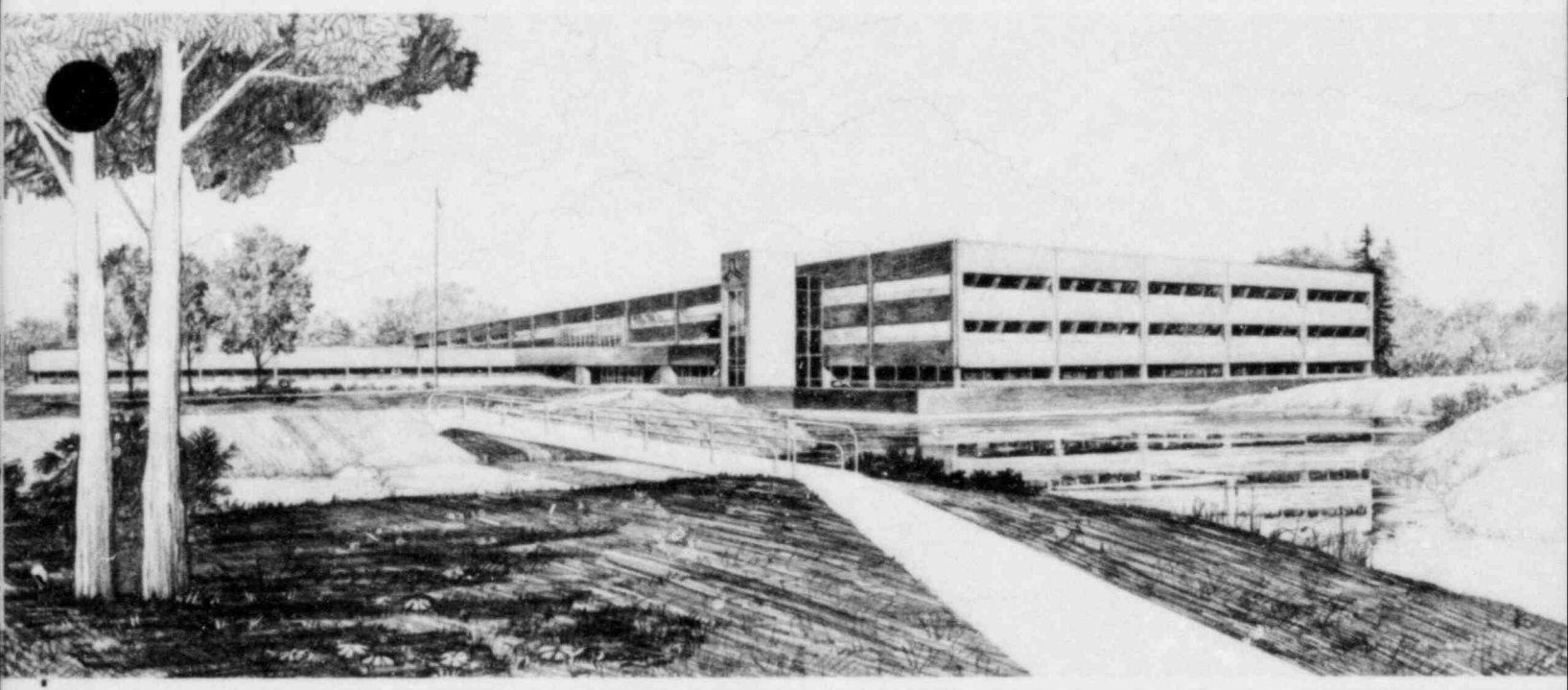

This is an informal report intended for use as a preliminary or working document

Prepared for the
U.S. Nuclear Regulatory Commission
Under DOE Contract No. DE-AC07-76ID01570
FIN No. A6047

EG&G Idaho

EG&G Idaho, Inc.

FORM EG&G 398
(Rev. 03-82)

INTERIM REPORT

Accession No. _____

Report No. EGG-NTAP-5984

Contract Program or Project Title: NRC Technical Assistance Program Division

Subject of this Document: TRAC-BD1 Computer Code Assessment Calculations of General Electric TLTA DBA and Small Break Tests

Type of Document: Technical Report

Author(s): M. A. Bolander

Date of Document: August 1982

Responsible NRC Individual and NRC Office or Division: F. Odar, NRC-RES

This document was prepared primarily for preliminary or internal use. It has not received full review and approval. Since there may be substantive changes, this document should not be considered final.

EG&G Idaho, Inc.
Idaho Falls, Idaho **83415**

Prepared for the
U.S. Nuclear Regulatory Commission
Washington, D.C.
Under DOE Contract No. **DE-AC07-76ID01570**
NRC FIN No. 6047

INTERIM REPORT

ABSTRACT

In this report, the results of TRAC-BD1 Version 11 and Version B002 code assessment calculations for four General Electric Two-Loop Test Apparatus tests are documented. Two high powered Design Base Accident type tests (6423 and 6424) were simulated using Version 11. Two small break tests (6431 and 6432) were simulated using Version B002. Results from the code calculated behavior compared to experimental data are presented. Conclusions and recommendations gleaned from the assessment study are given. The study described in this report has been performed as part of the Idaho National Engineering Laboratory's support to the Nuclear Regulatory Commission for the independent assessment of advanced, best estimate, reactor safety analysis computer codes.

NRC Technical Assistance Program Division

FIN No. A6047

SUMMARY

In this report, calculations are documented for the purpose of assessing the Transient Reactor Analysis Code, TRAC-BD1 Version 11 and B002. TRAC-BD1 Version 11 and B002 are advanced best estimate computer programs developed at the Idaho National Engineering Laboratory for the purpose of simulating the thermal-hydraulic behavior of Boiling Water Reactors. The tests chosen for the assessment study described herein were General Electric Two-Loop Test Apparatus Tests 6423, 6424, 6431 and 6432. Tests 6423 and 6424 were high powered Design Base Accident Tests and Tests 6431 and 6432 were small break tests. Version 11 was used to perform the Design Base Accident tests and Version B002 was used for the small break tests.

Major conclusions resulting from the calculations are summarized as follows:

1. Overall data trends and system behavior were reasonably calculated by both versions of TRAC-BD1.

2. TRAC-BD1 Version 11 overcalculated the suction line break flow rate.

3. System differential pressure trends were reasonably calculated by Version 11.

4. TRAC-BD1 Version 11 and B002 tended to undercalculate liquid down flow in the TLTA facility. CCFL limitations at the upper tie plate limited calculated ECC liquid penetration into the bundle and bypass from the upper plenum. Further investigation into this limitation should be performed in future assessment activities.

5. Water packing and guide tube modeling resulted in code failures and time step reduction in Version 11. The water packing option was turned on and the guide tube TEE secondary was modeled as a cone. These changes resolved the code failures and improved the results.

6. Break mass flow rates were well characterized by TRAC-BD1 Version B002.

7. TRAC-BD1 Version B002 did not calculate countercurrent flow in the bubbly flow regime with low void fraction. This led to a system mass distribution different to that of the experiment. It is recommended that this known code deficiency be further investigated.

ACKNOWLEDGEMENT

The author expresses appreciation to Dawnie Judd for her assistance in generating plots and nodalization drawings.

CONTENTS

FIGURES

TABLES

1. INTRODUCTION

The TRAC-BD1 computer code is a transient reactor analysis computer code developed at the Idaho National Engineering Laboratory (INEL), designed specifically for Boiling Water Reactor (BWR) transient analysis. An independent assessment of the code is being conducted at the INEL to identify and document the capability and limitations of the code. To assist in the assessment, data from several BWR related experiments are being used. This document reports four assessment calculations using General Electric (GE) Two-Loop Test Apparatus (TLTA) facility data from Tests 6423, 6424, 6431, and 6432. Tests 6423 and 6424 are Design Base Accident (DBA) tests conducted at peak power. Tests 6431 and 6432 are small break tests with and without degraded emergency core cooling system.

Two versions of the code were used for the assessment calculations reported in this document: Version 11 and Version B002. Assessment of TRAC-BD1 was initiated using Version 11. The early assessment results (which included the DBA calculations) indicated continued cost effective studies would be better accomplished with a subsequent version (B002). This change was effected and subsequent studies (including the small break tests) were performed.

Section 2 describes the G.E. TLTA test facility, the DBA tests and the small break tests. Section 3 describes the TRAC-BD1 computer code and the models used in the calculations. Section 3 also presents the initial boundary conditions used for both the tests and the calculations. Sections 4 and 5 present the DBA and small break calculations compared with experimental data respectively. Conclusions and recommendations resulting from the four assessment calculations are presented in Section 6.

2. FACILITY AND TEST DESCRIPTION

This section will present a brief overview of the TLTA experimental test facility and the DBA and small break tests used for the assessment described in this document. For a more detailed description of the test facility and tests, the reader should refer to References 1, 2, and 3.

2.1 Test Facility Description

The TLTA facility was a 1/624 scaled, two loop nonnuclear experimental test facility used to simulate various thermal/hydraulic transients that may occur in a BWR. The reference commercial BWR used for scaling purposes was a BWR/6-218. All major flow paths of the primary system of the BWR/6-218 were represented in the TLTA facility. Also included were the ECC system, the automatic depressurization system (ADS), TLTA auxiliary systems used for experimental set up and execution, and instrumentation system. Figures 1, 2, and 3 are schematic representations of the TLTA facility set up for the DBA and small break tests.

The test vessel was composed of the major sections of the referenced BWR, i.e., lower plenum, core, bypass, upper plenum, steam separator, steam dome, downcomer annulus and jet pumps. The lower plenum region housed the discharge pipe of the jet pumps and four guide tubes. Connected to each guide tube was a core bypass tube which extended up to the upper plenum region. Approximately 10% of the jet pump flow bypassed the core region via the guide tubes and bypass tubes. Core flow entered the core through the side entry orifice (SEO) tube, which was connected to the bottom of the bundle and extended into the lower plenum. The flow traveled over electrically heated rods and exited the bundle in the upper plenum region. The bundle housed 62 heater rods and two dummy water rods. Hydraulic communication between the bundle and the bypass tubes was through small connection tubes near the bottom of the heated bundle. The core flow entered the upper plenum region and mixed with the bypass flow in the mixing section. The vapor/water flow then entered the upper plenum. From the upper plenum section to the steam separation region the flow passed

through stationary swirl vanes. The vanes gave a swirling motion to the vapor/water flow, separating the water from the vapor by centrifugal force. The steam continued upward into the steam dome and out the steam line. At various elevations, the separated liquid was diverted from the separation region to the downcomer annulus. From the downcomer annulus, liquid was drawn into the lower plenum via the jet pumps. There was no thermal communication between the bundle and bypass tube as in the reference BWR, however, there was heat transfer between the bundle and downcomer and the bypass tubes and downcomer.

Two recirculation loops comprised the major flow paths external to the vessel. Each loop consisted of a suction line, drive pump and drive line. Loop flow was drawn into the suction line from the downcomer annulus by the drive pump. After traversing through the suction line and drive pump, the loop flow was discharged into the drive line. From the drive line, the flow entered the rams head and was discharged into the throat of the jet pump. Loop 1, the intact loop, was isolated from the rest of the system by two isolation valves during the transients. Loop 2, the broken loop, had only one isolation valve located in the drive line. Two blowdown lines connecting the broken loop suction and drive lines to the blowdown suppression tank were used to simulate the DBA tests (see Figure 1). A single blowdown line connecting the broken loop suction line to the blowdown suppression tank was used to simulate the small break tests (see Figure 2).

The ECC system was comprised of four systems: the high pressure core spray (HPCS) system, the low pressure core spray (LPCS) system, the low pressure core injection (LPCI) system, and the automatic depressurization system (ADS). Different injection locations for the HPCS, LPCS and LPCI systems were provided for experimental flexibility. The core spray systems injected liquid into either the upper plenum or the mixing plenum and the core injection system injected liquid into the four bypass tubes or the intact loop recirculation drive line. The ADS was located in the steam line piping of the TLTA facility and was used for the small break tests.

The instrumentation system was composed of pressure and differential pressure transducers, thermocouples, conductivity probes, turbine meters and drag disks. The data collected from the instrumentation was recorded on a comprehensive measurement and data acquisition system.

2.2 Test Description

The tests simulated by the assessment calculations were two DBA tests and two small break tests. This section will briefly describe each test. For more information on these tests the reader should refer to References 2 and 3.

The DBA tests used for this assessment were peak power, large break, loss of coolant accident tests. Test 6423 simulated an ECC system with low flow rate and high injection liquid temperature. The results of the test showed the ECC system was effective in cooling down the system. Test 6424 simulated an ECC system with average flow rate and average injection liquid temperature. The system response showed that the bundle reflooded completely at approximately 150 s following bypass region refill from LPCI flow and countercurrent flow limiting (CCFL) breakdown.

The small break tests simulated BWR small break scenarios with and without degraded ECC systems. Test 6431 assumed all ECC systems operable. HPCS injection recovered and maintained the system inventory. The mixture levels remained above the core and trip levels for the main steam isolation valve (MSIV) closure and activation of the ADS.

Test 6432 assumed the HPCS was inactive. In this test the MSIV was closed and the ADS tripped open. After ADS activation, bulk flashing occurred throughout the system. Also, large steam generation in the system led to CCFL at the upper tie plate, top of the bypass, and the bundle.

BWR/6 calculations have shown the water level in a small break accident will drop sufficiently to trip the MSIV and ADS, and may drop below the top of the bundle. For this type of transient it was necessary

to simulate the liquid transient carefully. To achieve this mass depletion in Test 6432, a second break was added to discharge the excess mass in TLTA (see Figure 4). Also, the TLTA vessel being shorter than a BWR, although a full sized bundle was used in the core region, made it impossible to initiate a test with water level at the BWR elevation as related to the core elevation. Therefore, neither break was initiated until the time the downcomer water level in a BWR/6 calculation equaled the initial liquid level in the TLTA test (approximately 138 s). The second break was closed when the ADS was tripped (286 s).

All major events in the tests were tripped on time. In events such as ECCS initiation, the event was tripped on time, however the subsequent rate of ECC flow was a function of system pressure.

3. MODEL DESCRIPTION AND INITIAL CONDITIONS

This section presents a description of the TRAC-BD1 computer code, TRAC-BD1 modeling of the TLTA facility for the DBA and small break tests, and the initial conditions used for the calculations.

3.1 TRAC-BD1 Computer Code Description

The Boiling Water Reactor (BWR) version of the transient reactor analysis code (TRAC), TRAC-BD1, is a basic best estimate code providing the capability for the analysis of design basis loss-of-coolant accidents in BWR systems (Reference 4). The code was developed at the Idaho National Engineering Laboratory (INEL). Unique features of the code include: (a) a full nonhomogeneous nonequilibrium two-fluid thermal-hydraulic model, (b) detailed model of BWR fuel bundles, (c) jet pump and separator dryer models, and (d) countercurrent flow limiting model for BWR-like geometries.

Two versions of the TRAC-BD1 code were used in the assessment calculations reported in this document. Several calculations (including the DBA calculations) were performed using Version 11 of the TRAC-BD1 code identified internally as TRAC1A011 and stored under Configuration Control Number 005998. Several errors in the coding and code models were discovered during the calculations. These errors were corrected and a new version of the code created, TRAC-BD1 Version B002. This version, identified internally as TRC1B002 and stored under Configuration Control Number F00874, was used to perform the small break calculations.

3.2 TRAC-BD1 TLTA Facility Model

Three TRAC-BD1 models of the TLTA facility were used for the DBA and small break calculations described in this document. The major difference in the three models was the modeling of the break and vessel. This section will present a description of the models.

3.2.1 TRAC-BD1 TLTA DBA Model

The TRAC-BD1 model of the TLTA facility used for the DBA calculations is shown schematically in Figure 5. The model contained 25 components (totaling 95 cells) and 30 junctions. The model represented all major flow paths of the facility, i.e., vessel, intact and broken recirculation loops, jet pumps, feed water system, main steam line and ECC system. Table 1 summarizes the relationship between the physical components of the TLTA facility and the correspondin mathematical components of the TRAC-BD1 model.

Heat transfer was modeled in the core heater rods, the guide tube TEE, and the jet pumps. Heat transfer from the bundle to the bypass was modeled, however no heat transfer occurred because the surface area of the bundle wall was set to zero internal to the code (TRAC-BD1 Version 11). The heat storage capacity of the system was modeled. Ambient heat loss was not modeled because of the nature of the tests.

The following TRAC-BD1 options were selected for the DBA calculations:

1. The maximum of Iloeje and Henry-Berenson correlations was used in the CHAN component for minimum film boiling temperature.

2. The choking model was used in the broken loop drive line/jet pump connection, broken loop drive line break plane, and broken loop suction line nozzle plane.

3. The countercurrent flow limiting (CCFL) model was used in the jet pump throat, the upper tie plate, bundle side entry orifice (SEO), and guide tube to lower plenum connection.

4. The velocity versus pressure option in the FILL components was used to model the ECC system.

5. The velocity versus time option in the FILL component was used to model main steam line and feedwater line closure.

These options were selected based upon past user experience and the nature of the tests to be simulated. Other user select options were set to default or other values recommended in the TRAC-BD1 input manual (Reference 4).

3.2.2 TRAC-BD1 TLTA Small Break Models

The TRAC-BD1 models of the TLTA facility used for the small break calculations are shown in Figures 6 and 7. The major difference between the two models was the break configuration; Test 6432 required two breaks. The models contained 19 components (totaling 112 cells) and 24 junctions for Test 6431, and 25 components (totaling 121 cells) and 30 junctions for Test 6432. The models represented all major flow paths of the facility, i.e., vessel, intact and broken recirculation loops, jet pumps, feedwater system, main steam line, ADS (Test 6432 only), HPCS (Test 6431 only), and LPCS, LPCI (Test 6432 only). Tables 2 and 3 summarize the relationship between the physical components of the TLTA facility and the corresponding mathematical components of the TRAC-BD1 model for Tests 6431 and 6432, respectively.

External and internal heat transfer was modeled in the small break models. The external heat transfer involved modeling the environmental heat loss from the system. At the initiation of the small break tests, system energy loss was approximately 50 kW. The energy loss was modeled, using the basis for heat loss dispersion outlined in Reference 5, i.e., through the two recirculation loops and the vessel. The energy loss was divided equally among the three components. A constant environmental heat sink temperature of 294 K was used in the models. Constant heat transfer coefficients of 11.72, 11.68 and 4.2266 $W/m^2 \cdot K$ were used for the broken loop, intact loop and vessel, respectively.

Internal heat transfer included heat transfer between the jet pumps and the vessel, guide tube TEE and the vessel, bypass and downcomer, upper plenum and separator and the downcomer, CHANNEL (bundle) and bypass, heater rod to channel wall, and rod to rod. TRAC-BD1 input required rod groups which describe one or more rods. The heater rods were modeled in five rod groups; four groups with heater rods and one group with simulated water rods. The rod group configuration is shown in Figure 8. The rod grouping was based upon geometry and radial peaking factors outlined in a previous study (Reference 6) which involved radiation heat transfer. Radiation heat transfer was not expected in the calculations, therefore, the rod group modeling recommended in Reference 6 was simplified.

The following TRAC-BD1 options were selected for the small break calculations:

1. The maximum of Iloeje and Henry-Berenson correlations was used in the CHAN component for minimum film boiling temperature.

2. The choking model was used in the broken loop break plane and ADS line.

3. The countercurrent flow limiting model was used in the jet pump throat, the upper tie plate, bundle side entry orifice (SEO), and guide tube TEE secondary side.

4. The velocity versus pressure option in the fill components was used to model the ECC system, and the ADS (Test 6432 only).

5. The pressure versus time option in the BREAK component was used to model the main steam line (Test 6432 only).

These options were selected based upon past user experience and the nature of the tests to be simulated. Other user select options were set to default or other values recommended in the TRAC-BD1 input manual (Reference 1).

3.3 Initial Conditions

This section presents the initial conditions used for the DBA and small break calculations. For each test simulation, initial conditions were obtained by running a steady state calculation with the TRAC-BD1 code until conditions of the calculation were within the uncertainty of the test initial conditions.[a] Two methods were used to obtain initial conditions: (1) manual and (2) automatic adjustment. TRAC-BD1 Version 11 had no built-in control system, therefore, initial conditions for the DBA calculations were obtained through manual adjustment, i.e., manually adjusting pump speed, etc. Initial conditions for the small break calculations were obtained using the built-in control package of Version B002.

3.3.1 Initial Conditions for DBA Calculations

Steady state operating conditions were not established prior to the transient initiation of Tests 6423 and 6424. The TLTA facility had a limited supply of feedwater and could not operate for long periods of time at high power. The downcomer liquid was high initially and the rod power low. Loop circulation was established and the facility warmed up. Just prior to initiation of the transient, the power was increased to the desired value. The downcomer liquid level decreased until it reached a predetermined level, at which time the blowdown valves were activated, beginning the transient. This mode of operation necessitated duplication of instantaneous test conditions in the TRAC-BD1 steady state runs, rather than initializing to steady state conditions. The transient pretest operating conditions made it difficult to initialize the TRAC-BD1 model.

---

a. The TRAC-BD1 model with initial conditions for each test is stored at the INEL under Configuration Control Number F00924.

Initialization of the TRAC-BD1 DBA calculations included the following: (a) setting the steam dome pressure by adjusting the pressure in the main steam line BREAK component, (b) setting recirculation loop pump speeds, and (c) adjusting the feedwater flow to equal the steam line flow. Bundle friction was also adjusted to obtain the proper core differential pressure. A short steady state run was made until system perturbation had diminished. The results were compared to differential pressure data, flow data, temperature data, etc. If the results were within the uncertainty band of the data, the steady state calculation was terminated. If the results were outside the data uncertainty bands, adjustments were made to the above parameters and the steady state calculation rerun. Several iterations were required to achieve satisfactory initial conditions for the transient calculations. The initial conditions used for the DBA calculations are presented in Tables 4 and 5.

During the steady state initialization, several problems were encountered. One of the major problems was bubble entrainment in the downcomer. After running a short time, significant voids in the downcomer and lower plenum would appear. These voids were a result of vapor carryover. Feedwater was injected into the level just below the downcomer liquid level, subcooling the liquid in that region. Vapor above the downcomer liquid level condensed on the subcooled liquid. Perturbations in the liquid level occurred, drawing vapor into the liquid region. The vapor was carried down the downcomer, through the jet pump and into the lower plenum. Similar results were encountered in a concurrent study involving the same TRAC-BD1 TLTA model and similar test conditions (Reference 7). In that study, it was discovered that the transient results were highly dependent upon the downcomer void fractions calculated in the steady state runs. It was also discovered that resetting the void fractions below the downcomer liquid level to 0.0 gave the best results in the transients. Therefore, in the DBA calculations, after acceptable initial conditions were achieved, the downcomer void fractions were reset to zero. Other problems encountered in the initialization process are described in detail in Reference 7.

In summary, obtaining initial conditions using manual adjustment was costly because of the trial and error procedure. It is recommended that the control package in the present version (Version B002) of the code be used for future initialization runs.

3.3.2 Initial Conditions for Small Break Calculations

The initial pretransient boundary conditions for the small break tests allowed the system to run at steady state before initiation of the transient. This steady state mode made initialization of the TRAC-BD1 TLTA small break model much simpler than the DBA model.

To initialize the TRAC-BD1 TLTA small break model, the control package contained in TRAC-BD1 Version B002 was used. The control package automatically adjusted the following preselected parameters to obtain steady state conditions: main steam line valve area to control steam dome pressure, recirculation pump torque to control jet pump mass flow and consequently core flow, and feedwater flow to control downcomer liquid level. The control system for the TRAC-BD1 TLTA model was adapted from a control system used for a TRAC-BD1 model simulating a commercial size BWR plant. Some of the gains, constants, and initial input values were adjusted to reflect the TLTA system. Figure 9 shows a schematic of the control system used for the steady state runs.

Tables 6 and 7 present the initial conditions generated in the steady state calculations. At the termination of the steady state calculations small decaying sinusoidal perturbations from the controllers in the control package were present. These perturbations resulted in a few of the calculated initial conditions being slightly outside the error band of the measurement, such as the bypass flow in Test 6431, and the downcomer temperature below the feedwater sparger and the bundle inlet subcooling in Test 6432. The perturbations were insignificant compared to the overall system response and further calculations were not considered cost effective or necessary.

The initial downcomer liquid level in the two tests was set at 7.1882 m (measured from the bottom of the vessel). In the TRAC-BD1 model, a vessel level was input at this elevation to distinguish the liquid level more accurately. The downcomer liquid level controller had problems in controlling around a modeled cell boundary, therefore, for steady state purposes the liquid level was artificially set .31 m higher (between vessel Levels 15 and 16). The effect of raising the level higher was minimal on the overall steady state initialization. The liquid level was reset to the correct height at the beginning of the transient.

4. DBA TRANSIENT CALCULATION RESULTS

The results of the DBA assessment calculations are presented in this section. The results are presented through the form of key assessment parameters jointly established by the Nuclear Regulatory Commission and EG&G Idaho. The key assessment parameters are divided into two categories: quantitative parameters (single valued) and qualitative parameters (time histories). The DBA calculations are presented in three sections. Section 4.1 presents the quantitative parameters of Tests 6423 and 6424 and the corresponding TRAC-BD1 calculations. Section 4.2 compares the qualitative parameters of Test 6423 and the corresponding TRAC-BD1 calculation. Section 4.3 compares the qualitative parameters of Test 6424 and its corresponding TRAC-BD1 calculation. A short summary of the DBA calculations is given in Section 4.4.

4.1 DBA Calculation Quantitative Parameters

Quantitative parameters of test events compared to the TRAC-BD1 calculations are shown in Tables 8 and 9 for Tests 6423 and 6424, respectively. Both tests showed two rod heat up periods: one resulting from boiling transition during the pump coastdown period and another due to subsequent dry out. Significant differences from the experimental peak clad temperatures were evident in both calculations. The timing of these events for the 6423 calculation lagged the pump coastdown dryout and led the subsequent dryout by a significant amount, while the timing of the events for the 6424 calculation agreed quite well with the data. Further discussion of these events will be included in the rod temperature comparisons for each calculation in Sections 4.2 and 4.3.

The calculation of the jet pump and suction line uncovery compared well with the data, with the calculation slightly leading the data. The timing of these events was determined by tracking the collapsed liquid level in the downcomer and lower plenum.

In the tests, the ECC system was activated based on time. The HPCS immediately came on and the LPCS and LPCI was initiated after the system pressure dropped below a specified value. After the calculations were complete, an error in the HPCS initiation set-up was noted. The HPCS FILL was tripped at time zero, however, the velocity versus pressure table in the FILL component did not allow flow until the correct HPCS initiating pressure of the test was reached. Fortunately, the calculated pressure response during the initiation of HPCS was well characterized and it was not necessary to go back and correct the mistake. However, in future calculations the timing of this event should be correctly input in accordance with the test procedure. The timings of the LPCS and LPCI initiation in the calculations showed significant differences compared to the experiments. The ECC system was modeled as velocity versus pressure FILL, therefore, the accuracy of matching the time of ECC initiation with the experiments depended upon how well TRAC-BD1 calculated the system depressurization. Further discussion of the ECC timing events is contained in the discussion of the system depressurization in Sections 4.2 and 4.3.

The minimum downcomer differential pressure and the timing of the event compared to experimental data were significantly different from data in both calculations. The difference was due partially to modeling and code limitations and the nature of the break. The broken loop suction line was connected to the bottom cell of the vessel downcomer in the TRAC-BD1 model (see Figure 5). The code does not calculate phase separation, i.e., it treats the two phases as a homogeneous mixture. Therefore, when the bottom cell in the downcomer began to void more liquid was swept out the break in the calculation than was shown in the experiment. Also, any ECC liquid penetrating the downcomer was quickly swept out the break through the broken loop suction line because of the homogeneous mixing in the connecting vessel cell and high velocities in the suction line. It was not until later in the calculations, after the broken loop suction line velocities had subsided that any significant amount of liquid began to collect in the downcomer. The addition of a vessel level below the suction line connection level may have conserved some of the downcomer liquid.

Other events important in the tests are shown in Table 10. These events were time trips and were modeled as such in the calculation.

4.2 Qualitative Parameters for Test 6423 Calculation

This section presents the qualitative parameters of the key assessment parameter list for the TRAC-BD1 calculation of TLTA Test 6423. Section 4.2.1 presents the break flow comparisons, Section 4.2.2 compares the calculated differential pressures with data, Section 4.2.3 presents the steam dome and break inlet pressure comparisons, Section 4.2.4 presents the ECC mass flow comparisons and finally Section 4.2.5 presents the rod temperature comparisons.

4.2.1 Break Flow Comparisons

Preparatory to a discussion of the break flow comparisons, break inlet conditions will be presented.

The break inlet temperature is compared to data in Figure 10. The calculated temperature followed the saturation curve and reflected the vessel depressurization rate calculated by TRAC-BD1. The oscillations in the calculated temperature reflect vessel pressure oscillations induced by the code. The data indicated a dryout at around 100 s indicating the thermocouple may be affected by stored heat in the vessel wall rather than superheated steam in the downcomer.

Figures 11 and 12 compare the calculated suction line break inlet void fraction and subcooling to data. The main interest in these figures is the duration of the liquid blowdown portion of the transient. Figure 11 shows departure from liquid blowdown commencing at approximately 2 s in the calculation while in the test it did not occur until approximately 8 s. Only a short term comparison was made of the inlet subcooling because the liquid blowdown was of main interest. Calculated subcooling was initially higher than the data as shown in Figure 12. By 2 s the calculated subcooling had become zero. This lasted for approximately 4 s, then a slight subcooling for approximately 7 s was noted. The slight subcooling after 6 s in the calculation appeared to be a result of subcooled liquid

from vessel downcomer Level 5 dropping into Level 4, decreasing the break inlet void fraction as shown in Figure 11. The data showed approximately 4 K subcooling initially which became saturated liquid by approximately 1 s into the transient as shown in Figure 12. It remained saturated liquid until approximately 8 s at which time two phase fluid began to enter the break as shown in Figure 11.

Figures 13 and 14 compare the calculated drive line break inlet void fraction and subcooling to data. The differences in the two curves in Figure 13 were due to the fact that the instrumentation was in the downcomer, whereas the calculation was in the drive line near the jet pump suction. Similar results were observed in the drive line break inlet subcooling as in the suction line break inlet subcooling as observed in Figure 14. The departure time from single phase blowdown to two phase in the drive line in the calculation agreed quite well with the data as evident in Figure 13.

The break comparisons are made on a mass flow basis rather than a volumetric flow. A problem of erroneous calculation of the pressure downstream of the suction line flow nozzle precluded valid volumetric flow comparisons. An in-depth discussion of this problem is found in Reference 7 for those interested readers.

Figure 15 compares the suction line break flow with data. The calculated suction line break flow rate was overcalculated. This was a result of early two phase flow initiation in the calculation as shown in Figure 11 and an overcalculation of pressure drop through the suction line flow nozzle (see Reference 7). At approximately 11 s two phase flow was well underway as a result of recirculation line uncovery in the calculation affecting the mass flow rate as shown in Figure 15. After 15 s, lower plenum flashing occurred, reversing the jet pump mass flow rate and allowed more fluid to exit the break. Beyond 60 s the calculated mass flow rate compared reasonably well with the data.

Figure 16 compares the drive line mass flow rate with data. TRAC-BD1 undercalculated the mass flow for the first 8 s. During this time, subcooled liquid calculated by the code maintained a constant mass flow rate. At approximately 8 s, the jet pump suction uncovered in the test accounting for the rapid change in mass flow rate shown in Figure 16. After 8 s, the calculated drive line break mass flow rate agreed quite well with the data.

4.2.2 Differential Pressure Comparisons

This section compares calculated and measured differential pressures. This method of comparison was selected over mass inventory comparisons because the differential pressures were direct measurements rather than derived data. Some of the differential pressure comparisons were significantly offset because of elevation mismatch between the model cells and the experimental differential pressure taps. The calculation values were not adjusted for the elevation difference because the calculated mixture density history was not available. The oscillatory behavior in the calculated differential pressure response appeared to be related to condensation effects from the condensation model in the code. Even though condensation was localized, the effects were observed globally. Similar results were observed in the 6424 calculation.

Figure 17 compares the calculated downcomer differential pressure to data. The calculated value compared well with the data for the first 10 s, however, after that time the code undercalculated the data. The undercalculation after 10 s was a result of the way the suction line was connected to the vessel in the model explained in Section 4.1. Also the higher calculated suction line break mass flow rate contributed to the mass depletion inferred by the differential pressure.

Figure 18 compares the calculated lower plenum differential pressure with data. An elevation difference of 0.51 meters existed between the data measurement and the calculation. Even though the comparison is mismatched interesting trends are observed. Early in the transient the data shows an increase in the pressure differential due to the initiation of the break,

the code does not show this trend. Lower plenum bulk flashing and jet pump exit plane uncovery, however, were well characterized as shown in Figure 18. The trend in the data was calculated by the code after the jet pump exit plane uncovery. The oscillations in the calculation after 35 s appeared to be condensation instabilities in the code.

Figures 19 and 20 compare the calculated core and bypass differential pressures with data respectively. As shown, good agreement existed between the data and the calculation. After approximately 120 s, the calculated bypass began to deviate from the data, due to ECC liquid hold up in the upper plenum from CCFL calculated by the code. CCFL and upper plenum liquid hold up will be discussed in section 4.3.

The calculated upper plenum differential pressure is compared to data in Figure 21. The code undercalculated the upper plenum differential pressure response out to approximately 30 s. The difference was partially due to a mismatch between the model noding and the differential pressure taps. At 15 s, lower plenum flashing occurred sending a surge of liquid up the core and bypass into the upper plenum. This liquid continued to travel up the upper plenum, through the steam separator and dissipated in the downcomer, in the calculation. The data indicated that the liquid remained in the upper plenum. After HPCS injection at 27 s, the data indicated upper plenum drainage into the bypass. The calculation showed no upper plenum differential pressure increase due to ECC injection until after LPCS initiation.

At approximately 100 s, the code overcalculated the upper plenum differential pressure. After LPCS was initiated, liquid began to collect in the upper plenum, increasing the differential pressure. However, the upward core steam flow was high enough that the CCFL correlation was prohibiting any liquid downflow, therefore the liquid collected in the upper plenum showing an overcalculation of the data. A sensitivity study was performed in which the CCFL correlation was removed from the model, improving the results. Further discussion on this will be included in a later section.

4.2.3 Pressure Comparisons

Figures 22 and 23 compare calculated pressure response with data for the steam dome and break inlet respectively. The break inlet pressure was equivalent to vessel Level 5; instrumentation in the break lines were not active. The two pressure curves are very similar, therefore, only the steam dome pressure curve will be discussed. Due to an overcalculation of the suction line break mass flow rate, the system depressurized faster than the data for the first 5 s. At approximately 5 s, the steam line began to close and the system repressurized. At 11.5 s, the steam line had completely closed, indicated by the apex of the repressurization in the curves. The calculation repressurization was not as pronounced as the data. At approximately 15 s, lower plenum bulk flashing occurred and slowed the system depressurization rate. At this time, good agreement between the calculation and data was reached. At approximately 35 s, the jet pump exit plane uncovered in the calculation, resulting in unity void fraction in the break planes and a faster depressurization rate. The faster depressurization rate in the calculation led to an earlier initiation of LPCS and LPCI flows as shown in Table 8. After approximately 150 s, the depressurization rate was reasonably calculated. The oscillations in the calculation between 60 and 120 s were numerically induced by the code.

4.2.4 ECC Comparisons

The ECC system was controlled by velocity versus pressure in the calculation, i.e., given a pressure a specified velocity is output. The ECC system was tripped on time then governed by the system depressurization.

Figures 24, 25, and 26 compare the calculated HPCS, LPCS and LPCI flows with data respectively. As explained earlier, an error was found in modeling the HPCS activation, however because of good agreement in the system depressurization at the time of HPCS initiation the error was not corrected. As discussed previously, after jet pump exit plane uncovery occurred, the calculation system depressurization rate was more rapid than the data, resulting in early initiation of LPCS and LPCI flows as shown in Figures 25 and 26. The oscillations in the calculated LPCS and LPCI curves

at the initiation of the flows were a result of local condensation in the ECC lines. Saturated steam condensed on the subcooled ECC liquid, lowering the pressure locally. More subcooled liquid entered the pipe condensing more steam. The pipe filled with liquid, pressurized locally, then expelled the liquid. This occurred for a short time until the system stabilized. An in-depth study was performed on improving this instability and interested readers should refer to Reference 7.

The bypass tubes were modeled as vessel Levels 4 through 8, ring 1, with LPCI injecting liquid into Level 7. When liquid entered Level 7 it remained there until the volume was liquid full. When water packing in that volume occurred, the liquid was released. It was also noted that similar behavior was occurring in the guide tube TEE secondary side. This behavior resulted in code failures and a reduction of time step size from 6 ms to 1 ms. Two solutions were required to overcome the problem: (a) the water packing option was turned on and (b) the guide tube TEE secondary was modeled as a cone as shown in Figure 27. Better results were calculated with these fixes implemented as illustrated by the void fraction behavior shown in Figures 28 and 29.

4.2.5 Rod Temperature Comparisons

This section presents the rod temperature comparisons. The bundle was modeled with four rod groups and one group representing the simulated water rods as shown in Figure 30. The radial peaking factor was modeled as unity. At the time the rods were modeled it was felt that the modeling was adequate, however a subsequent study (Reference 6) demonstrated that careful modeling of the rods should be exercised.

The rod temperature comparisons were done on a rod group (calculation), rod location (data), elevation basis. The experimental data consisted of the mean of all the thermocouples within the calculated rod group and elevation level, and in addition, the minimum and maximum of those data.

Figures 31 through 37 compare the calculated rod temperatures with data at each of the 7 modeled rod levels. The bottom three rod levels

(Figures 31, 32 and 33) show rod temperatures were reasonably calculated. The bottom level showed no heatup as in the data but followed saturated temperature. The other two bottom levels demonstrated a heatup. Departure from nucleate boiling (DNB) and rod quench occurred at approximately the same time as in the data for Level 2 (Figure 32). The calculated rod temperature at Level 3 (Figure 33) showed an early heatup due to reduced core flow from pump coastdown and a delayed core power decay. After the power decay was initiated, enough liquid upflow cooled the rods. Because of further reduced core flow, DNB at rod Level 3 occurred earlier in the calculation than in the data. Enough LPCI liquid from the bypass had entered the core through the core bypass path that the rods at Level 3 quenched around 165 s in the calculation, approximately 35 s earlier than the data.

Rod temperature comparison of the middle three rod levels (Levels 4 through 6, Figures 34, 35 and 36) showed significant deviation from the data. The early calculated rod heat up was a result of bundle dryout due to pump coastdown (lower core mass flow rate) and delayed core power decay. These effects were observed in the data only at higher elevations. An upward surge of liquid from the lower plenum turned over the rod temperatures as a result of lower plenum flashing at approximately 15 s. The surge of liquid was not enough to cool the rod midplane to saturation (the rod midplane was the maximum axial power level). At approximately 50 s, bundle dryout occurred and the rod temperature began to increase. This corresponded approximately to dryout times in the data. Enough LPCI liquid entered the core through the bypass leakage holes to maintain the rod temperatures, but not enough to remove the decay heat in the rods and reduce steam generation. After 140 s steam upflow from the bypass to the mixing plenum decreased enough that upper plenum liquid began to drain into the bypass and eventually in the core via the core bypass connection. At approximately 150 s, the midplane of the heater rods began to decrease.

The upper level rod temperatures showed good agreement with the data as shown in Figure 37. Rod temperatures were adequately calculated during the pump coastdown period. A rod heatup shortly after 100 s in the data was not calculated by the code. This heatup may have been the result of local dryout due to the bundle grid spacer located at that elevation.

4.3 Qualitative Parameters for Test 6424 Calculation

The results of the TRAC-BD1 Test 6424 calculation were very similar to Test 6423. Many of the problems encountered in the Test 6424 calculation were encountered in the Test 6423 calculation, therefore discussion of the Test 6424 calculation will not be as detailed except where the author feels it is warranted. Section 4.3.1 will present the break flow results, Section 4.3.2 will present the differential pressure comparisons, Section 4.3.3 will compare calculated pressure to data, Section 4.3.4 will discuss the ECC time histories, and Section 4.3.5 will present the rod temperature comparisons.

4.3.1 Break Flow Comparisons

As in the Test 6423 comparison, preparatory to presenting the break flow comparisons, break inlet conditions will be presented.

Figure 38 compares the calculated break inlet temperature to data. The calculated temperature followed the saturation curve and reflected the vessel depressurization rate calculated by the code. The oscillations in the calculation after 50 s were depressurization oscillations induced by the code. During the first 11-14 s of the calculated transient, subcooled conditions existed at the break as shown in Figures 39 and 40. The increase in subcooling between 6 and 11 s appeared to be liquid dropping from one level to another in the calculation. Little subcooling was shown in the data, however, it is believed the thermocouples were experiencing vessel wall effects.

Departure from liquid blowdown is illustrated in the break inlet void fraction comparison for the suction line and drive line in Figures 41 and 42 respectively. Good agreement existed in the time of departure from liquid blowdown. These times correspond to the jet pump suction and suction line uncovery shown in Table 9.

Figures 43 and 44 compare the calculated suction line and drive line break mass flow rates with data. Unlike the Test 6423 calculation, the suction line break mass flow rate was undercalculated until the suction line uncovered at approximately 8.5s. Two phase flow then began to exit the break resulting in an overcalculation of the break flow. After 120 s, the break flow was again undercalculated resulting from calculated liquid holdup in the upper plenum discussed in Section 4.3.2.

The calculated drive line break flow in Figure 44 was reasonably calculated. The undercalculation of the drive line break flow between 3 and 8 s was related to the voiding of the break as shown in Figure 42. After the steam line closure at 8 s, good agreement with the data existed in the drive line break flow calculation. The perturbation in the data at approximately 160 s and out to the end of the calculation appear to be condensation related.

4.3.2 Differential Pressure Comparisons

Figure 45 compares the calculated downcomer differential pressure with data. Generally the calculation of the downcomer differential pressure compared well with the data. The code undercalculated the data slightly, however this may be partially due to a slight mismatch in differential pressure taps and vessel level noding. Also, as discussed in Section 4.1 the location of the suction line in the bottom level of the downcomer may be contributing to the undercalculation.

Figure 46 compares the calculated lower plenum differential pressure with data. Again, the vessel noding mismatched the instrumentation differential pressure taps of the test. Also a slight difference in the lower plenum liquid temperature contributed to the difference. After the main steam line valve closed the calculated differential pressure showed good agreement with the data. The oscillations after approximately 35 s appear to be condensation modeling related.

Figures 47 and 48 compare core and bypass differential pressures with data respectively. The comparison of the two curves with data show an

overcalculation of the differential pressure. The difference was attributed to model noding and instrumentation differential pressure tap mismatch. After LPCI injection in the bypass commenced, liquid build-up in the bypass was more in the calculation than in the data due to oscillatory flow in the guide tube. After 150 s the core differential pressure was undercalculated as a result of CCFL at the upper tie plate. Again, the sharp oscillatory behavior appeared to be related to condensation effects.

The calculated upper plenum differential pressure is compared with data in Figure 49. Good agreement existed early in the transient. At 27 s, HPCS was initiated and the upper plenum began to fill with ECC liquid. In the calculation, the ECC liquid was carried up through the separator and into the downcomer. At approximately 100 s ECC liquid began to penetrate the core and bypass. The calculation, however, showed an increase in liquid due to CCFL at the upper tie plate. The effects of CCFL will be discussed in the section describing the rod temperature behavior.

4.3.3 Pressure Comparisons

The steam dome and break inlet pressure calculation is compared to data in Figures 50 and 51 respectively. The first 6 s of the pressure response compared very well with the data. This was a result of the low break flow calculation during that time. The undercalculated break flow resulted in a better comparison in the volumetric break flow rate and allowed a better calculation of the pressure response. At 6 s, the steam line valve began to close and a repressurization of the system occurred. At 8 s the valve had completely closed. The code overcalculated the repressurization after the valve closure. Lower plenum bulk flashing occurred at approximately 14 s, slowing the depressurization rate. At approximately 32 s the jet pump exit plane uncovered the depressurization rate increase in the calculation. Similar to the Test 6423 calculation the increased depressurization rate led to early initiation of the LPCS and LPCI. Between 50 and 160 s the oscillations in the calculated pressure response were numerically induced by the code.

4.3.4 ECC Comparisons

Figures 52, 53 and 54 compare the HPCS, LPCS and LPCI with Test 6424 data respectively. Due to the overcalculation of the depressurization rate the HPCS did not activate until 28 s compared with 27 s in the data. Early activation of the LPCS and LPCI flows shown in Figures 53 and 54 was a result of a faster depressurization rate calculated by TRAC-BD1.

4.3.5 Rod Temperature Comparisons

The same rod group modeling used in the Test 6423 was used in this calculation.

Figures 55 through 61 compare the calculated rod temperatures with data at each of the 7 rod bundle levels. The first four levels show reasonable agreement between the calculation and the data. After quenching, the calculated rod temperature followed the saturation line of the system depressurization.

The calculated rod temperature at Level 5 in Figure 59 shows similar results as those in the Test 6433 calculation, i.e., not enough cooling from the ECC liquid to remove the decay heat. The trend, however, shows a dryout and rewet in the calculated temperature about the same time the data shows a dryout and rewet.

Figures 60 and 61 show good agreement with the rod temperature comparisons at the two highest levels in the rods. However, after 100 s a second rod heatup occurred. It appeared that the second rod heatup was due to CCFL limitations at the upper tie plate. This heatup period corresponded to the increased upper plenum differential pressures at that time.

In the two DBA calculations CCFL at the upper tie plate limited calculated ECC liquid penetration into the bundle and bypass from the upper plenum, resulting in higher rod temperatures in the TLTA Test 6423 calculation and a small, second rod heatup after 100 s in the TLTA Test 6424 calculation. The CCFL model was removed at the upper tie plate

in the TLTA Test 6424 calculation and rerun commencing at 100 s. Liquid in the upper plenum from ECC injection penetrated the bundle and bypass resulting in no rod heatup as shown in Figures 62 through 64. Currently TRAC-BD1 uses two CCFL modeling options: CCFL calculated using upper tie plate constants and SEO constants. As illustrated in the previous discussion the CCFL model restricts the liquid downflow to values which may be too low for the modeled facility. This may be an over-conservative formulation of the CCFL coefficients. It should be noted, however, that CCFL is highly configuration dependent and the existing coefficients may also be insufficiently general for the many experiment and reactor designs.

In general, it was noted that calculated rod temperature behavior in Test 6424 agreed with the data better than did the calculation simulating Test 6423. The degree of ECC subcooling between the two calculations was the major factor in the better comparison of Test 6424.

4.4 Summary of DBA Calculations

In general, TRAC-BD1 calculated the trends in the data, i.e., lower plenum flashing, rod heatup due to pump coastdown and subsequent dryout, etc. The code tended to overcalculate the suction line break mass flow rate which led to a faster depressurization and consequently early initiation of LPCS and LPCI initiation. Generally, the calculated differential pressures were reasonable. CCFL at the upper tie plate was overcalculated resulting in ECC liquid holdup in the upper plenum and consequently higher rod temperatures in the upper half of the bundle.

It was also discovered that water packing in the guide tube TEE secondary and initiation of ECC subcooled liquid in the bypass resulted in code failures and a significant reduction in time step size. The guide tube TEE secondary was modeled to resemble a cone and the water packing option was turned on. These fixes smoothed the oscillations and the calculation ran at a reasonable time step.

5. SMALL BREAK CALCULATION RESULTS

The results of the small break assessment calculations are presented in this section. As in the presentation of the DBA results the small break results are presented through the key assessment parameters. Section 5.1 presents the quantitative parameters for each calculation, Section 5.2 presents the qualitative results for the TLTA Test 6431 calculation, and Section 5.3 presents the qualitative results for the TLTA Test 6432 calculation. A short summary of the small break calculations is given in Section 5.4.

5.1 Small Break Calculation Quantitative Parameters

Quantitative parameters of test events compared to the TRAC-BD1 calculations are shown in Tables 11 and 12 for Tests 6431 and 6432 respectively. Most of the test events were tripped on time, therefore, these events were also tripped on time in the calculation. LPCS and LPCI inlet valves were tripped on time, however, the subsequent rate of ECC flow was a function of system pressure. The occurrence of these events compared with data very well.

5.2 Qualitative Comparisons for Test 6431 Calculation

This section presents a qualitative comparison of the TRAC-BD1 calculation with TLTA Test 6431 data. The comparisons include the established key assessment parameters. Section 5.2.1 presents the depressurization comparison, Section 5.2.2 the break flow comparison, Section 5.2.3 the differential pressure comparison, Section 5.2.4 the ECCS mass flow comparison, and finally Section 5.2.5 presents the rod temperature comparisons.

5.2.1 Depressurization Comparisons

Figures 65 and 66 compare the steam dome pressure and break inlet pressure with data, respectively. The first increase in pressure was a result of increased core steam generation due to delayed power decay and a

rapid decrease in core mass flow resulting from pump coastdown. At approximately 7 s power decay began, steam generation decreased and the pressure decreased. The main steam line valve was closed at 17.5 s, reducing the system mass removal rate, resulting in a second pressure increase. At 26.8 s the HPCS system was initiated, injecting subcooled liquid into the upper plenum, condensing the steam and decreasing the pressure. As shown in Figures 65 and 66, TRAC-BD1 calculated the pressure response very well. The pressure response was undercalculated beginning at approximately 500 s, however, the deviation was within the uncertainty bands of the data until approximately 1000 s. After 1000 s the calculated pressure response was outside the uncertainty bands. The deviation appeared to be a result of a deviation in the break inlet subcooling as shown in Figure 67 and the break inlet temperature shown in Figure 68. Further explanation of the break inlet subcooling deviation will be discussed later in this section.

5.2.2 Break Flow Comparison

The calculated break mass flow rate is compared to data in Figure 69. As shown, the break mass flow rate was well characterized by TRAC-BD1. The controlling factor in the break flow rate was the differential pressure across the break plane orifice. It was felt the undercalculation of the break mass flow between 50 and 300 s was a result of coarse noding in the break pipe. A better calculation of the pressure drop and thus the break flow in the break pipe may result from finer noding. Further investigation into break noding should be done.

The oscillation in the calculated break flow rate around 500 s was a result of small voids ($0.0 \leq \alpha \leq 0.02$) formed in the break pipe.

5.2.3 Differential Pressure Comparisons

This section presents a comparison of the downcomer, lower plenum, core, bypass, and upper plenum differential pressures. The differential pressures reflect the mass distribution throughout the system. It was discovered that during low void, bubbly flow regime the code would not

calculate countercurrent flow. This situation was observed in the calculation after HPCS was initiated. The code did not calculate reverse core flow as was observed in the data (see Figure 70), resulting in a calculated mass distribution (i.e., differential pressure) throughout the system somewhat different than the data as shown in the following figures. As in the DBA calculations, the oscillatory behavior in the calculated differential pressure response appeared to be related to condensation effects from the condensation model in the code. Also, similar results were observed in the 6432 calculation.

Figure 71 compares the calculated downcomer differential pressure with data. At approximately 20 s the code undercalculated the downcomer differential pressure indicating less mass in the downcomer. This mass was redistributed into the core and bypass. Between 20 and 200 s the two curves paralleled each other indicating that the mass depletion rate in the downcomer was the same.

At about 200 s the calculated downcomer differential pressure response agreed reasonably well with the data. Similar to the core mass flow, the calculated jet pump mass flow rate did not reverse direction, therefore any liquid that entered the downcomer came from the upper plenum via the steam separator. The liquid coming from the upper plenum was a mixutre of the subcooled ECC liquid and saturated steam from the core. The liquid coming from the upper plenum into the downcomer picked up enough heat from the vessel wall and internals that it was nearly saturated by the time it exited the break as shown in Figure 67. The calculated oscillations in Figure 71 appear to be related to condensation spikes calculated by the code.

Past 700 s TRAC-BD1 undercalculated the downcomer differential pressure response as a result of positive core and jet pump flow and system mass distribution as discussed below.

The lower plenum differential pressure comparison is shown in Figure 72. As shown, TRAC-BD1 did not characterize the lower plenum differential pressure response very well. Figure 73 shows calculated integrated core flow (at SEO), integrated combined jet pump flow, and

integrated quide tube flow (secondary side). The core flow demanded more than the jet pump and guide tube flows could offer, therefore, fluid from the lower plenum was swept up through the core, thus the deviation in the calculated lower plenum differential pressure. Also, the subcooled ECC injected liquid had become saturated by the time it reached the lower plenum, converse to that of the data.

Figure 74 compares the calculated core differential pressure with data. Reasonable agreement existed between the calculation and data until approximately 180 s. At that time, the measured core flow reversed direction as a result of ECC liquid head build-up in the upper plenum and the liquid in the upper plenum drained into the core. As stated before, the code will not calculate countercurrent flow in the low void, bubbly flow regime. These were the conditions in the calculation, therefore the core flow remained positive and no ECC liquid entered the core through the upper tie plate. The core began to void, because core outflow was higher than the core inflow as indicated by the integrated mass flow rates shown in Figure 75.

Figure 76 compares the calculated bypass differential pressure with data. Shortly after the steam line and loop isolation valves closed, in the calculation, the bypass flow reversed direction and liquid accumulation in the bypass commenced. This was converse to the data as shown in Figure 76. Liquid accumulation in the test began at approximately 80 s. Near the termination of the calculation the calculated differential pressure in the bypass agreed with that measured. As mentioned earlier the spikes in the calculation appear to be condensation spikes from injecting subcooled liquid into the system.

The calculated upper plenum differential pressure is compared to data in Figure 77. TRAC-BD1 reasonably calculated the data response up to approximately 180 s. At that time the ECC liquid collected in the upper plenum, drained into the core, reversing the core flow in the data. TRAC-BD1 did not calculate this phenomena because of the code limitations discussed earlier. In the calculation, the ECC liquid injected into the

upper plenum mixed with the two phase fluid coming from the core decreasing the degree of subcooling. Some of this liquid drained into the bypass, but a majority of the liquid exited the upper plenum through the steam separator and entered the downcomer. The liquid either remained in the downcomer as indicated in Figure 71, exited the break, or entered the lower plenum as a result of positive jet pump flow. From the lower plenum the liquid entered the core and exited in the upper plenum.

5.2.4 ECCS Mass Flow Comparison

Only the HPCS of the ECCS system was activated during Test 6431. The activation of this system was done on time (26.8 s), therefore, to be consistent with the test, the HPCS in the calculation was also tripped on time. After that time the flow was controlled by system pressure in the calculation. Figure 78 compares the calculated HPCS mass flow with data. Because the system pressure was well characterized in the calculation, the HPCS mass flow trend in the calculation was also well characterized.

5.2.5 Rod Temperature Comparisons

To present the rod data with the calculation, the same technique used to present the DBA rod data was incorporated, i.e., the mean of all rod data within a calculated rod group level and the minimum and maximum of that data.

Figures 79-84 compare the calculated rod temperature histories at various elevations with data. Because there was sufficient fluid in the bundle no rod heat up occurred. The significant difference in the comparison was again related to the inability of the code to calculate countercurrent flow in the low void, bubbly flow regime. When the experimental core flow reversed direction at approximately 180 s, subcooled ECC liquid in the upper plenum entered the bundle cooling the rods below the saturation temperature. Because the calculated core flow did not reverse direction, the subcooled ECC liquid did not penetrate the bundle directly, but rather entered the core from two directions: (a) liquid

dropping into the bypass tubes from the upper plenum and entering the core via the bypass leakage path, and (b) upper plenum liquid entering the downcomer via the steam separator, traversing the downcomer, entering the lower plenum via the jet pumps, and entering the core via the SEO. In either case, by the time the ECC liquid entered the core all of the subcooling was lost. As a result, the rods in the calculation followed the depressurization saturation temperature.

5.3 Qualitative Comparisons for Test 6432 Calculation

This section presents a qualitative comparison of the TRAC-BD1 calculation with TLTA Test 6432 data. Section 5.3.1 presents the depressurization comparison, Section 5.3.2 the break flow comparison, Section 5.3.3 the differential pressure comparison, Section 5.3.4 the ECC mass flow comparison, and finally Section 5.3.5 presents the rod temperature comparisons.

5.3.1 Depressurization Comparisons

Steam dome and break inlet depressurization comparisons with data are shown in Figures 85 and 86 respectively. Early in the transient, steam dome pressure was held constant (approximately 6.69 MPa) by adjusting the main steam line valve. In the calculation this was accomplished using a BREAK component with a pressure vs time table. At approximately 165 s the main steam line valve closed and a pressure increase was observed. The calculated pressure increase was higher than the data due to an undercalculation of the break flow. At approximately 286 s the ADS was tripped open and rapid depressurization began.

5.3.2 Break Flow Comparison

The calculated break mass flow rate is compared with data in Figure 87. In the test, two breaks were used, one representing the small break the other for excess mass removal. The breaks were not opened until 138 s because of scaling differences and downcomer liquid level matching between the referenced BWR and TLTA. At the initiation of the break,

TRAC-BD1 undercalculated the break mass flow rate. The undercalculated mass flow rate resulted in an overcalculation of the pressure response discussed above. The break flow calculation might have been improved if finer noding around the break was done. However, the code calculated the break flow reasonably well. At 286 s the second break was closed, accounting for the rapid decrease in mass flow rate. After ADS initiation, break inlet conditions became saturated and remained saturated throughout the transient calculation as shown in Figures 88 and 89. The data in Figure 88 shows that superheated steam existed early in time. This may be a result of a zero off-set in the instrumentation at that location.

In addition to the break mass flow comparison, it is important to briefly discuss the steam line/ADS mass flow rate. The steam line remained open until 165 s, therefore, steam line mass flow was important in downcomer liquid mass tracking. As mentioned earlier the steam line was modeled using a BREAK component with a pressure versus time table to calculate the constant pressure early in the transient. Using this setup, mass flow versus time out the BREAK was not available. Another alternative would have been to model the steam line with a negative FILL with a velocity vs time table, and letting the code calculate the pressure. Using the BREAK with pressure versus time to maintain constant pressure was deemed more important than using the negative FILL to control the mass flow rate out the steam line.

Figure 90 compares the calculated steam line/ADS mass flow rate with data. The calculated high mass flow early in time was a result of downcomer level swell into the steam dome and downcomer liquid exiting through the steam line. The level swell appeared to be code induced. Several modeling techniques were tried to limit the high mass flow rate. The successful technique was to connect the steam line PIPE component to Ring 2 in the steam dome level of the VESSEL component and set the levels in Ring 2 above the downcomer liquid level to an alpha equal to 1.0. This gave the best result. After 20 s the calculated behavior reasonably matched the data.

5.3.3 Differential Pressure Comparisons

This section presents the differential pressure comparisons for the downcomer, lower plenum, core, bypass, and upper plenum. The differential pressures reflect the mass distribution through the system.

The calculated downcomer differential pressure is compared with data in Figure 91. The high calculated mass flow out the steam line, discussed above, depleted the downcomer liquid as indicated in Figure 91. The calculated downcomer differential pressure remained below the measured pressure until the initiation of the second break at 138 s. The undercalculation of the break flow induced a better downcomer differential pressure agreement. Between 138 and 286 s the calculated differential pressure essentially paralleled the data. Shortly after 200 s a sharp decrease in the calculated differential pressure and a leveling off until 286 s was observed. This was attributed to a small flow reversal followed by essentially zero flow through the jet pumps. At 286 s the second break was closed and the ADS opened, resulting in a level swell indicated by the increase in differential pressure in Figure 91. From 286 s to the termination of the calculation, TRAC-BD1 calculated the trend of the data. The spikes in the calculation appear to be condensation related.

Figure 92 compares the calculated differential pressure in the lower plenum with data. As shown, reasonable agreement existed between the calculation and the data out to ADS initiation at 286 s. At the initiation of ADS the lower plenum partially voided due to lower plenum steam generation from the rapid system depressurization rate. In the calculation the lower plenum was voided to the jet pump exit plane, where it remained until approximately 438 s. The liquid that voided out of the lower plenum, in the calculation, appeared in the downcomer, core and bypass. During this time a slight level swell was observed in the data due to the rapid system depressurization. Also lower plenum steam generation due to ADS activation led to CCFL at the SEO in both the calculation and the data.

At approximately 438 s the jet pump mass flow began oscillating around zero, tending to be more reverse than positive flow. The reverse flow out the jet pumps further reduced the liquid inventory in the lower plenum as observed in the calculated lower plenum differential pressure curve in Figure 92. Also at 438 s the LPCS flow was initiated and began filling the upper plenum with subcooled liquid. The liquid head in the upper plenum produced by LPCS injection changed the pressure balance in the system such that positive core flow was reduced and any steam generation in the lower plenum from system depressurization exited through the jet pumps. In the data this behavior was slightly different. The liquid inventory in the lower plenum did not begin to decrease until after 500 s, at which time a higher hydrostatic head in the core, from ECC liquid in the upper plenum, began to drive the lower plenum liquid out the jet pumps until the jet pump exit plane uncovered. At the uncovery of the jet pump exit plane, steam generated in the lower plenum had an alternate escape route. This changed the CCFL conditions at the SEO and allowed bundle liquid to enter the lower plenum. With less steam flow up the bundle, liquid from the upper plenum began to penetrate the bundle and cool the rods. This liquid continued down the bundle and into the lower plenum until subcooled liquid entered the SEO and subcooled CCFL break down at the SEO occurred followed by a rapid refill of the lower plenum (approximately 610 s). The refill of the lower plenum in the calculation did not occur until approximately 630 s as a result of incomplete flow reversal in the core. CCFL at the upper tie plate was intermittent, therefore most of the liquid regained in the lower plenum came from LPCI injection in the bypass via the core bypass and SEO or the guide tube. By the time the liquid entered the lower plenum it was saturated.

Figure 93 compares the calculated core differential pressure with data. After ADS initiation, liquid from the lower plenum was observed in the core region in the calculation. At approximately 400 s reasonable agreement existed between the calculation and the data. At approximately 550 s liquid from the upper plenum began to increase the core mass inventory in the data where as in the calculation this did not occur until approximately 30 s later. As stated earlier the oscillations in the calculation appear to be condensation effects on the subcooled injected liquid.

The calculated bypass differential pressure is compared to data in Figure 94. As in the core differential pressue comparison, liquid from the lower plenum was observed to keep the bypass differential pressure higher in the calculation than in the data. At approximately 458 s LPCI injection was activated and shortly after that liquid inventory in the bypass began to increase the differential pressure in both the calculation and the data. TRAC-BD1 reasonably calculated the bypass differential pressure response after LPCI initiation.

The upper plenum differential pressure comparison is shown in Figure 95. The change in the differential pressure at approximately 80 s appeared to be related to the steam line mass flow behavior. Shortly after 200 s a sharp decline in differential pressure was noted in both the calculation and the data. This was a result of core flow reversal, draining upper plenum liquid into the core. After ADS initiation liquid swell from the rapid depressurization and mass inventory from the core and bypass entering the upper plenum resulted in the increased differential pressure shown in Figure 95. Unlike the data, the upper plenum liquid continued to go up through the separator and into the downcomer resulting in a rapid decrease in differential pressure shortly after ADS initiation. At 438 s the LPCS was initiated and upper plenum mass inventory began to increase in both the calculation and the data. At approximately 580 s the data shows upper plenum drainage into the core as a result of jet pump exit plane uncovery explained earlier. This did not occur in the calculation because of intermittent CCFL at the upper tie plate. Because of time constraints on the calculation, investigation into the CCFL modeling was not done, however, this investigation should be carried out in future assessment work.

5.3.4 ECC Mass Flow Comparisons

The ECC system mass flow rates are compared with data in this section. In this test, the HPCS system was not operable, therefore, only the LPCS and LPCI systems were initiated.

The calculated LPCS and LPCI mass flow rates are compared to data in Figure 96 and 97 respectively. The importance in showing these curves was the timing of the initiation of these flows. Because the system pressure was well characterized in the calculation the timing of LPCS and LPCI initiation was also well characterized. As shown, the activation of LPCS and LPCI occurred at 438 and 458 s respectively. The experimental LPCS initiation led the calculation by approximately 5 s. The positive flow shown by the data before LPCS and LPCI initiation was due to either zero offset in the instrumentation or pre-injection warmup circulation.

5.3.5 Rod Temperature Comparisons

The same technique used to present the rod data in the calculation of TLTA Test 6431 is used in presenting the rod temperature comparisons for Test 6432.

Figure 98-103 compare the calculated rod temperatures with data. As in Test 6431 no rod heatup was observed in either the calculation or the data. TRAC-BD1 tended to undercalculate the data, however, the temperature histories were reasonably calculated. The decrease in rod temperature due to subcooled liquid as discussed earlier was delayed in the calculation by approximately 20 s.

5.4 Summary of Small Break Calculations

In general, TRAC-BD1 Version B002 calculated the trends in the data. Break mass flow and system depressurization was well characterized by the code in both calculations. ECC liquid holdup in the upper plenum due to the inability of the code to calculate countercurrent flow in a low void, bubbly flow regime led to a system mass distribution different to that of the experiment in the simulation of Test 6431. In Test 6432, CCFL at the upper tie plate limited ECC liquid downflow into the bundle and bypass, similar to results in the DBA calculations. No rod heatup was observed in either the tests or the calculations.

6. CONCLUSIONS AND RECOMMENDATIONS

This section presents the conclusions and recommendations for the four TRAC-BD1 calculations described in this document. The conclusions and recommendations for the DBA calculations will be presented first, followed by the conclusions and recommendations for the small break calculations. It is recommended interested readers refer to Reference 7 for other conclusions relative to calculations similar to the DBA calculations documented in this report.

TRAC-BD1 Version 11 was observed to generally calculate the trends of the data. Problems, where they arose, were due to the immaturity of Version 11, model and input limitations and initialization difficulties.

TRAC-BD1 Version 11 overcalculated the suction line break flow rate. The overcalculation of the suction line break flow rate led to a faster depressurization rate and consequently early initiation of ECCS.

TRAC-BD1 Version 11 calculated the trend in the system differential pressure response.

The TRAC-BD1 Version 11 model tended to undercalculate liquid downflow in this facility.

CCFL at the upper tie plate limited calculated ECC liquid penetrations into the bundle and bypass from the upper plenum, resulting in higher rod temperatures in the TLTA Test 6423 calculation and a small, second rod heatup after 100 s in the TLTA Test 6424 calculation. The CCFL model was removed at the upper tie plate in the TLTA Test 6424 calculation and rerun commencing at 100 s. Liquid in the upper plenum from ECC injection penetrated the bundle and bypass resulting in no rod heatup. Version 11 uses two CCFL modeling options: CCFL calculated using upper tie plate constants and SEO constants. The analyses indicate the current coefficients in the CCFL model restrict the liquid downflow to values which may be too low for the modeled facility. It is suspected the coefficients

are formulated to be over-conservative. However, it is generally agreed that CCFL is highly configuration dependent and the existing coefficients may also be insufficiently general for the many experiment and reactor designs. It should be noted that Version B002, the version used in the small break calculations, has an option to adjust those coefficients.

Water packing and guide tube modeling resulted in code failures and time step reduction.

Pressure oscillations originating from the guide tube TEE resulted in code failures due to water packing in the TEE and required a significant reduction of the time step size to run. To smooth the pressure oscillations and increase the time step size, the side arm of the guide tube TEE was modeled as a cone with the large end next to the primary side and the water packing option turned on. The TLTA Test 6424 calculation was rerun for a short time beginning at 50 s, with the above changes to the model. The pressure oscillations in the guide tube were smoothed and the calculation ran at a reasonable time step. It is recommended that modeling the guide tube TEE as mentioned above be used as applicable.

Conclusions and recommendations relative to the small break calculations using TRAC-BD1 Version B002 are as follows:

Initialization of the small break calculations using the control package contained in TRAC-BD1 Version B002 was much simpler and more cost effective than the manual adjustment method used in Version 11.

TRAC-BD1 Version B002 calculated the general system response of the small break data reasonably well

Break mass flow rates were well calculated by TRAC-BD1 Version B002

TRAC-BD1 Version B002 did not calculate countercurrent flow in the bubbly flow regime with low void fraction.

As a result of this inability to calculate countercurrent flow in the bubbly flow regime, liquid holdup in the upper plenum was observed. This liquid holdup led to a different system mass distribution than indicated by the data. It also prevented core reverse flow, which was essential in bringing subcooled liquid to the rods. This problem is a recognized code deficiency and should be investigated further.

CCFL limitations at the upper tie plate in the TLTA Test 6432 calculation was observed to hold up liquid in the upper plenum.

This problem was similar to the one observed in the DBA calculations. The option of adjusting the CCFL coefficients should be investigated in future assessment activities. Even with the subject holdup, the code calculated sufficient liquid in the bundle to prevent rod heatups.

7. REFERENCES

1. W. J. Letering et al., "BWR Blowdown/Emergency Core Cooling Program Preliminary Facility Description Report for the BD/ECC1A Test Phase," NRC-EPRI-GE Cooperative Research and Development Report GEAP-23592, NRC-2, December 1977.

2. L. S. Lee et al., "BWR Blowdown/Emergency Core Cooling Program-64-Rod Bundle Core Spray Interaction (BD/ECC1A) Final Report-Volume I, Large Break Tests," General Electric Draft of Final Report GEAP-24912-1, EPRI NP-1783, NUREG/CR 2009, DRF EOV-66, March 1981.

3. W. S. Hwang et al., "BWR Small Break Simulation Tests With and Without Degraded ECC Systems BWR Blowdown/Emergency Core Cooling Program," NUREG/CR-2230, EPRI NP-1782, GEAP-24963, January 1982.

4. J. W. Spore, et al., "TRAC-BD1: An Advanced Best Estimate Computer Program for Boiling Water Reactor Loss-of-Coolant Accident Analysis," Vol. 1-3, NUREG/CR-2178, EGG-2109, October 1981.

5. R. J. Dallman, "TRAC-BD1 Calculation and Data Comparison of International Standard Problem 12", EGG-VAAD-5860, May 1982.

6. R. G. Hanson, "TRAC-BD1 Version 12 Assessment Using GPTA Data" EGG-CAAD-5868, May 1982.

7. E. Holcomb, "TRAC-BD1 Version 11 Code Assessment Calculations of General Electric TLTA ECC/NO ECC Tests 6425 and 6426," EGG-CAAD-5857, May, 1982.

TABLE 1. RELATIONSHIP BETWEEN THE PHYSICAL AND MATHEMATICAL COMPONENTS OF THE TRAC-BD1 TLTA DBA MODEL

Physical Component	Mathematical Component[a]
Break lines	TEE 4, TEE 7 (secondary)
Broken loop suction line	TEE 4, BREAK 24
Broken loop drive pump	PUMP 5
Broken loop drive line isolation valve	VALVE 6
Broken loop drive line	TEE 7, BREAK 25, JETP 8 (secondary)
Broken loop jet pump	JETP 8
Intact loop suction line	PIPE 26
Intact loop suction line isolation valve	VALVE 1
Intact loop drive pump	PUMP 2
Intact loop drive line isolation valve	PUMP 2
Intact loop drive line	PUMP 2, JETP 3 (secondary)
Intact loop jet pump	JETP 3
Heated bundle	CHAN20
Guide tube	TEE 21, FILL 27
Feed water line	PIPE 11, FILL 10
Main Steam line	PIPE 18, FILL 19
HPCS line	PIPE 17, FILL 16
LPCS line	PIPE 15, FILL 14
LPCI line	PIPE 13, FILL 12
Vessel and internals	VESSEL 9
Lower plenum	Levels 1-3, Cell 1 and 2
Downcomer	Levels 4-11, Cell 2
Bypass tubes	Levels 4-8, Cell 1
Mixing plenum	Levels 9, Cell 1
Upper plenum	Levels 10-11, Cell 1
Steam separator	Levels 12, Cells 1
Steam dome	Level 13, Cells 1 and 2

a. A TRAC component is made up or one or more cells. The VESSEL component is constructed with axial levels, radial rings and theta sections. One VESSEL cell is defined by one theta section in one radial ring of one axial level.

TABLE 2. RELATIONSHIP BETWEEN THE PHYSICAL AND MATHEMATICAL COMPONENTS OF THE TRAC-BD1 TLTA SMALL BREAK MODEL FOR TEST 6431

Physical Component	Mathematical Component[a]
Break line	TEE 1, (secondary)
Broken loop suction line	TEE 1, BREAK 5
Broken loop drive pump	PUMP 2
Broken loop drive line isolation valve	VALVE 3
Broken loop drive line	VALVE 3, JETP 4 (secondary)
Broken loop jet pump	JETP 4
Intact loop suction line	VALVE 8
Intact loop suction line isolation valve	VALVE 8
Intact loop drive pump	PUMP 9
Intact loop drive line isolation valve	VALVE 10
Intact loop drive line	VALVE 10, JETP 11 (secondary)
Intact loop jet pump	JETP 11
Heated bundle	CHAN 12
Guide tube	TEE 6, FILL 7
Feed water line	PIPE 25, FILL 26
Main Steam line	VALVE 14, BREAK 26
HPCS line	PIPE 19, FILL 20
Vessel and internals	VESSEL 27
Lower plenum	Levels 1-5, Cell 1 and 2
Downcomer	Levels 6-73, Cell 2
Bypass tubes	Levels 6-11, Cell 1
Mixing plenum	Levels 12, Cell 1
Upper plenum	Levels 13, Cell 1
Steam separator	Levels 14-15, Cells 1
Steam dome	Level 16, Cells 1 and 2

a. A TRAC component is made up or one or more cells. The VESSEL component is constructed with axial levels, radial rings and theta sections. One VESSEL cell is defined by one theta section in one radial ring of one axial level.

TABLE 3. RELATIONSHIP BETWEEN THE PHYSICAL AND MATHEMATICAL COMPONENTS OF THE TRAC-BD1 TLTA SMALL BREAK MODEL FOR TEST 6432

Physical Component	Mathematical Component[a]
Break line	TEE 28 (primary-break 1; secondary-break 2), BREAK 5, BREAK 29
Broken loop suction line	TEE 1,
Broken loop drive pump	PUMP 2
Broken loop drive line isolation valve	VALVE 3
Broken loop drive line	VALVE 3, JETP 4 (secondary)
Broken loop jet pump	JETP 4
Intact loop suction line	VALVE 8
Intact loop suction line isolation valve	VALVE 8
Intact loop drive pump	PUMP 9
Intact loop drive line isolation valve	VALVE 10
Intact loop drive line	VALVE 10, JETP 11 (secondary)
Intact loop jet pump	JETP 11
Heated bundle	CHAN 12
Guide tube	TEE 6, FILL 7
Feed water line	PIPE 25, FILL 26
Main Steam line	VALVE 14, BREAK 15
LPCS line	PIPE 21, FILL 22
LPCS line	PIPE 23, FILL 24
ADS line	PIPE 17, FILL 18
Vessel and internals	VESSEL 27
Lower plenum	Levels 1-5, Cell 1 and 2
Downcomer	Levels 6-13, Cell 2
Bypass tubes	Levels 6-11, Cell 1
Mixing plenum	Levels 12, Cell 1
Upper plenum	Levels 13, Cell 1
Steam separator	Levels 14-15, Cells 1
Steam dome	Level 16, Cells 1 and 2

a. A TRAC component is made up or one or more cells. The VESSEL component is constructed with axial levels, radial rings and theta sections. One VESSEL cell is defined by one theta section in one radial ring of one axial level.

TABLE 4. COMPARISON OF INITIAL CONDITIONS OF TLTA TEST 6423 AND TRAC-BD1 STEADY STATE CALCULATION

	Test	TRAC-BD1
Bundle Power (MW)	6.46 ± 0.03	6.46
Steam dome pressure (MPa)	7.1499 ± 0.0345	7.149
Lower plenum pressure (MPa)	7.34 ± 0.0345	7.363
Lower plenum temperature (K)	547.09 ± 4	550.07
Initial water level (m)	3.1242 ± 0.015	3.15
Feed water temperature (K)	294.26 ± 2	294.2
Bundle inlet to outlet DP (MPa)	0.1103 ± 0.0138	0.1003
Steam flow (Kg/s)	3.1749 ± 0.45	3.428
Feed water flow (Kg/s)	0.4536 ± 0.14	0.4536
Drive pump #1 flow (Kg/s)	3.6738 ± 0.45	3.773
Drive pump #2 flow (Kg/s)	3.7645 ± 0.45	3.950
Jet pump #1 flow (Kg/s)	7.7104 ± 0.91	7.244
Jet pump #2 flow (Kg/s)	8.6176 ± 0.91	7.875
Bundle inlet flow (Kg/s)	14.9673 ± 2.27	14.81
ECC fluid temperature (K)	366.48 ± 8.33	366

TABLE 5. COMPARISON OF INITIAL CONDITIONS OF TLTA TEST 6424 AND TRAC-BD1 STEADY STATE CALCULATION

	Test	TRAC-BD1
Bundle Power (MW)	6.49 ± 0.03	6.49
Steam dome pressure (MPa)	7.2809 ± 0.0345	7.28056
Lower plenum pressure (MPa)	7.4532 ± 0.0345	7.508
Lower plenum temperature (K)	548.15 ± 4	552.17
Initial water level (m)	3.1496 ± 0.15	3.15
Feed water temperature (K)	296.47 ± 2	296.4
Bundle inlet to outlet DP (MPa)	0.1379 ± 0.0138	0.10762
Steam flow (Kg/s)	3.6284 ± 0.45	3.534
Feed water flow (Kg/s)	0.4989 ± 0.14	0.4987
Drive pump #1 flow (Kg/s)	3.1749 ± 0.45	3.652
Drive pump #2 flow (Kg/s)	3.6284 ± 0.45	4.076
Jet pump #1 flow (Kg/s)	6.3498 ± 0.91	6.225
Jet pump #2 flow (Kg/s)	8.164 ± 0.91	7.642
Bundle inlet flow (Kg/s)	13.153 ± 2.27	13.79
ECC fluid temperature (K)	322.04 ± 8.33	322

TABLE 6. COMPARISON OF INITIAL CONDITIONS OF TLTA TEST 6431 AND TRAC-BD1 STEADY STATE CALCULATION WITH CONTROL PACKAGE

	Test	TRAC-BD1
Steam dome pressure (MPa)	7.1774 ± 0.034	7.1781
Downcomer liquid level (m)	7.19 ± 0.08	7.19
Bundle flow (Kg/s)	19.50 ± 2.27	19.29
Bypass flow (Kg/s)	1.13 ± 0.23	1.37
Steam flow (Kg/s)	0.91 ± 0.23	0.88
Bundle inlet subcooling (K)	8.89 ± 2.22	7.70
Downcomer temperature (K)		
Above F. W. Sparger	562.04 ± 2.22	560.9
Below F. W. Sparger	554.82 ± 22	554.6
Bundle Power (MW)	2.06672	2.06672

TABLE 7. COMPARISON OF INITIAL CONDITIONS OF TLTA TEST 6432 AND TRAC-BD1 STEADY STATE CALCULATION WITH CONTROL PACKAGE

	Test	TRAC-BD1
Steam dome pressure (MPa)	7.2257 ± 0.034	7.2258
Downcomer liquid level (m)	7.19 ± 0.08	7.19
Bundle flow (Kg/s)	15.42 ± 2.27	15.26
Bypass flow (Kg/s)	0.95 ± 0.23	1.14
Steam flow (Kg/s)	0.73 ± 0.23	0.84
Bundle inlet subcooling (K)	11.67 ± 2.22	9.00
Downcomer temperature (K)		
Above F. W. Sparger	562.59 ± 2.22	561.1
Below F. W. Sparger	550.93 ± 2.22	553.7
Bundle Power (MW)	1.97315	1.97315

TABLE 8. QUANTITATIVE PARAMETERS OF THE TRAC-BD1 TLTA 6423 CALCULATION COMPARED WITH DATA

	Data	TRAC-BD1
Peak clad temperature (K)		
Pump coastdown	822.0	950.0
Dryout	794.0	840.0
Time to peak clad temperature (s)		
Pump coastdown	5.0	15.0
Dryout	200.0	182.0
Time to inital rod dryout (s)		
Pump coastdown	1.7	0.5
Dryout	30.0	40.0
Time to core quench (s)	230.0	230.0
Time to jet pump suction uncovery (s)	7.6	8.3
Time to recirculation line uncovery (s)	11.0	10.3
Time to jet pump exit plane uncovery (s)	39.3	35.0
Time to ECCS activation (s)		
HPCS	27.0	27.0
LPCS	65.0	53.0
LPCI	72.0	56.0
Minimum downcomer differential pressure (MPa)	1.50×10^{-3}	1.13×10^{-4}
Time to minimum downcomer differential pressure (s)	82.0	124.0
Lower plenum bulk flashing (s)	15.0	15.0

TABLE 9. QUANTITATIVE PARAMETERS OF THE TRAC-BD1 TLTA 6424 CALCULATION COMPARED WITH DATA

	Data	TRAC-BD1
Peak clad temperature (K)		
Pump coastdown	844.0	875.0
Dryout	704.0	806.0
Time to peak clad temperature (s)		
Pump coastdown	10.0	12.0
Dryout	80.0	80.0
Time to inital rod dryout (s)		
Pump coastdown	1.3	0.7
Dryout	35.0	40.0
Time to core quench (s)	150.0	160.0
Time to jet pump suction uncovery (s)	7.2	6.4
Time to recirculation line uncovery (s)	10.8	8.5
Time to jet pump exit plane uncovery (s)	34.0	32.0
Time to ECCS activation (s)		
HPCS	27.0	28.0
LPCS	63.0	52.0
LPCI	71.0	56.0
Minimum downcomer differential pressure (MPa)	1.40×10^{-3}	1.10×10^{-4}
Time to minimum downcomer differential pressure (s)	76.0	150.0
Lower plenum bulk flashing (s)	14.0	14.0

TABLE 10. SEQUENCE OF EVENTS FOR TESTS 6423 AND 6424

	6423	6424
Blowdown valves open (s)	0.0	0.0
Bundle power decay initiated (s)	0.5	0.5
Feed water flow stops (s)	0.5	0.5
Steamline valve completely closed (s)	11.5	8.0
Loop 1 isolated (s)	20.0	20.0

TABLE 11. QUANTITATIVE PARAMETERS OF THE TRAC-BD1 TLTA 6431 CALCULATION COMPARED WITH DATA

	Data	Calculation
Pump coastdown initiation (s)		
Pump 1	0.0	0.0
Pump 2	4.0	4.0
Feedwater closure initiation (s)	0.0	0.0
Break open (s)	-0.9	0.0
Steam line valve closed (s)	17.5[a]	17.5
HPCS Activation (s)	26.8	26.8
Loop isolation valve closure (s)		
Intact loop	19.6	19.6
Broken loop	18.5	18.5

a. Based upon steam line flow data.

TABLE 12. QUANTITATIVE PARAMETERS OF THE TRAC-BD1 TLTA 6432 CALCULATION COMPARED WITH DATA

	Data	Calculation
Pump coastdown initiation (s)		
Pump 1	0.0	0.0
Pump 2	4.0	4.0
Feedwater closure initiation (s)	0.1	0.0
Break open (s)	-0.9	0.0
Line 1	138.0	138.0
Line 2	138 ≤t≤ 286	138 ≤t≤ 286
ADS open (s)	286.0	286.0
MSIV closure (s)	165.0	165.0
Loop isolation valve closure (s)		
Intact loop	20.0	20.0
Broken loop	18.2	18.2
ECCS activation (s)		
LPCS	433.0	438.0
LPCI	458.0	458.0

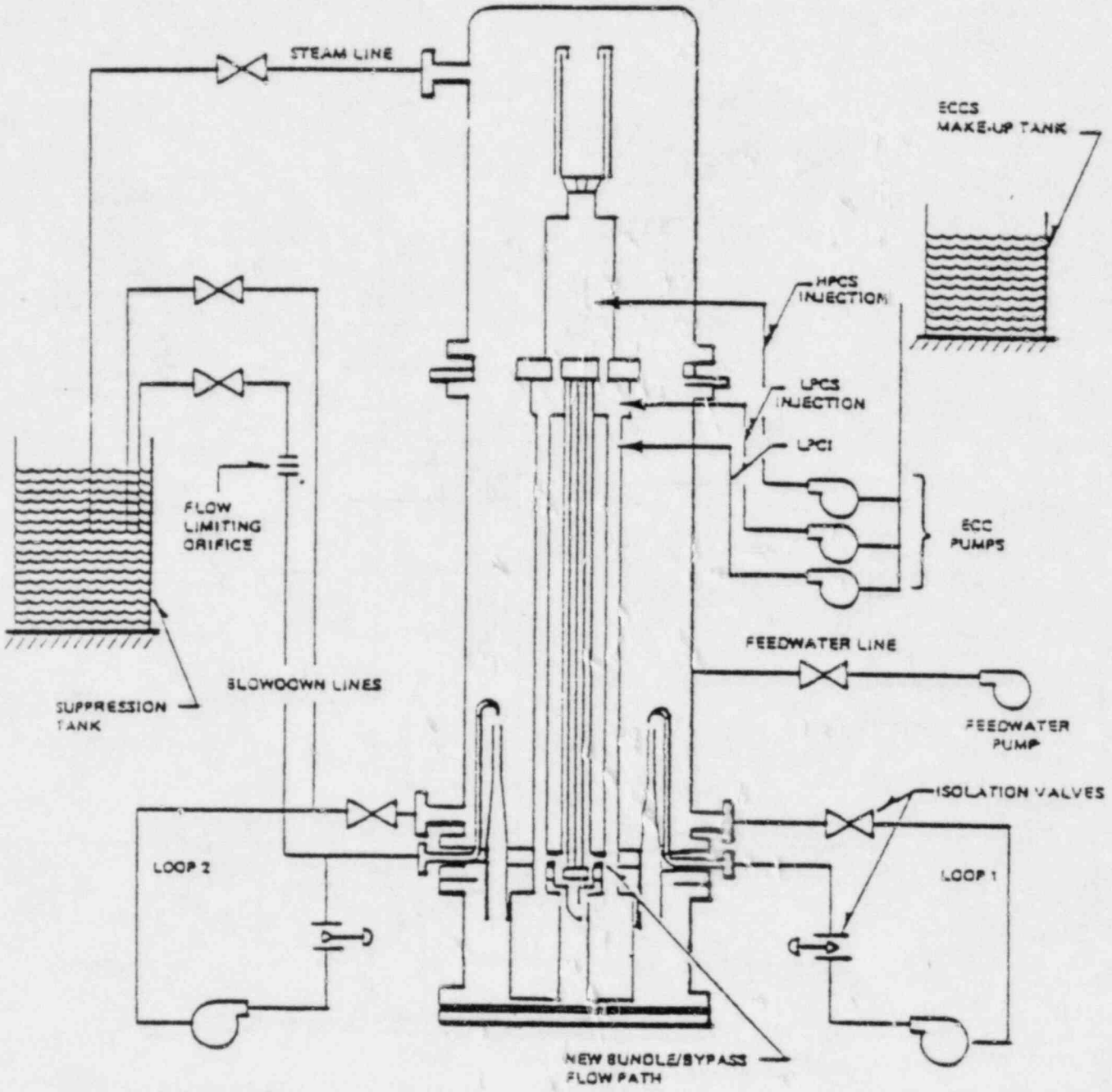

Figure 1. Two-Loop test apparatus configuration 5A (TLTA-5A) with emergency core cooling systems for DBA experiments.

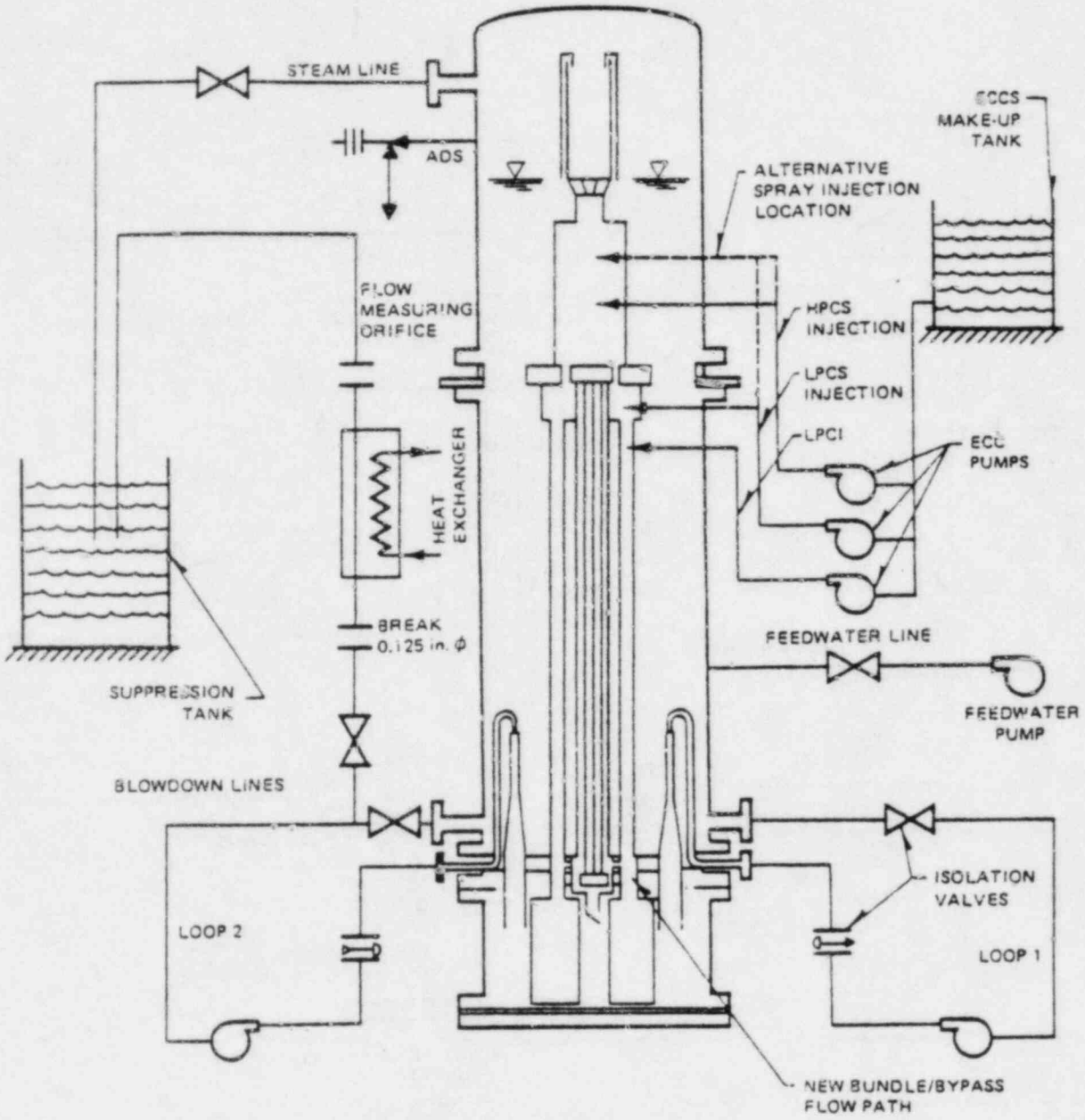

Figure 2. Two-Loop test apparatus configuration 5B (TLTA-5B)
(Small break test I configuration for test 6431).

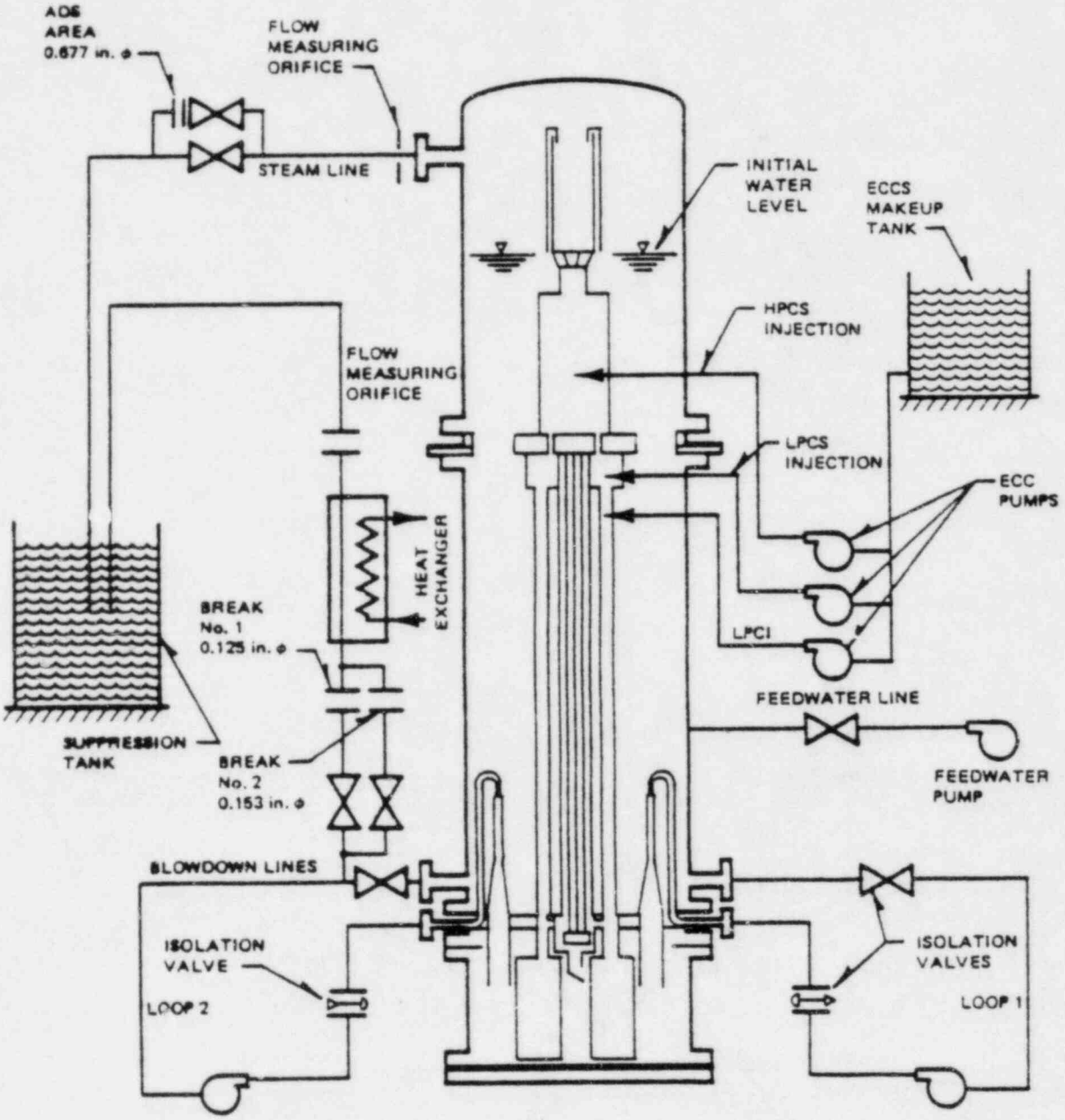

Figure 3. Two loop test apparatus configurations 5C (TLTA-5C)
(Small break test II configuration for test 6432).

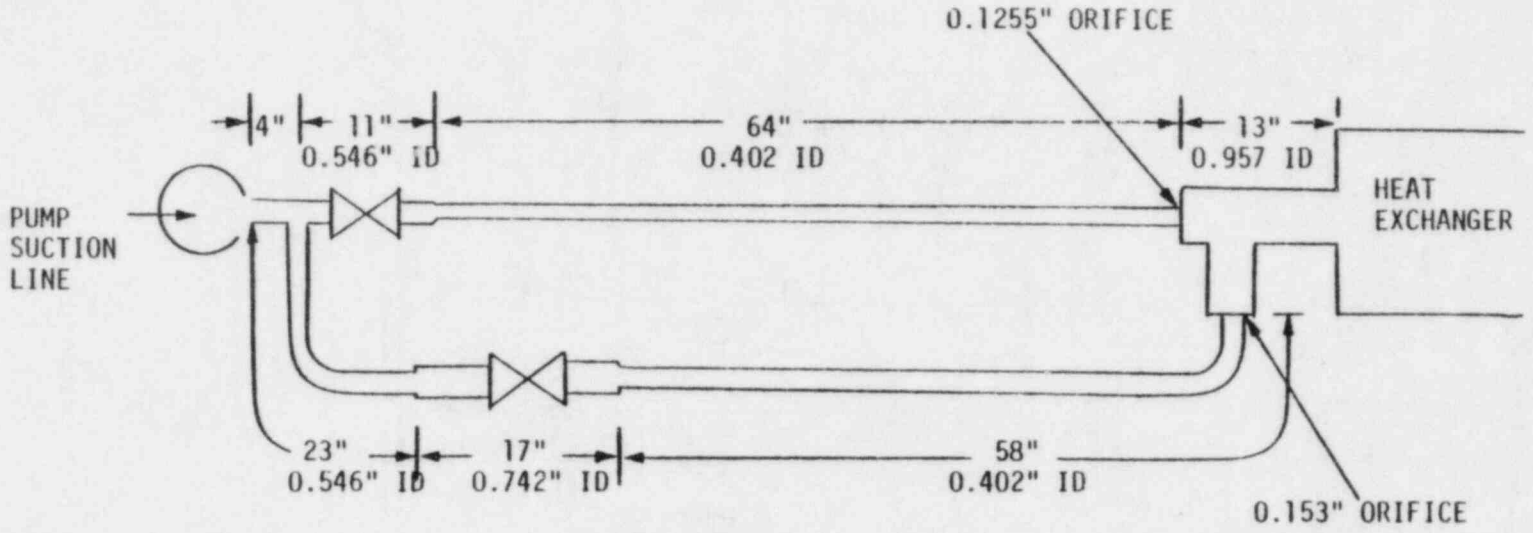

Figure 4. Small break piping for small test number 2 (test 6432).

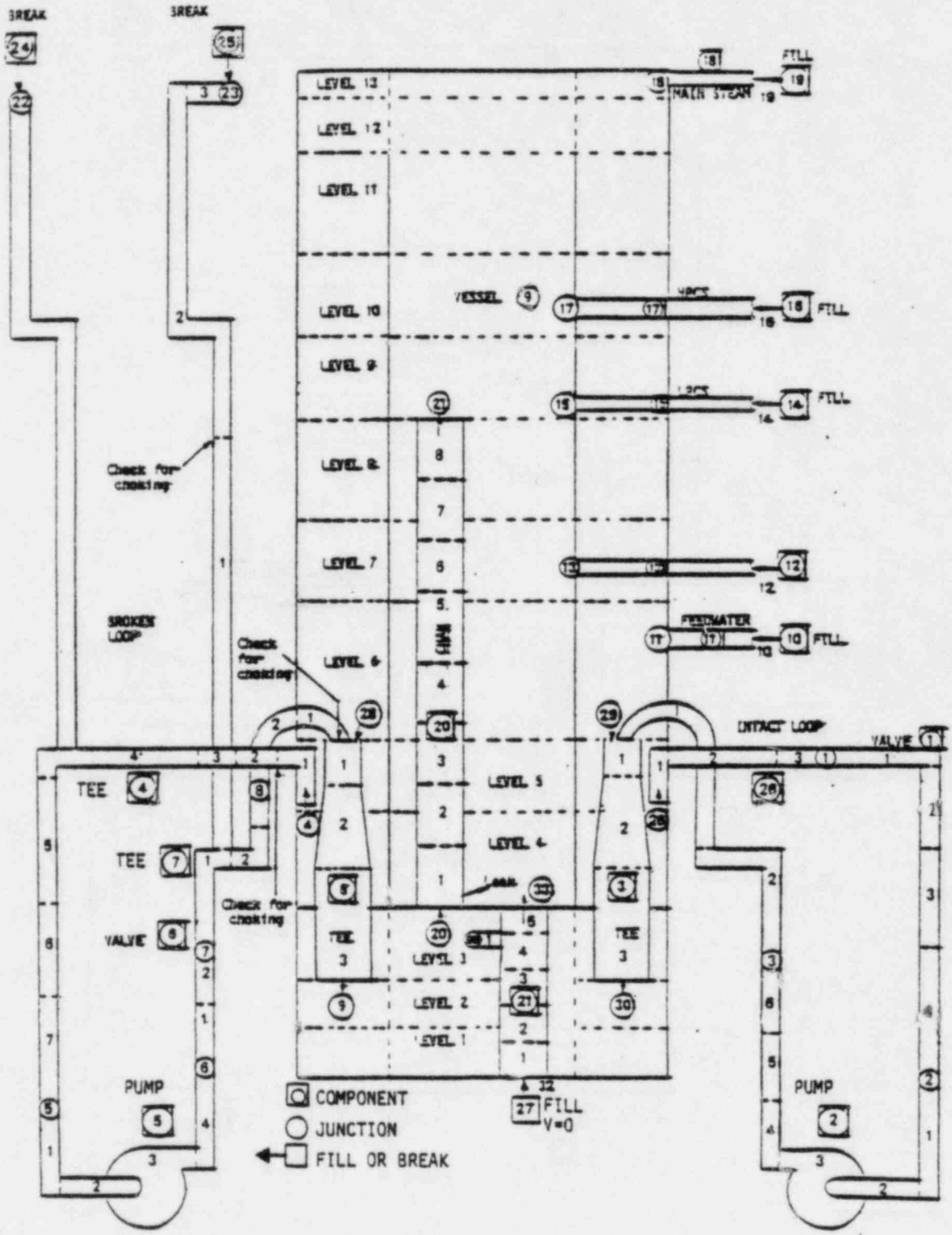

Figure 5. TRAC-BD1 representation of the TLTA-5 facility for DBA calculations.

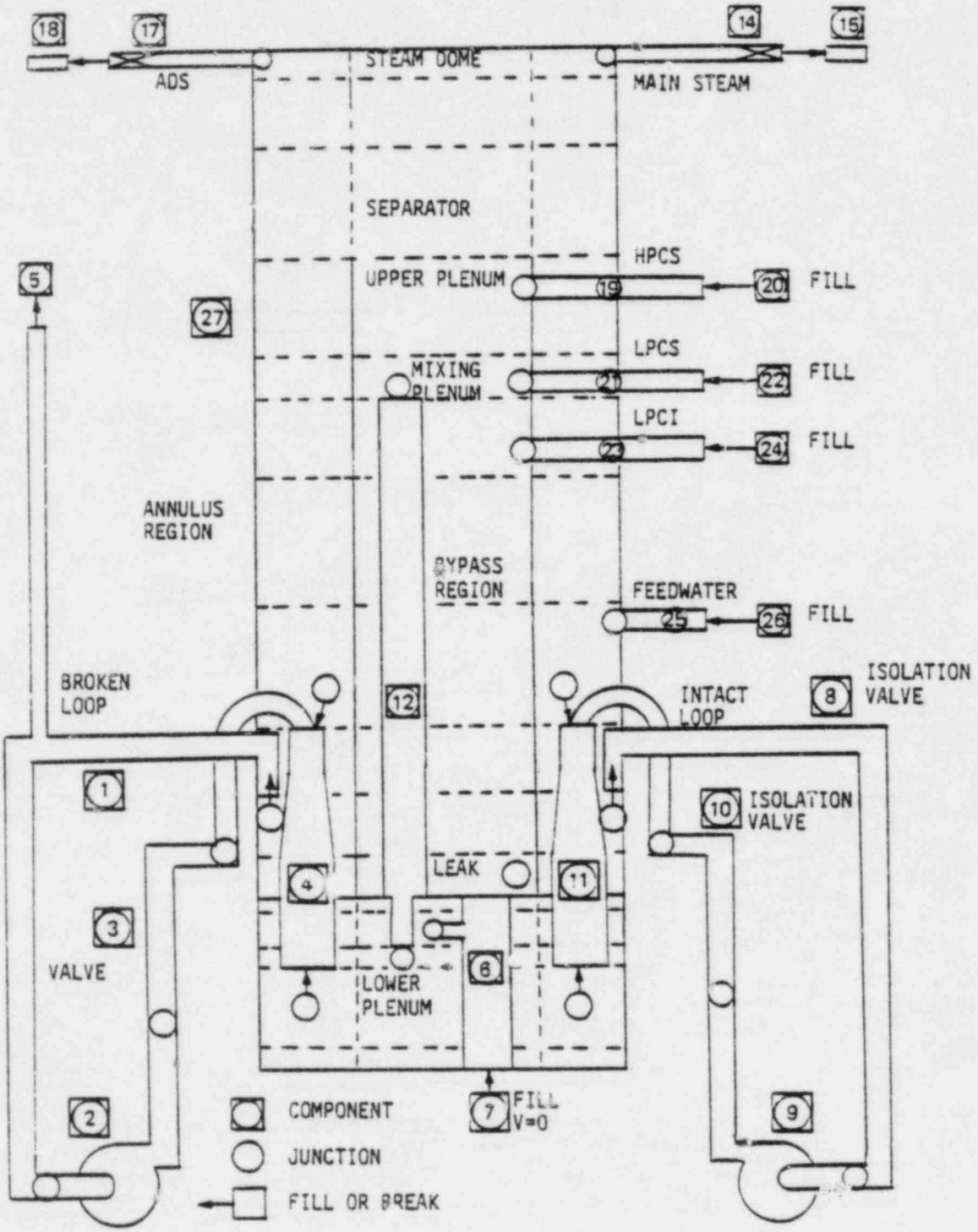

Figure 6. TRAC-BD1 representation of the TLTA-5 facility for the small break calculation of Test 6431.

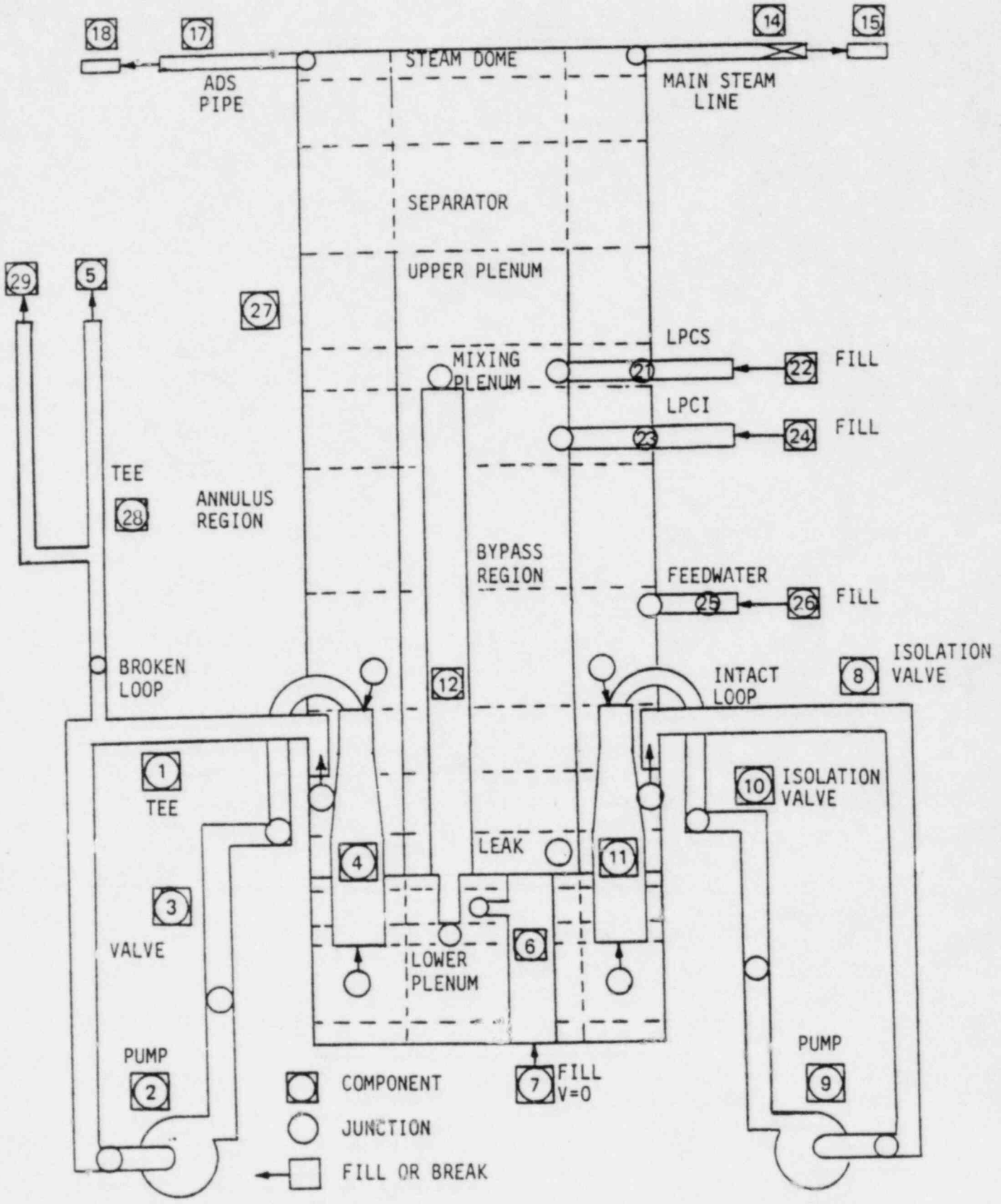

Figure 7. TRAC-BD1 representation of the TLTA-5 facility for the small break calculation of test 6432.

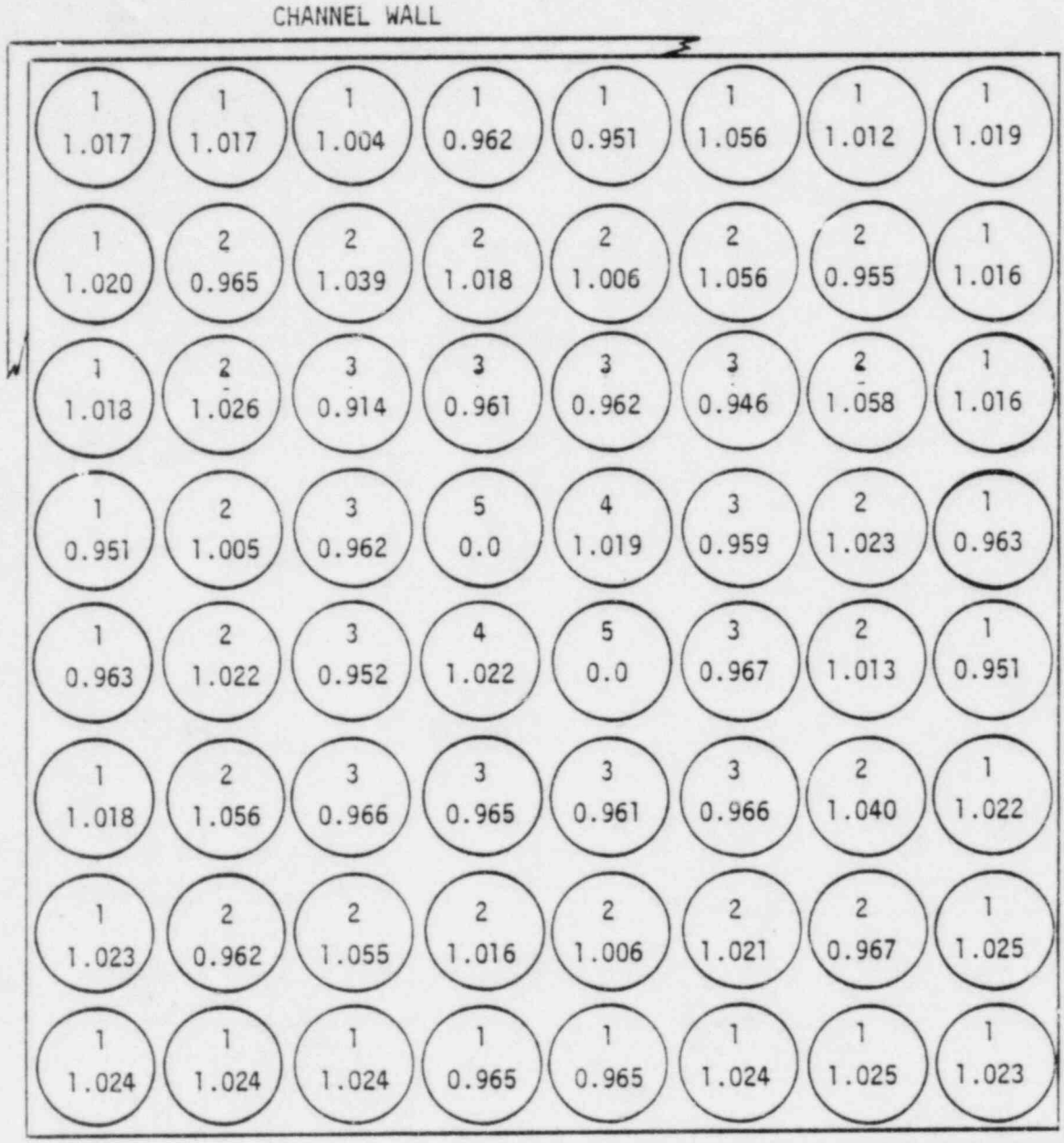

ROD GROUP #	# RODS IN GROUP	AVERAGE PEAKING FACTOR
1	28	1.0366
2	20	1.0491
3	12	0.9909
4	2	1.0541
5	2	0.0000

Figure 8. Rod group configuration for TRAC-BD1 TLTA small break calculations.

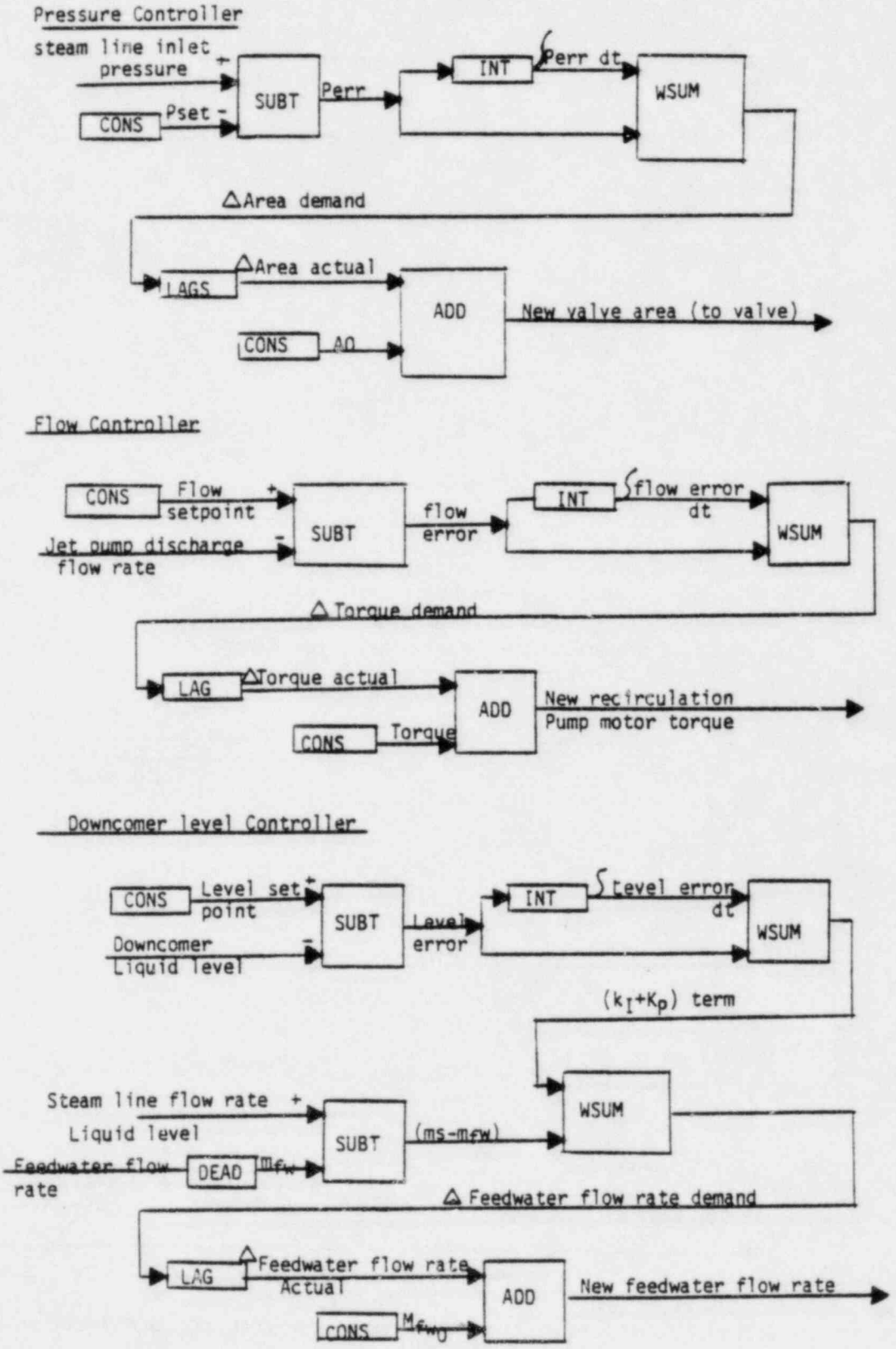

Figure 9. Control system schematic for the TRAC-BD1 TLTA small break steady state calculations.

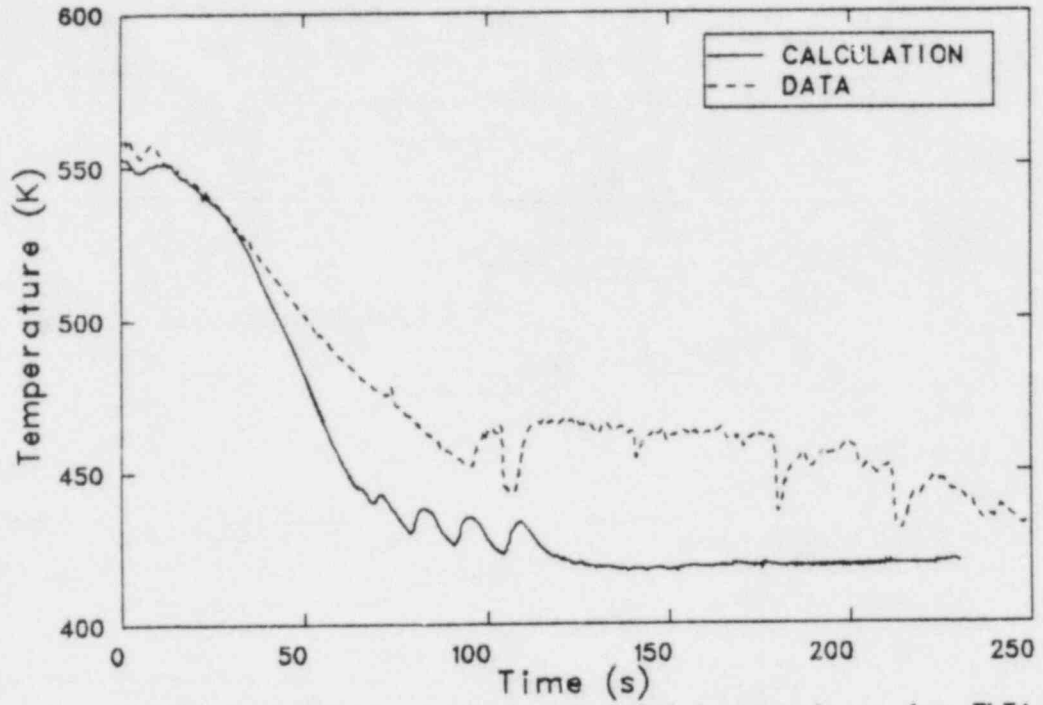

Figure 10. Comparison of the break inlet temperatures for TLTA Test 6423 at downcomer level 5.

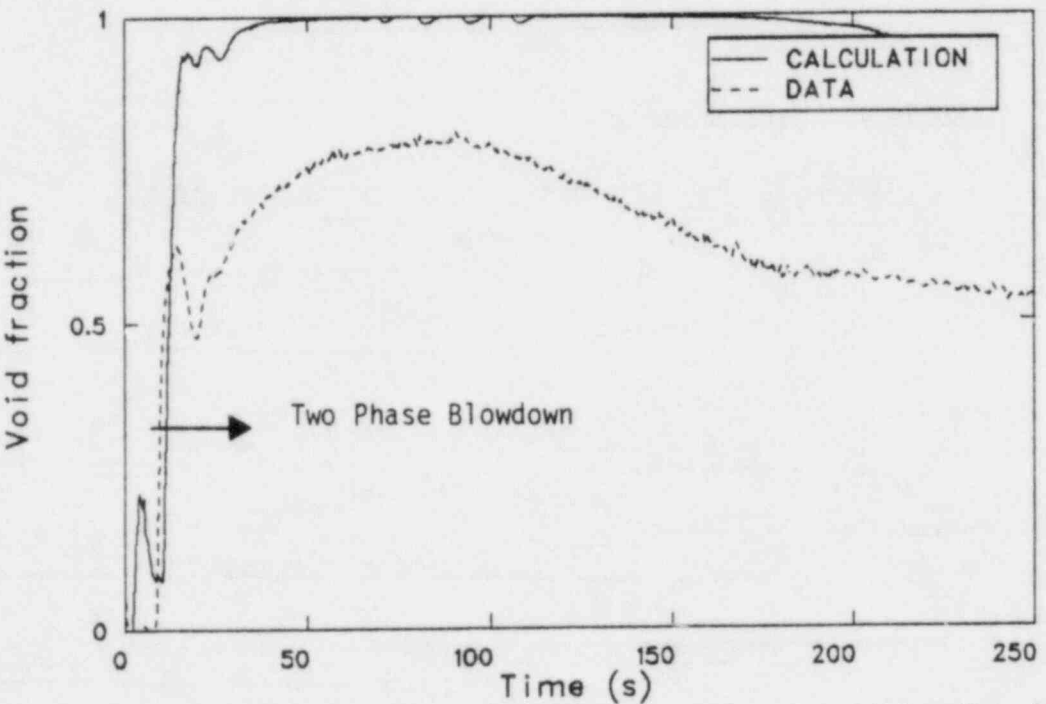

Figure 11. Comparison of suction line break inlet void fraction for Test 6423.

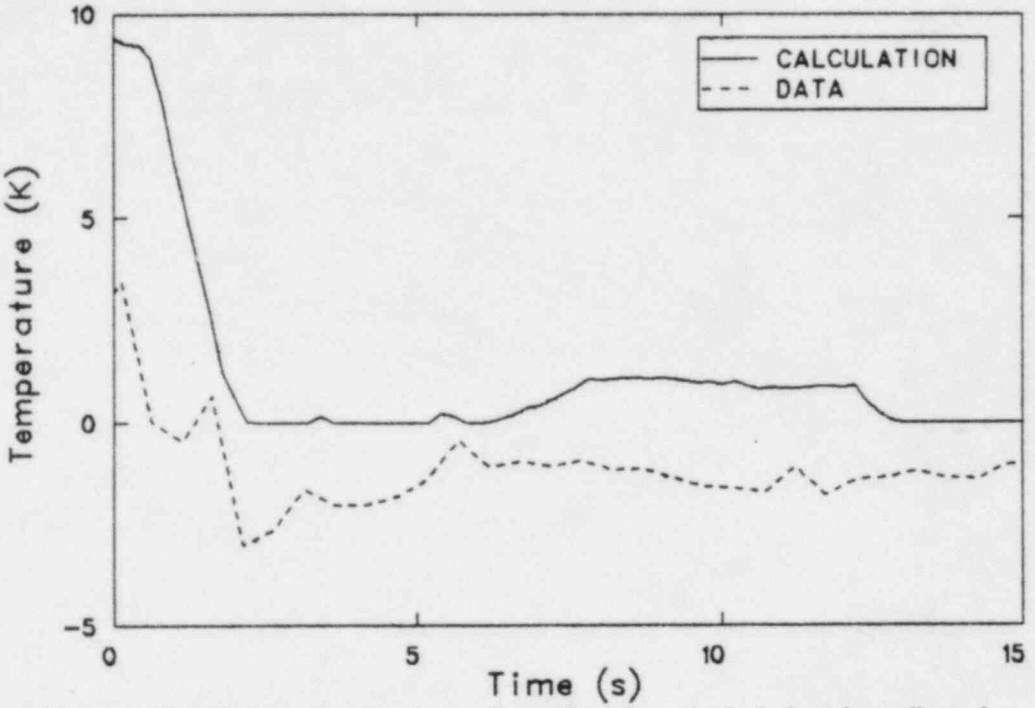

Figure 12. Comparison of suction line break inlet subcooling for Test 6423.

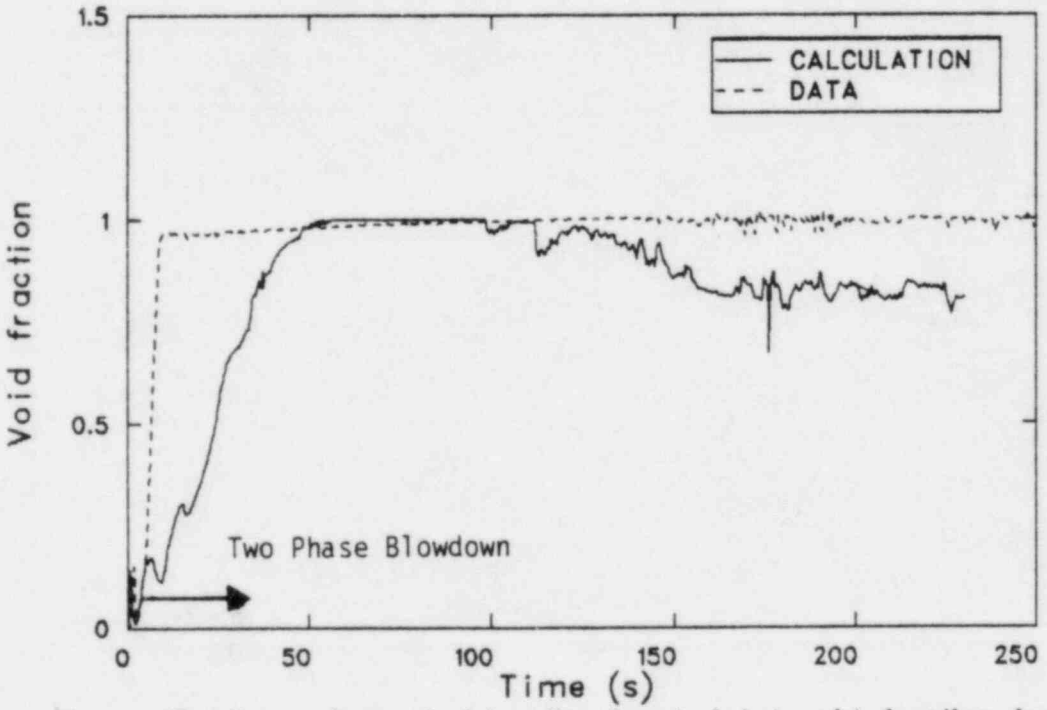

Figure 13. Comparison of drive line break inlet void fraction for Test 6423.

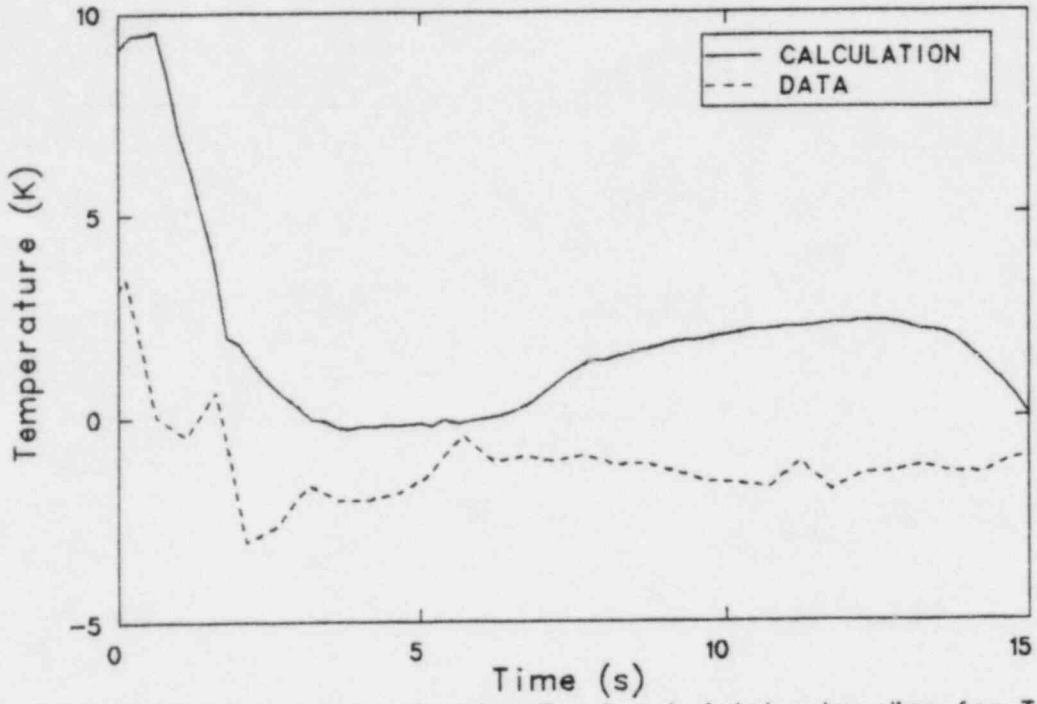

Figure 14. Comparison of drive line break inlet subcooling for Test 6423.

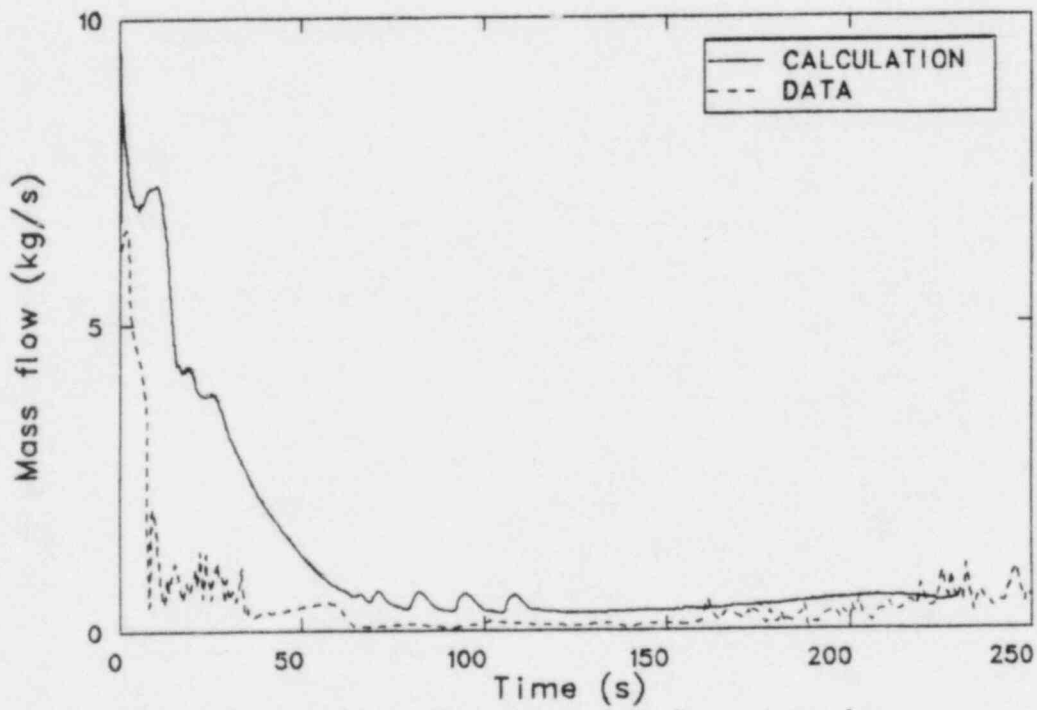

Figure 15. TLTA 6423 suction line break flow comparison

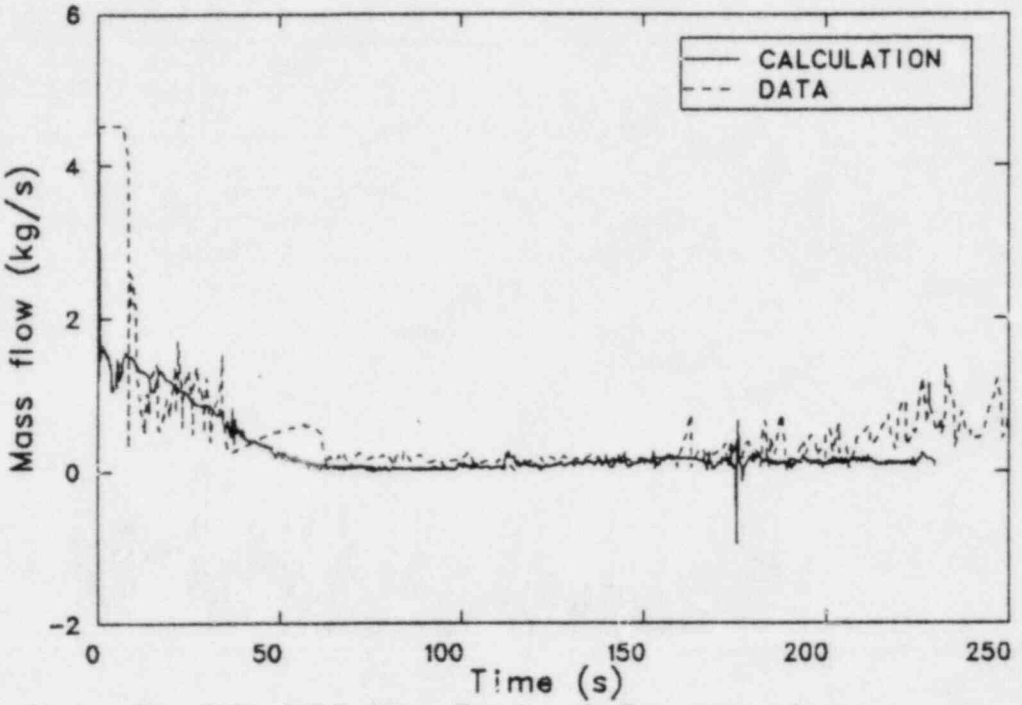

Figure 16. TLTA 6423 drive line break flow comparison.

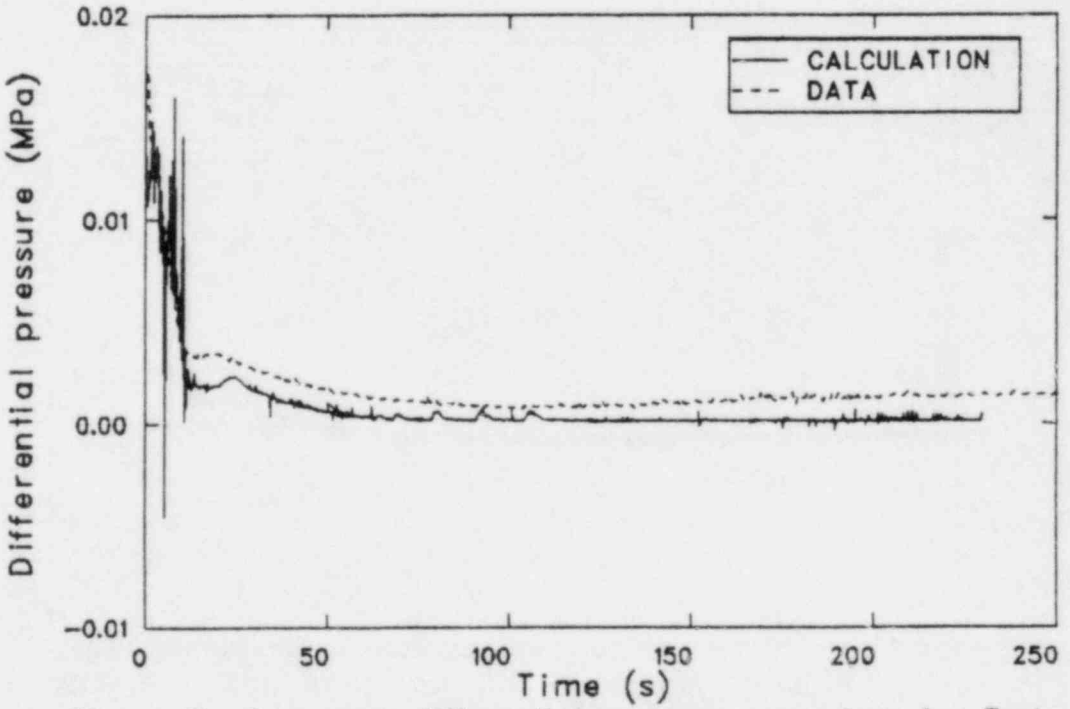

Figure 17. Downcomer differential pressure comparison for Test 6423.

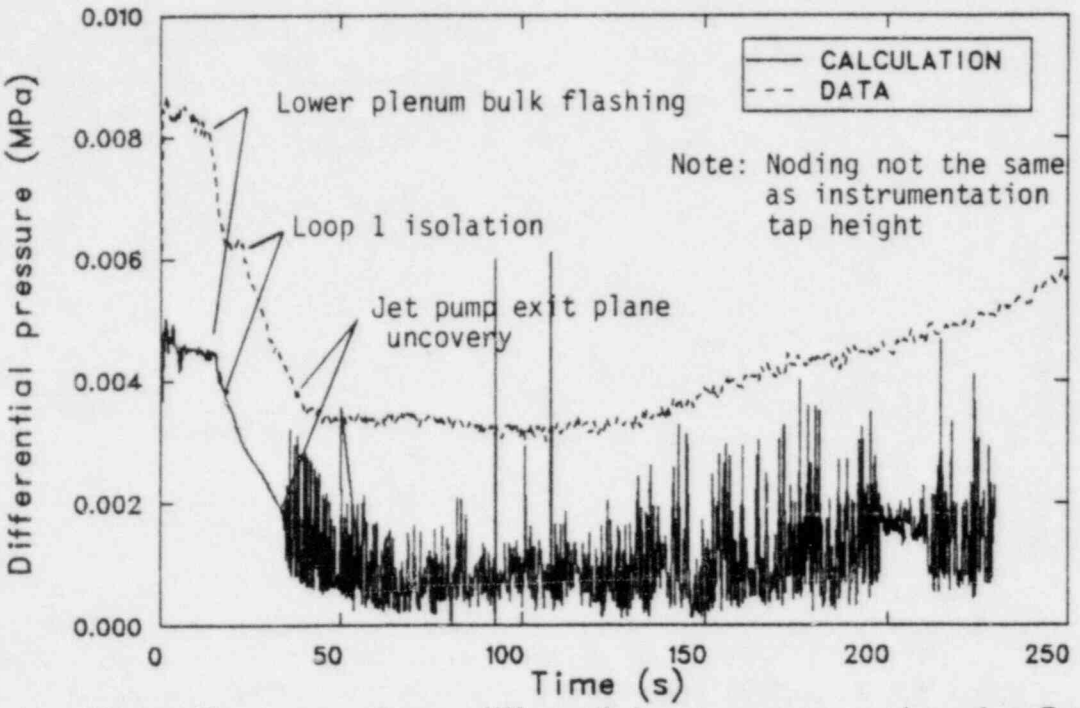

Figure 18. Lower plenum differential pressure comparison for Test 6423.

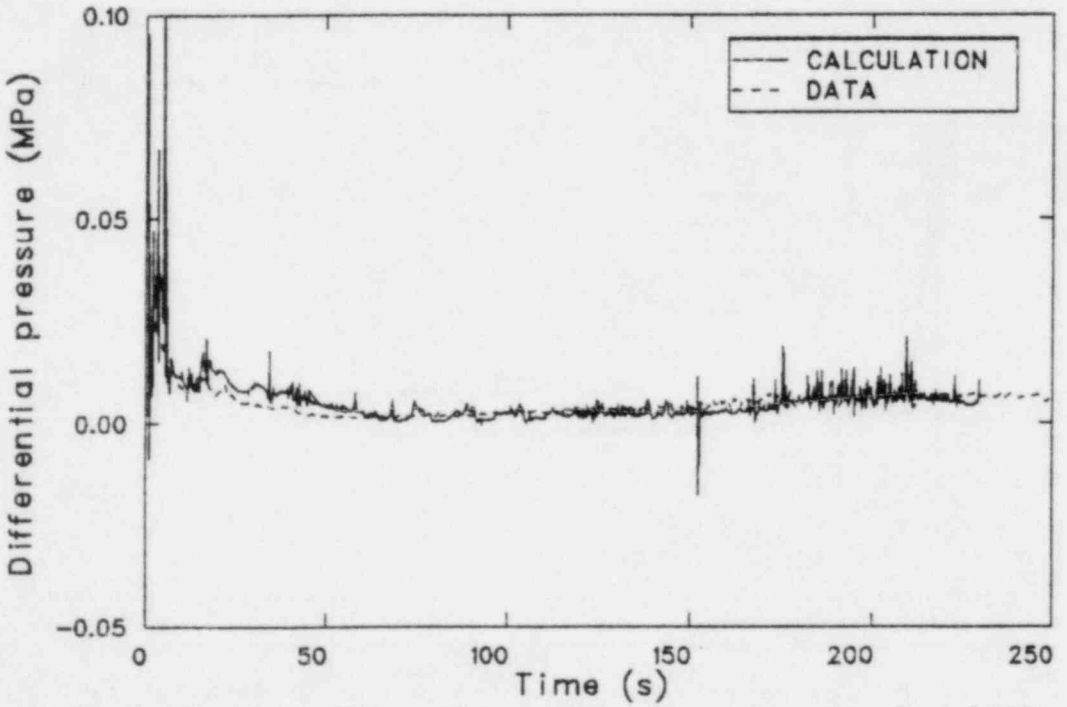

Figure 19. Core differential pressure comparison for Test 6423.

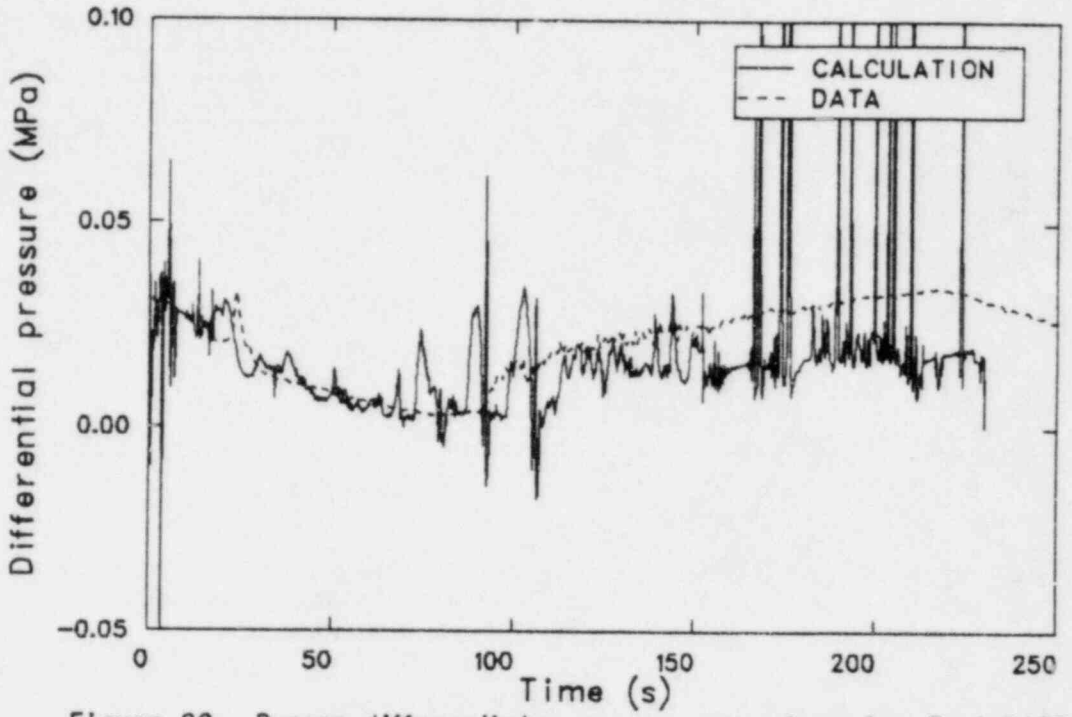

Figure 20. Bypass differential pressure comparison for Test 6423.

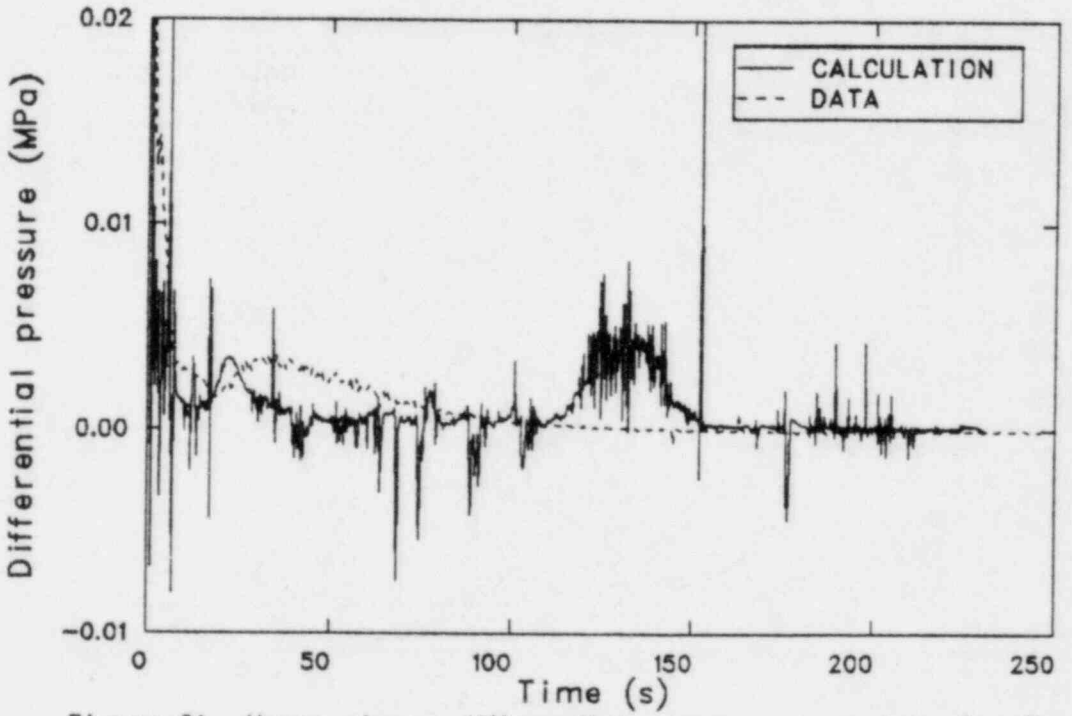

Figure 21. Upper plenum differential pressure comparison for Test 6423.

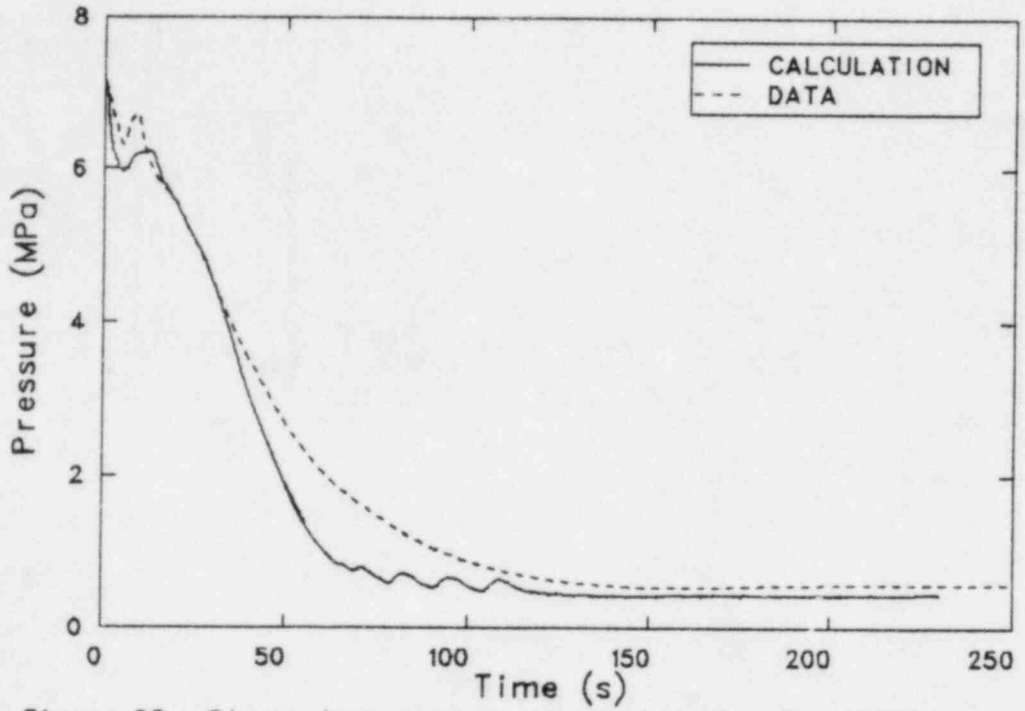

Figure 22. Steam dome pressure comparison for Test 6423.

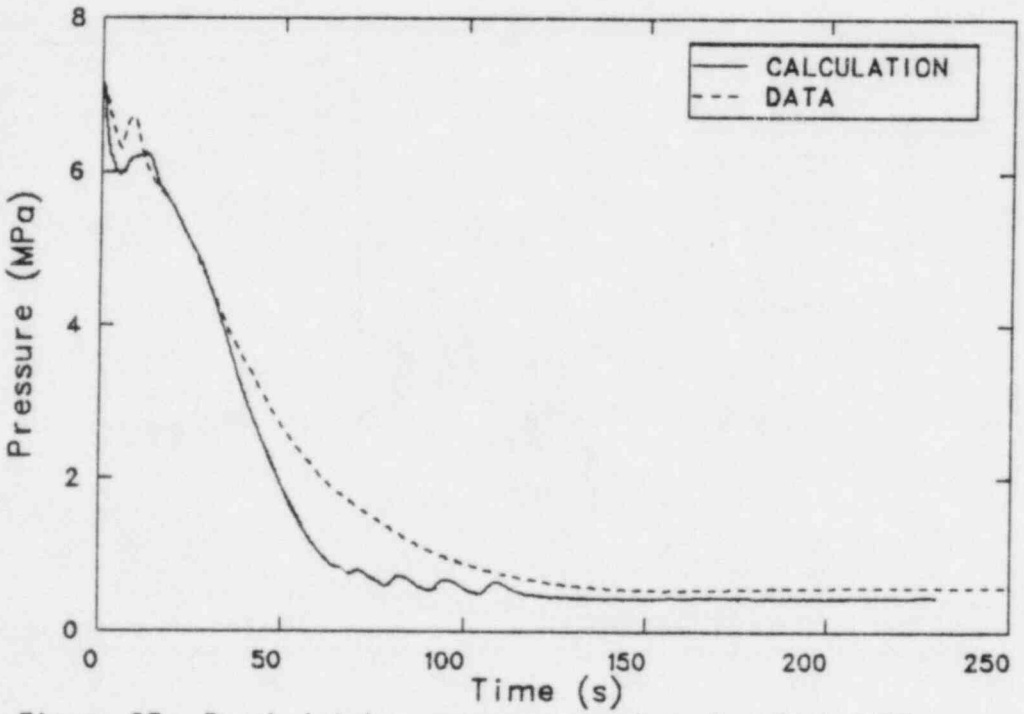

Figure 23. Break inlet pressure comparison for Test 6423.

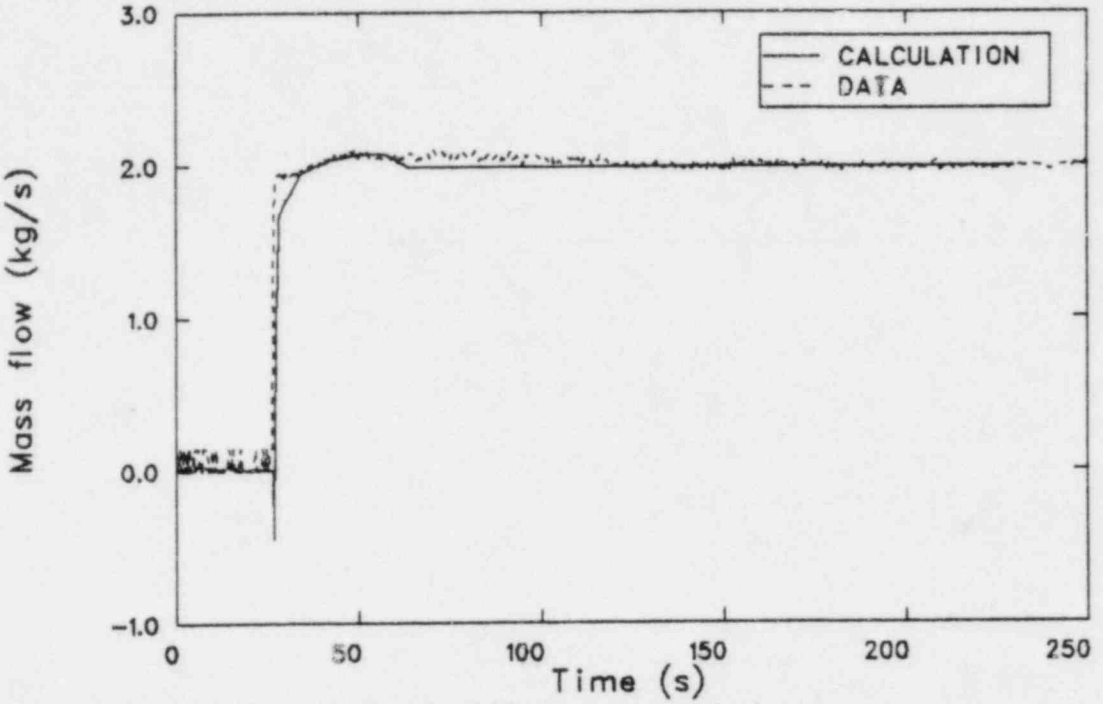

Figure 24. TLTA 6423 HPCS flow comparison.

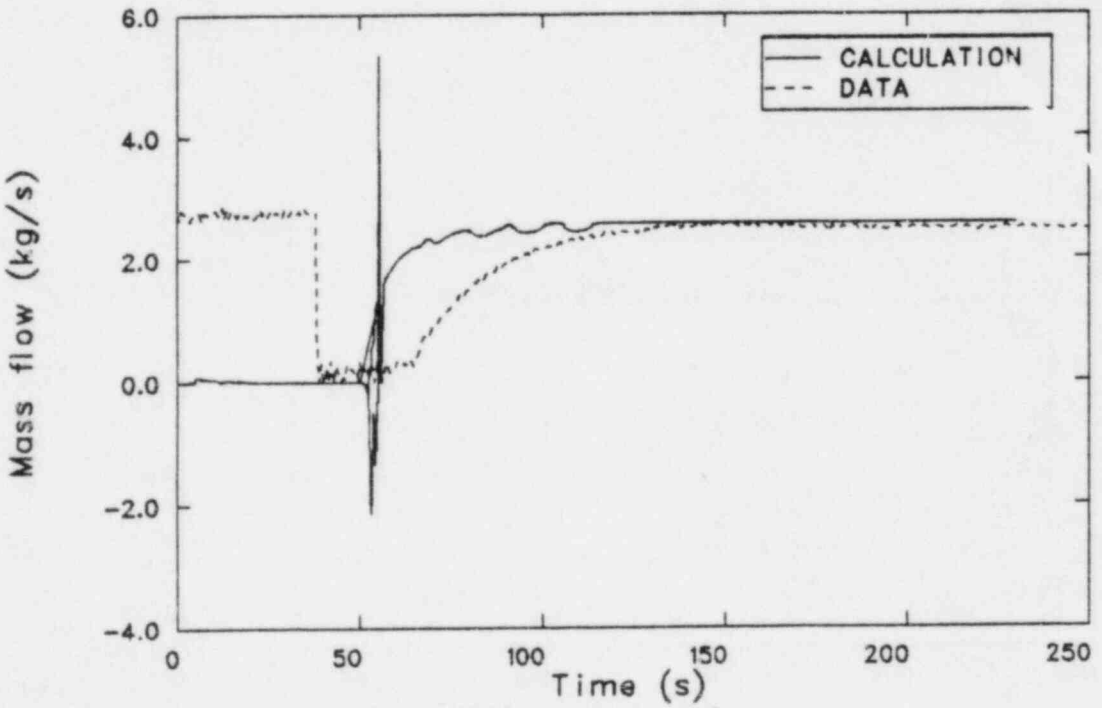

Figure 25. TLTA 6423 LPCS flow comparison.

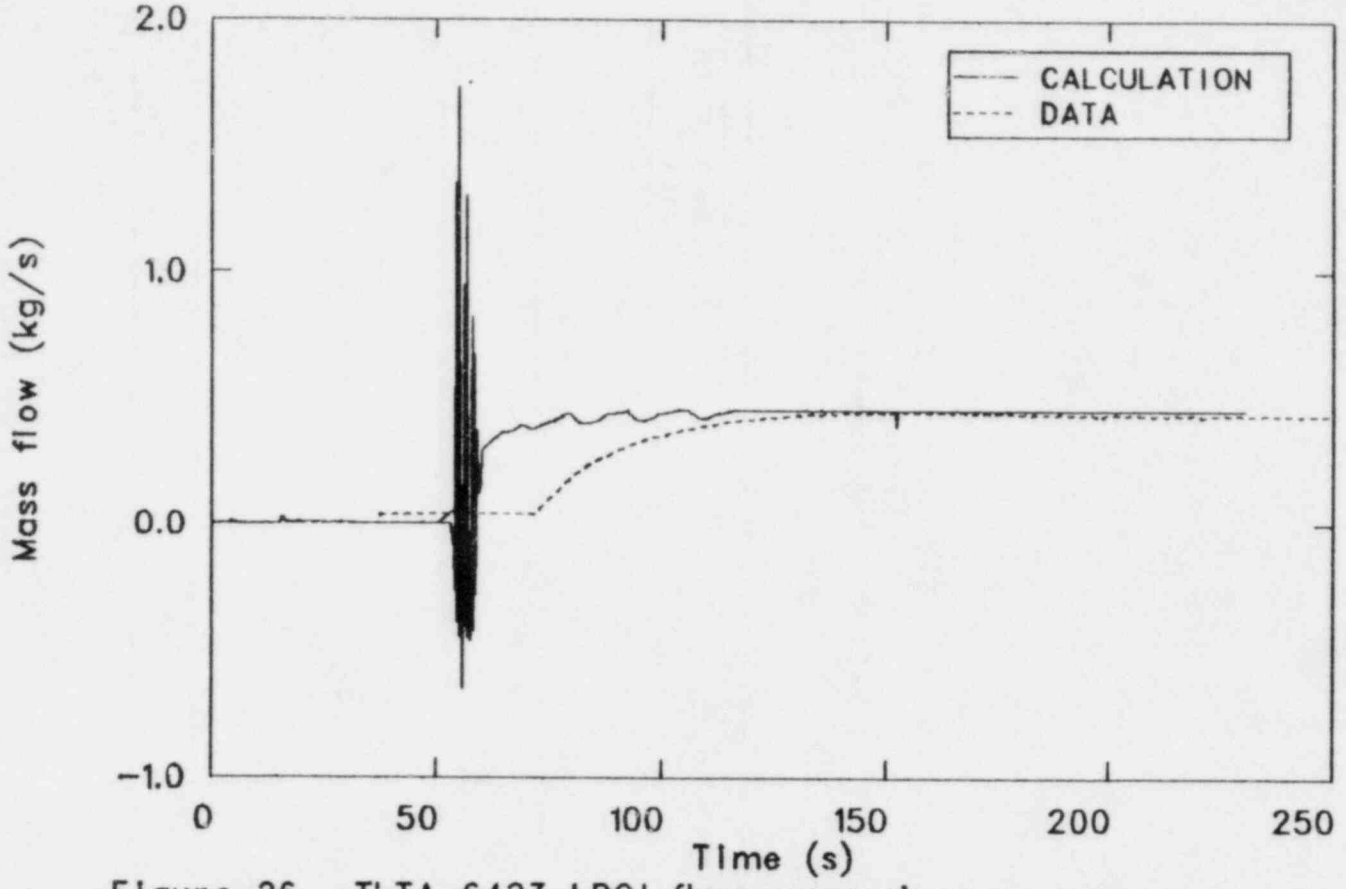

Figure 26. TLTA 6423 LPCI flow comparison.

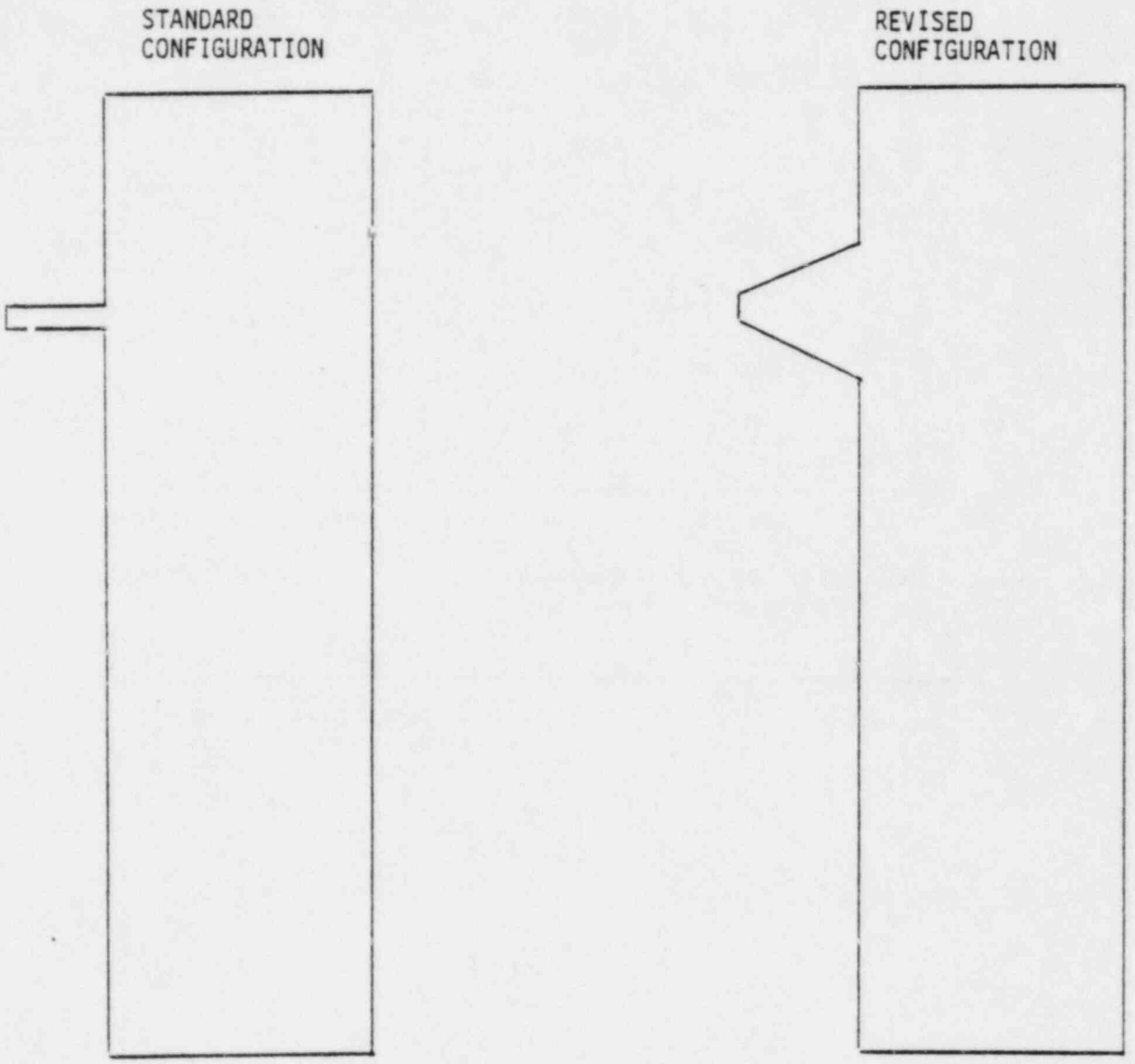

Figure 27. Guide tube models used in the DBA assessment calculations.

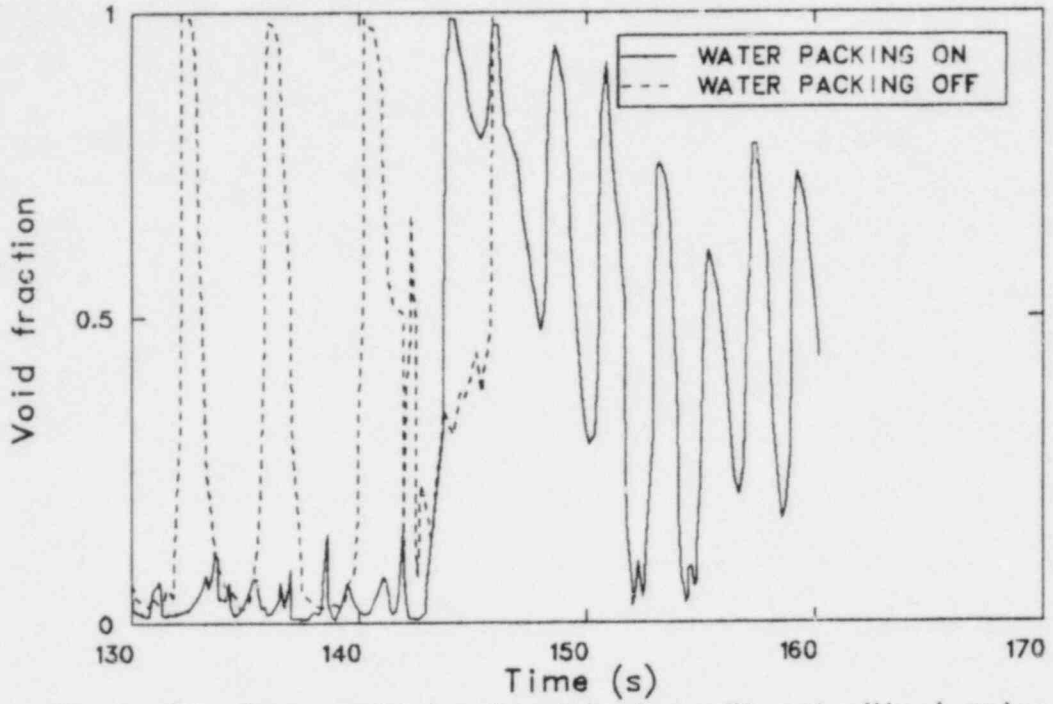

Figure 28. Bypass void fraction behavior with and without water packing option (Level 7).

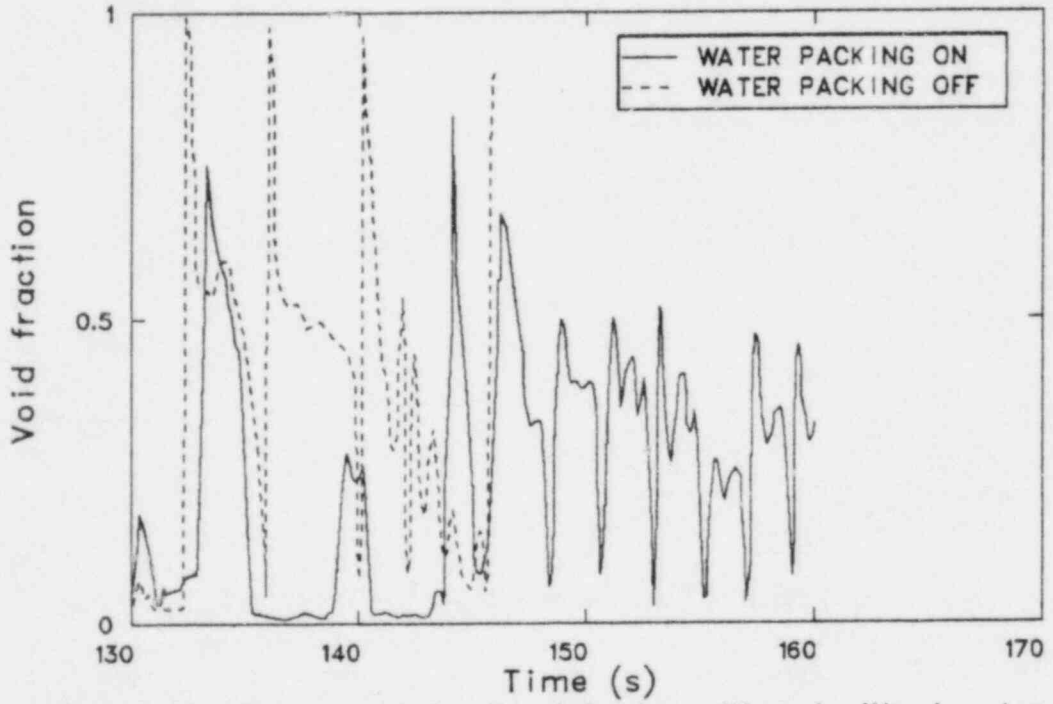

Figure 29. Bypass void fraction behavior with and without water packing option (Level 6).

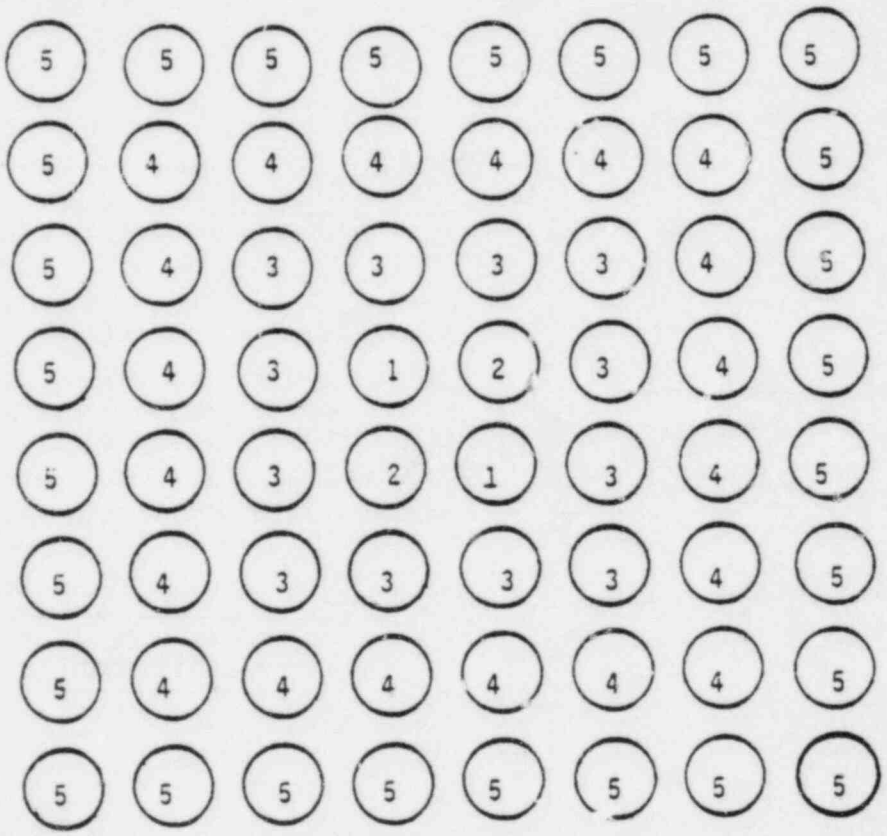

Group 1 - simulated water rods
Group 2-5 - heater rods

Figure 30. TRAC-BD1 computational rod grouping for the TLTA DBA calculations.

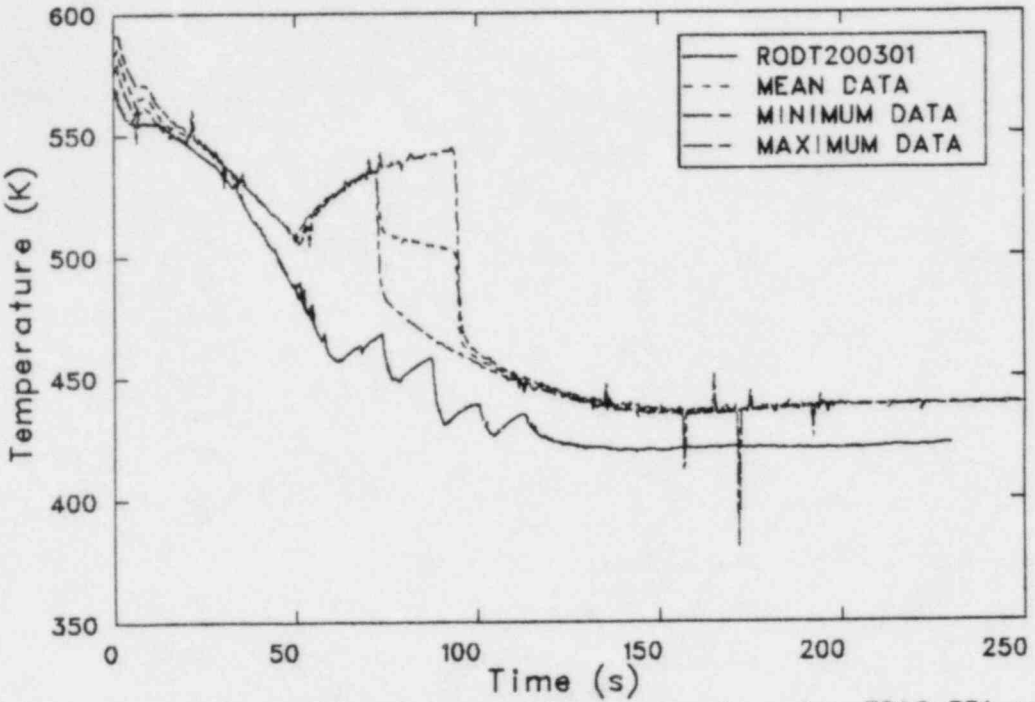

Figure 31. Test 6423 rod temperature comparison for TRAC-BD1 rod group 2 level 1 and rod thermocouple data at .25 m from bottom of heated length (BHL).

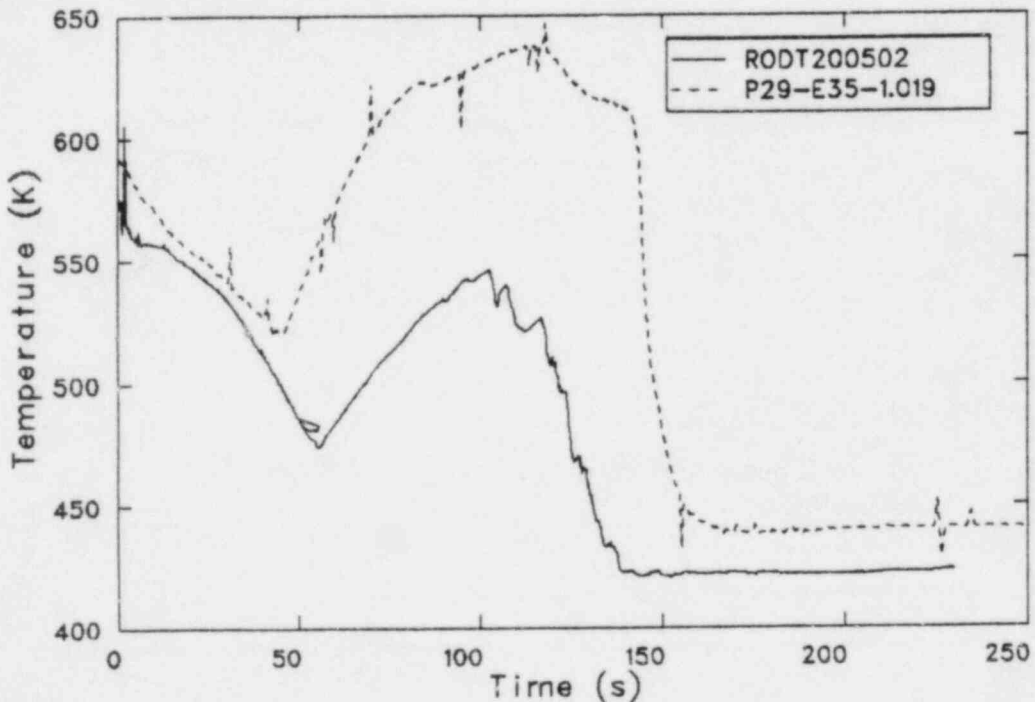

Figure 32. Test 6423 rod temperature comparison for TRAC-BD1 rod group 3 level 2 and rod thermocouple data at .89 m from BHL.

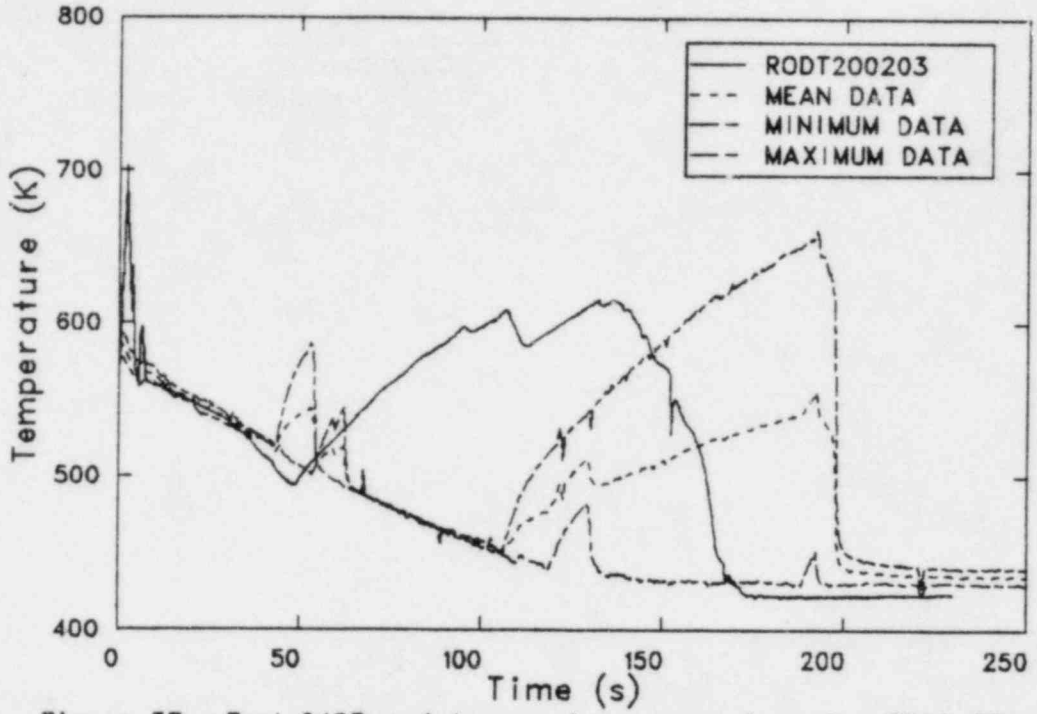

Figure 33. Test 6423 rod temperature comparison for TRAC-BD1 rod group 1 level 3 and rod thermocouple data at 1.27 m from BHL.

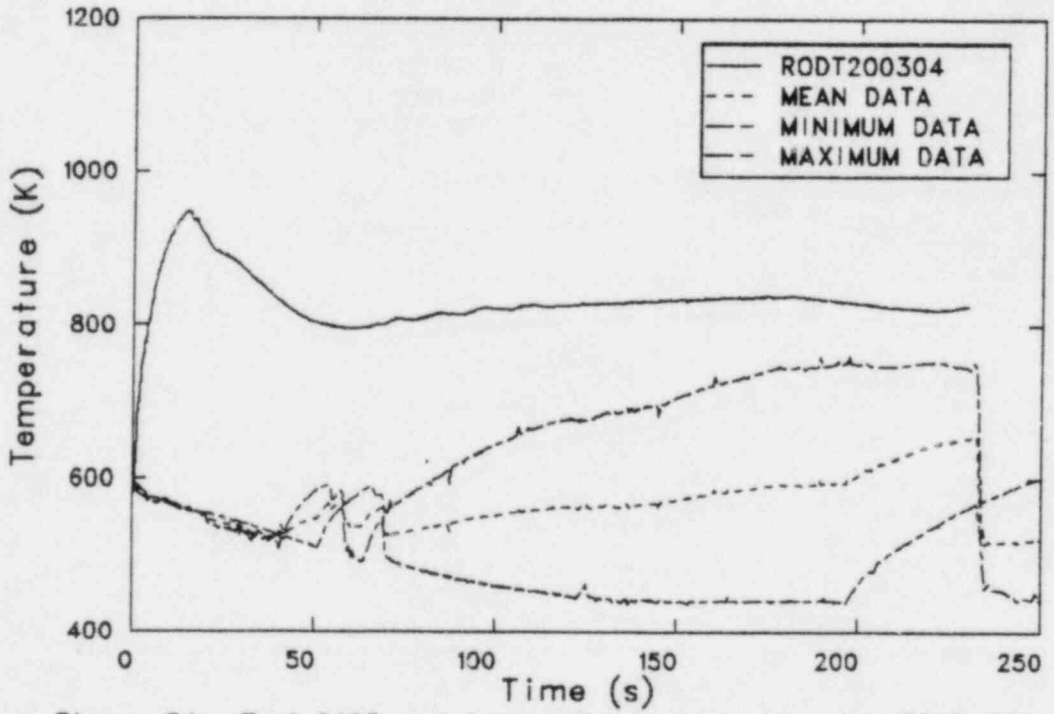

Figure 34. Test 6423 rod temperature comparison for TRAC-BD1 rod group 2 level 4 and rod thermocouple data at 2.00 m from BHL.

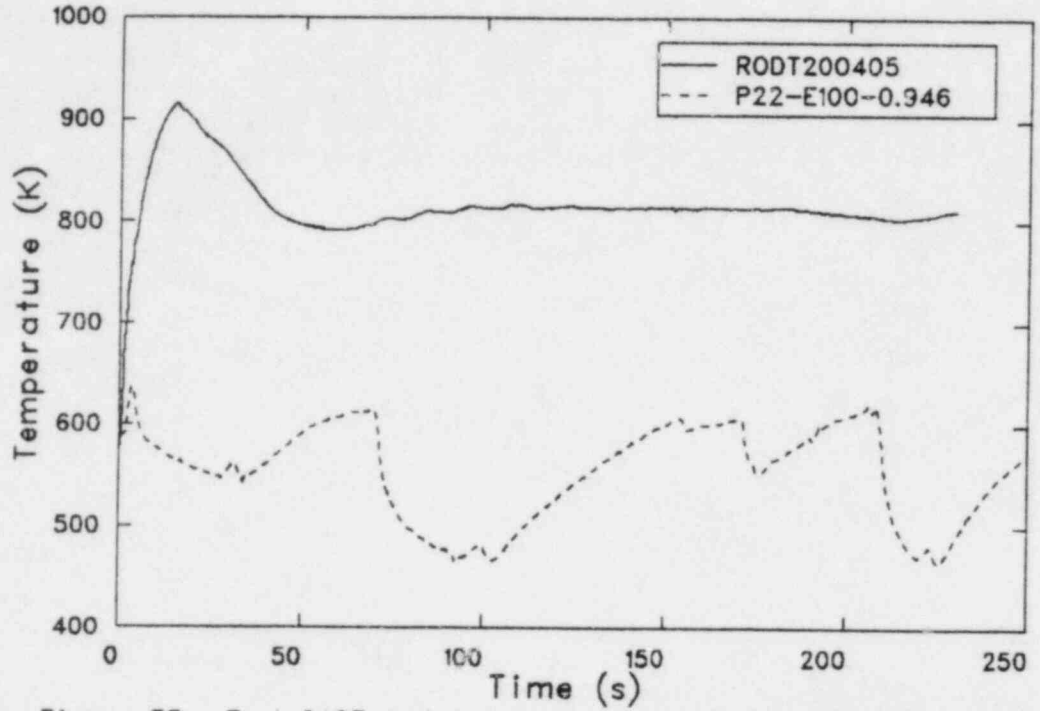

Figure 35. Test 6423 rod temperature comparison for TRAC-BD1 rod group 3 level 5 and rod thermocouple data at 2.54 m from BHL.

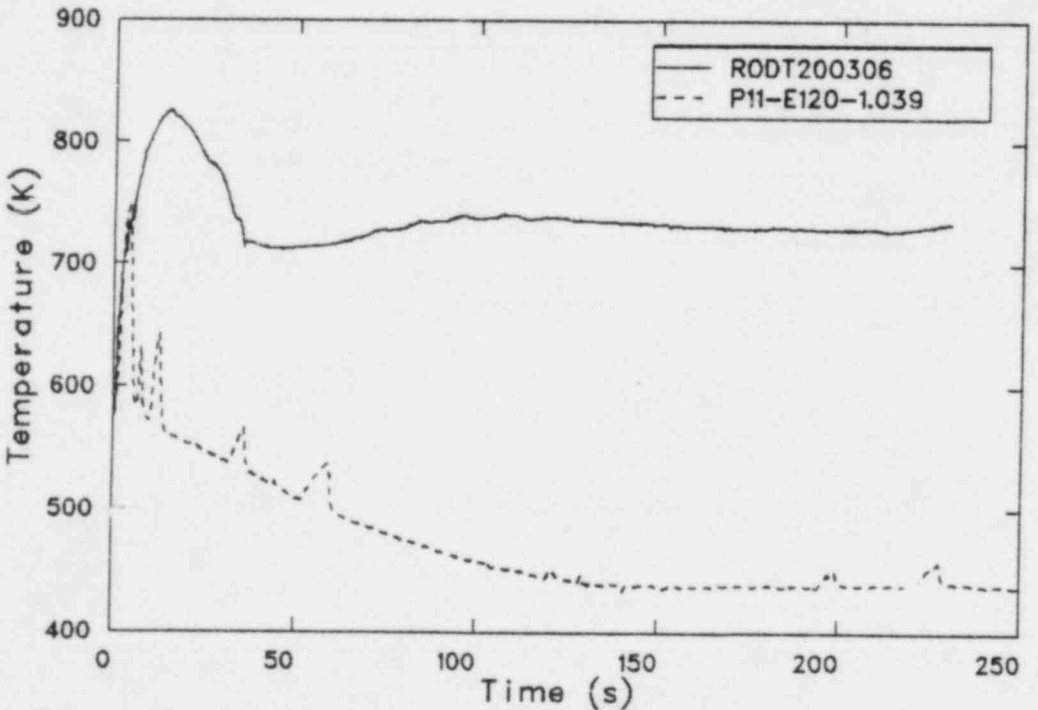

Figure 36. Test 6423 rod temperature comparison for TRAC-BD1 rod group 2 level 6 and rod thermocouple data at 3.05 m from BHL.

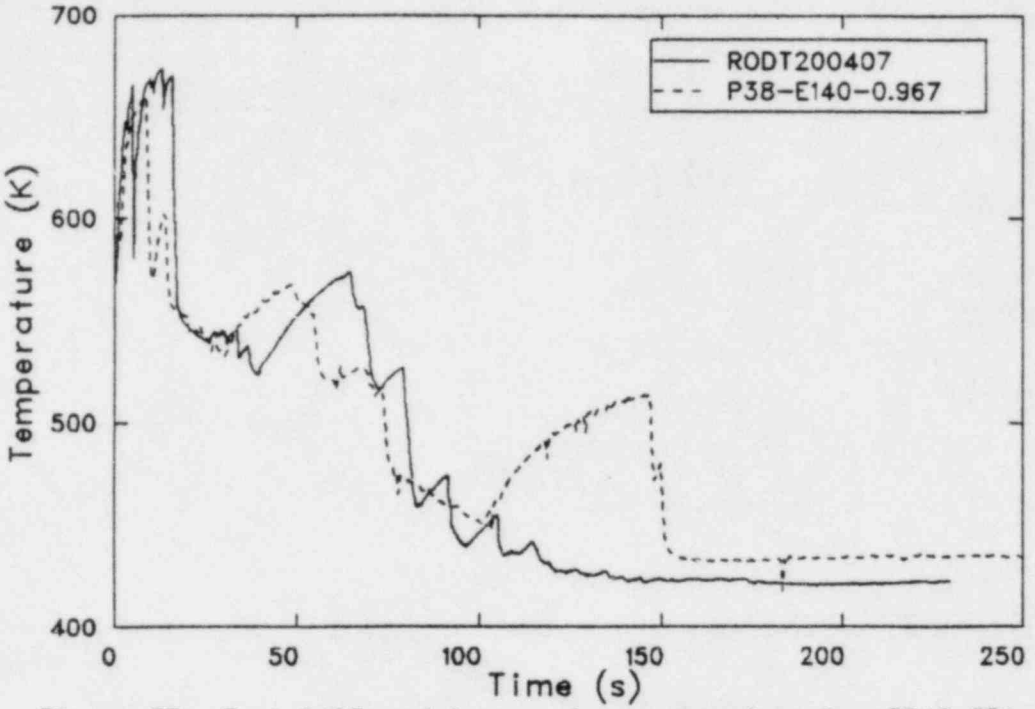

Figure 37. Test 6423 rod temperature comparison for TRAC-BD1 rod group 3 level 7 and rod thermocouple data at 3.556 m from BHL.

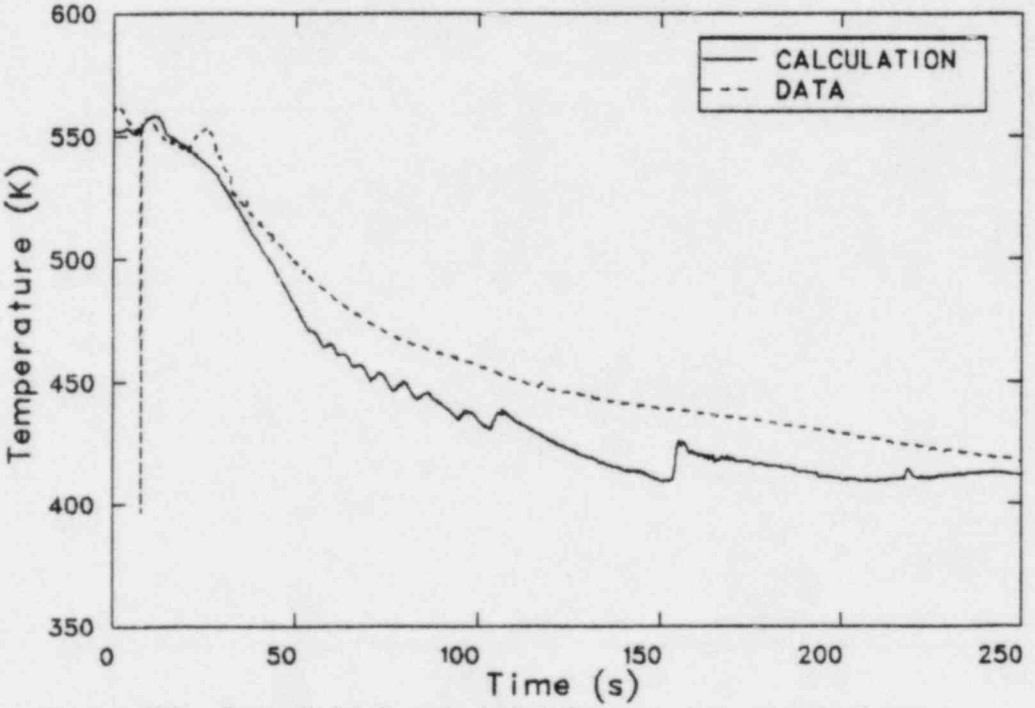

Figure 38. Test 6424 break inlet temperature comparison.

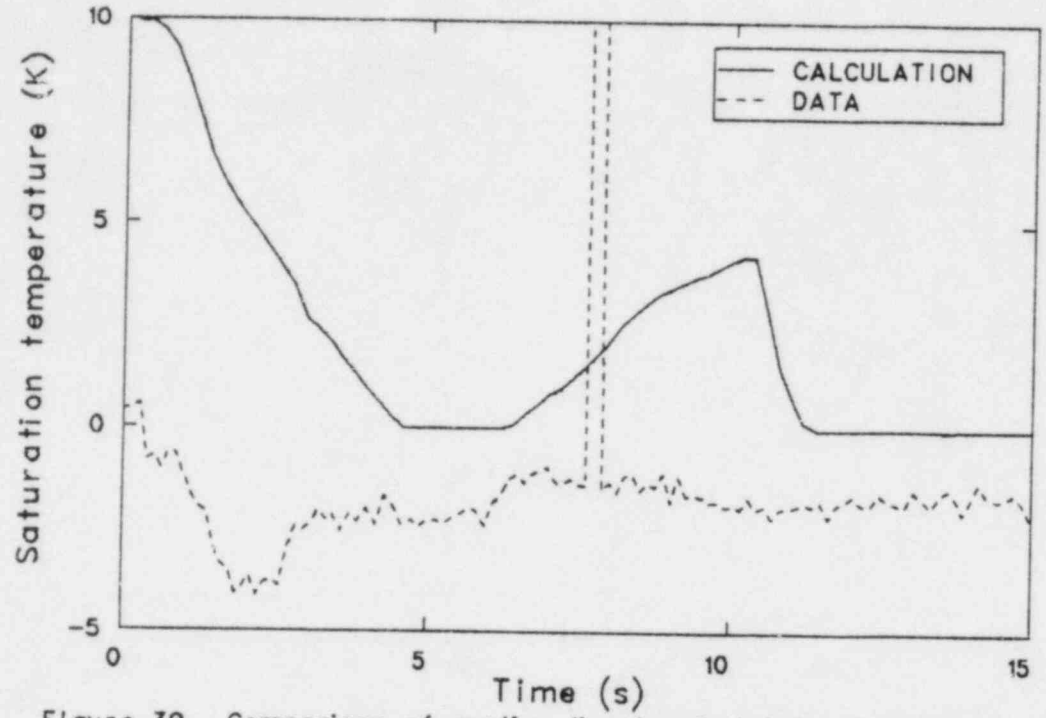

Figure 39. Comparison of suction line break inlet subcooling for Test 6424.

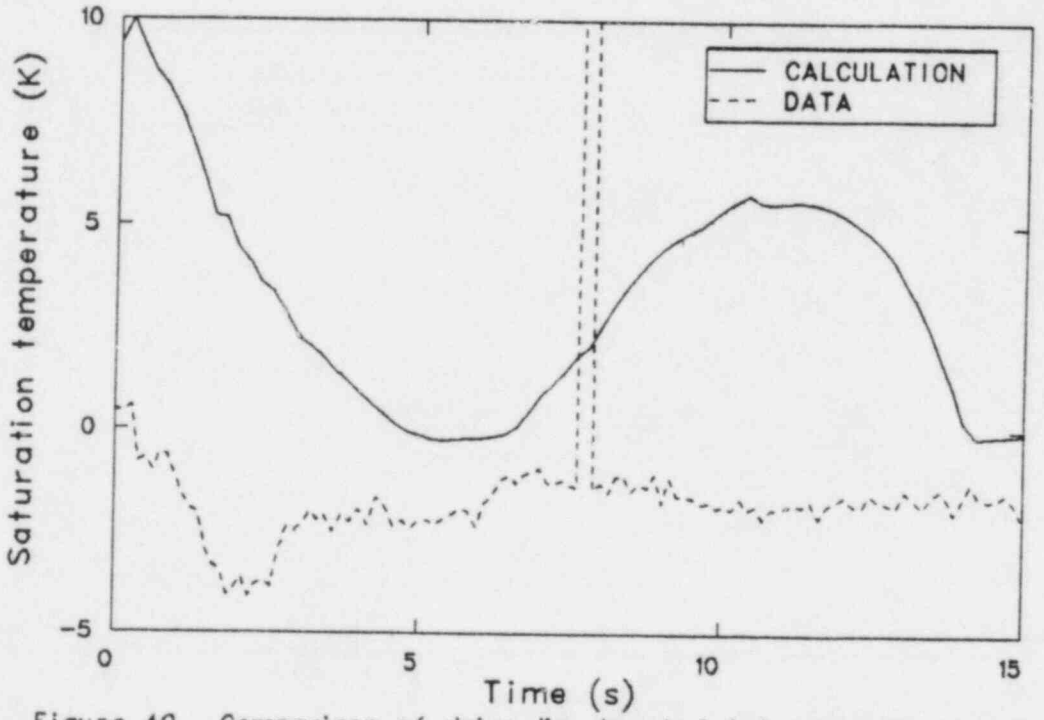

Figure 40. Comparison of drive line break inlet subcooling for Test 6424.

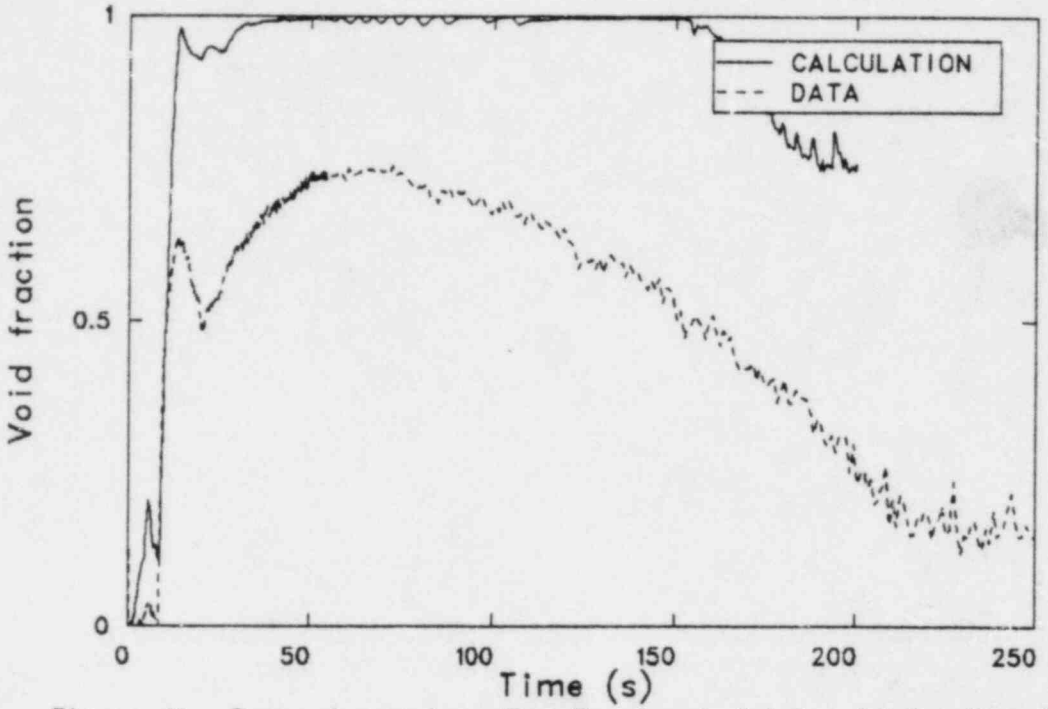

Figure 41. Comparison of suction line break inlet void fraction for Test 6424.

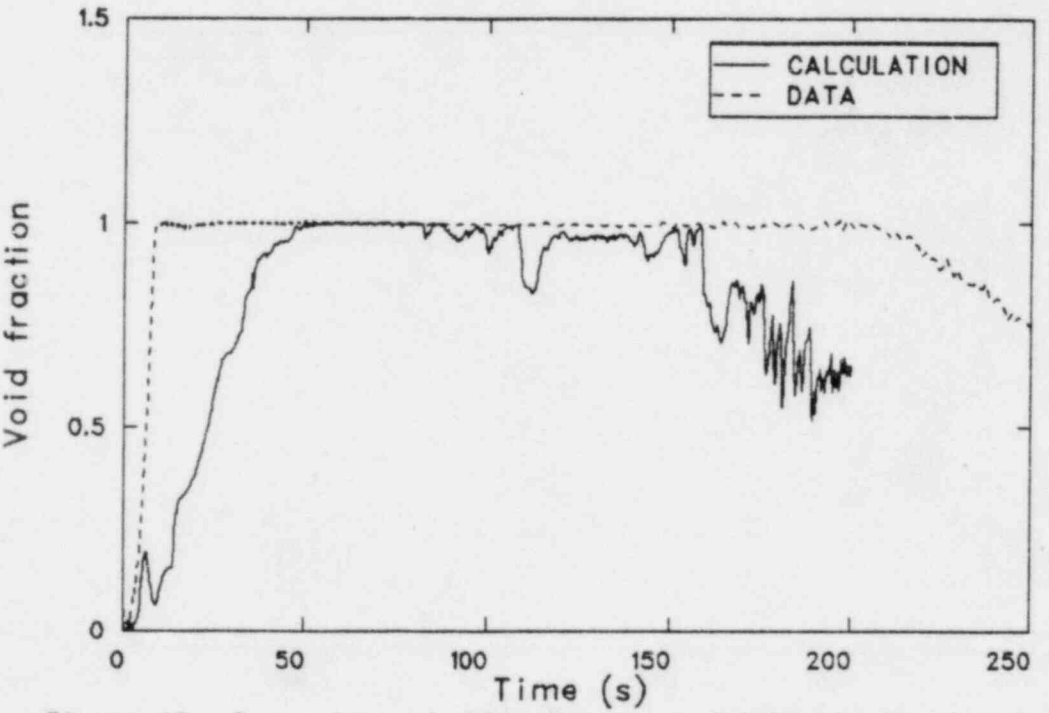

Figure 42. Comparison of drive line break inlet void fraction for Test 6424.

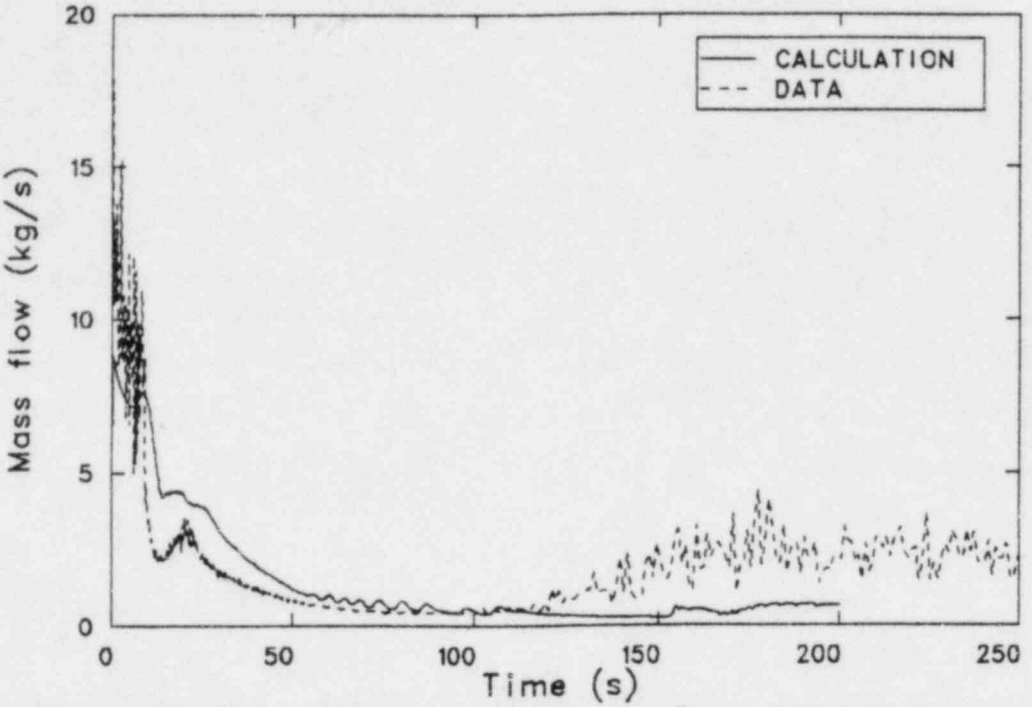

Figure 43. TLTA 6424 suction line break flow comparison.

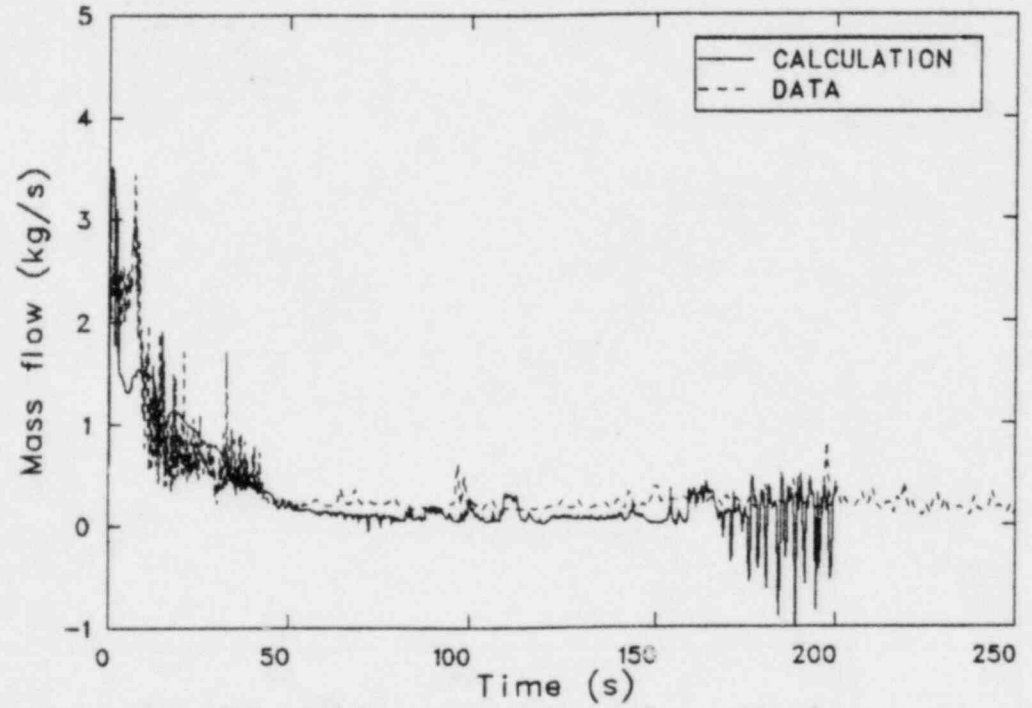

Figure 44. TLTA 6424 drive line break flow comparison.

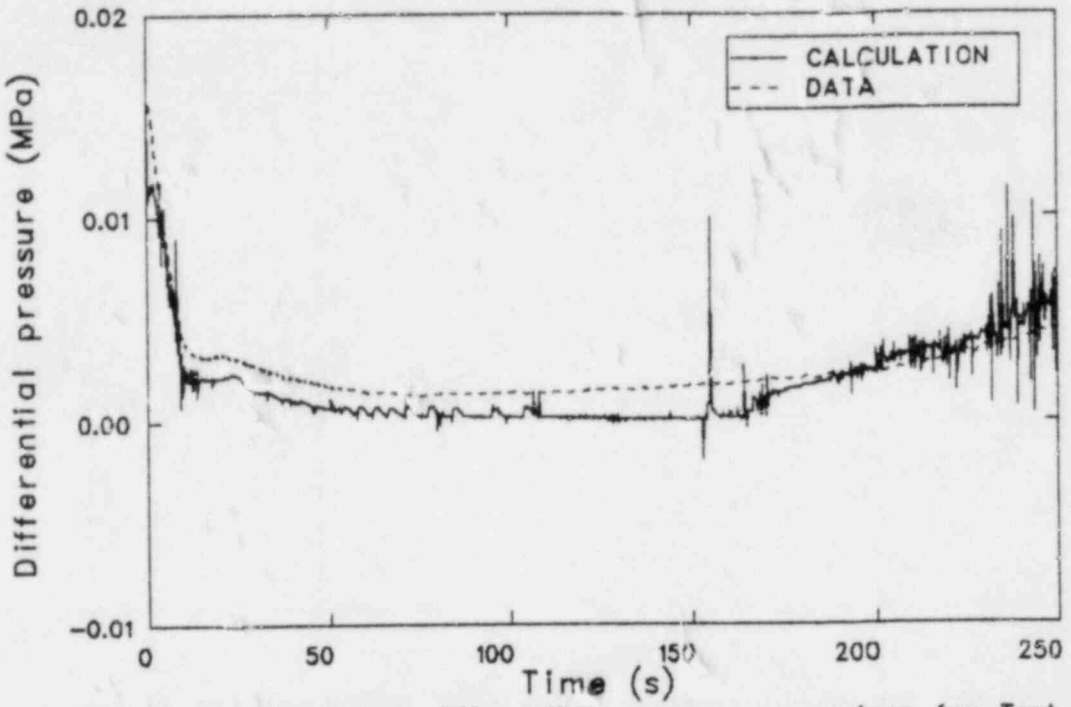

Figure 45. Downcomer differential pressure comparison for Test 6424.

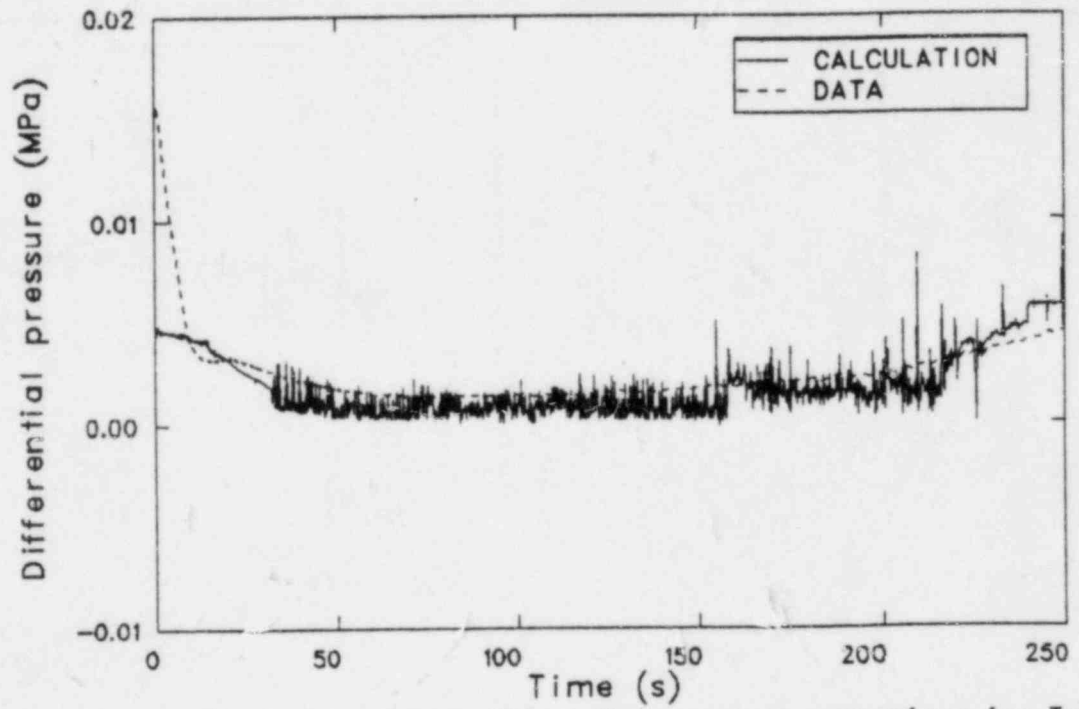

Figure 46. Lower plenum differential pressure comparison for Test 6424.

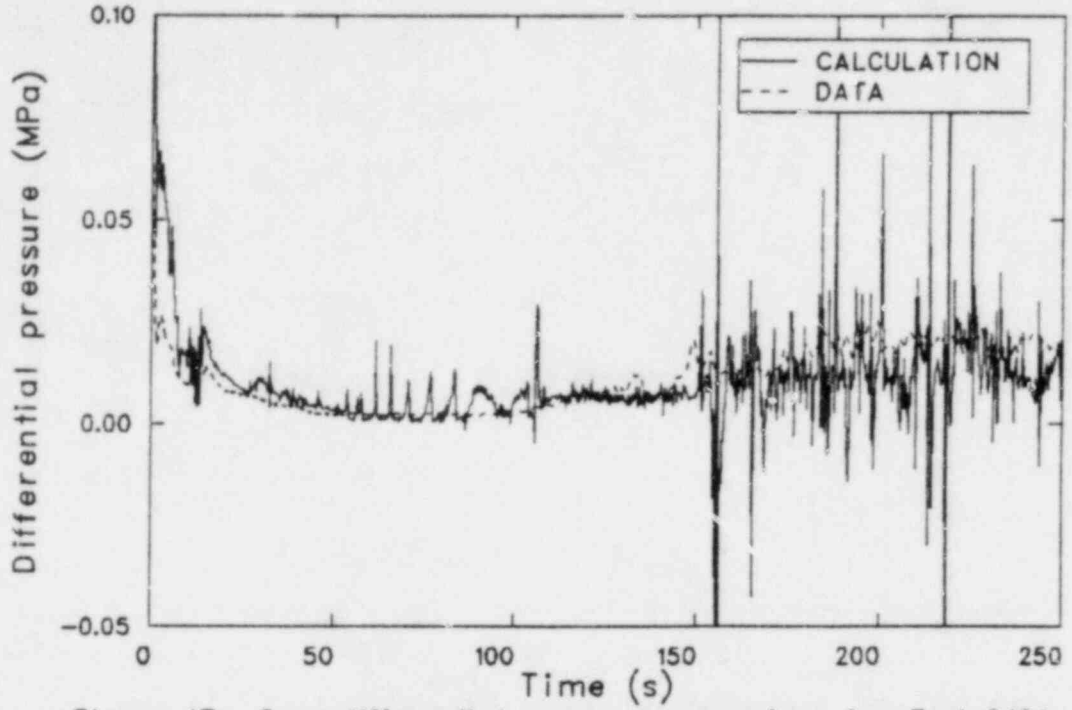

Figure 47. Core differential pressure comparison for Test 6424.

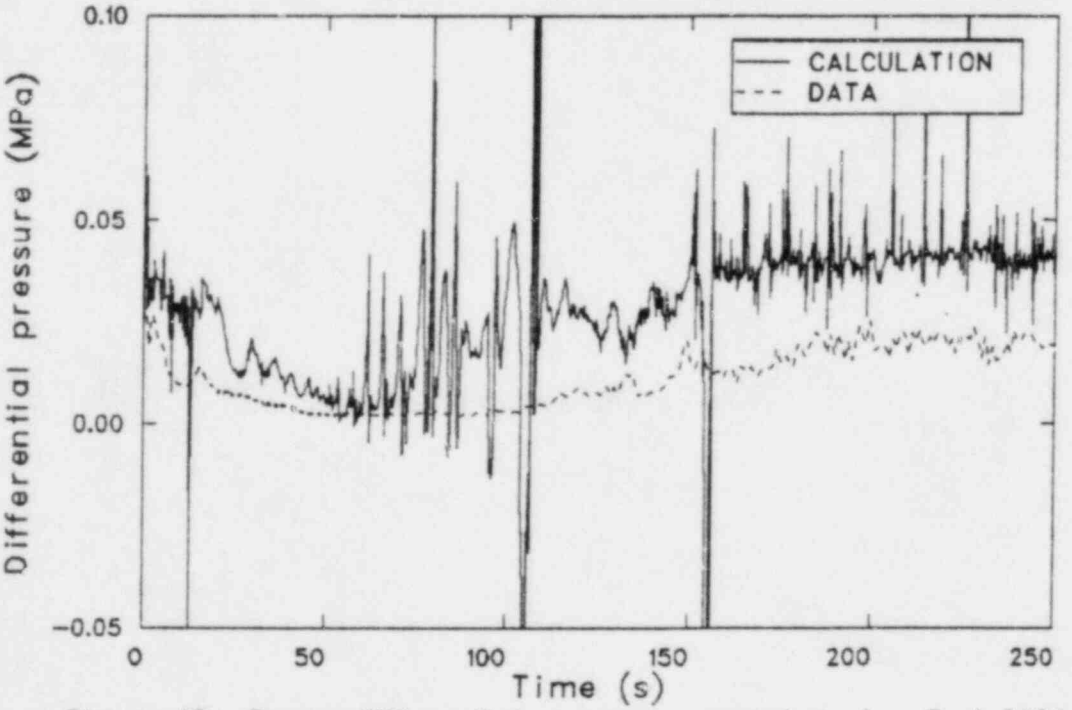

Figure 48. Bypass differential pressure comparison for Test 6424.

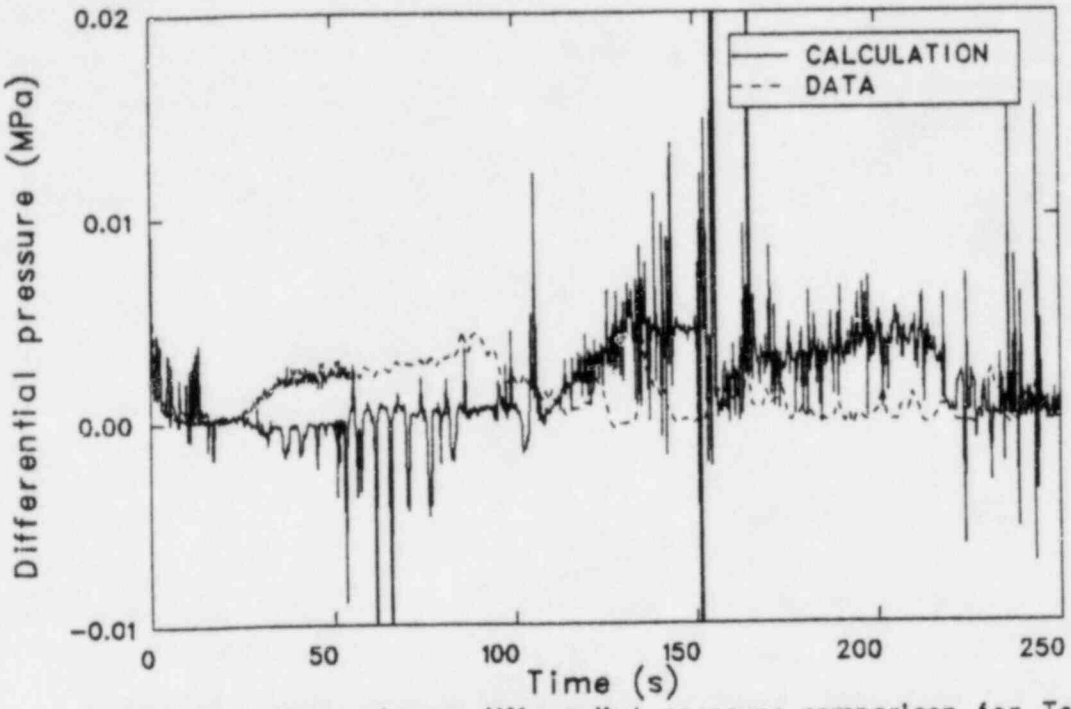

Figure 49. Upper plenum differential pressure comparison for Test 6424.

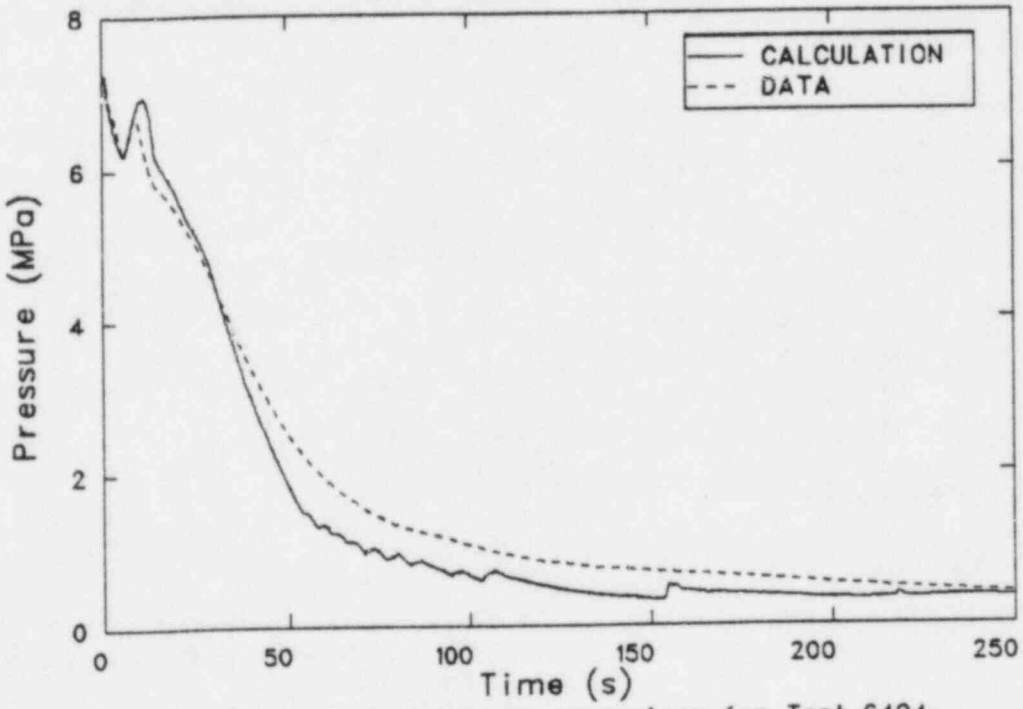

Figure 50. Steam dome pressure comparison for Test 6424.

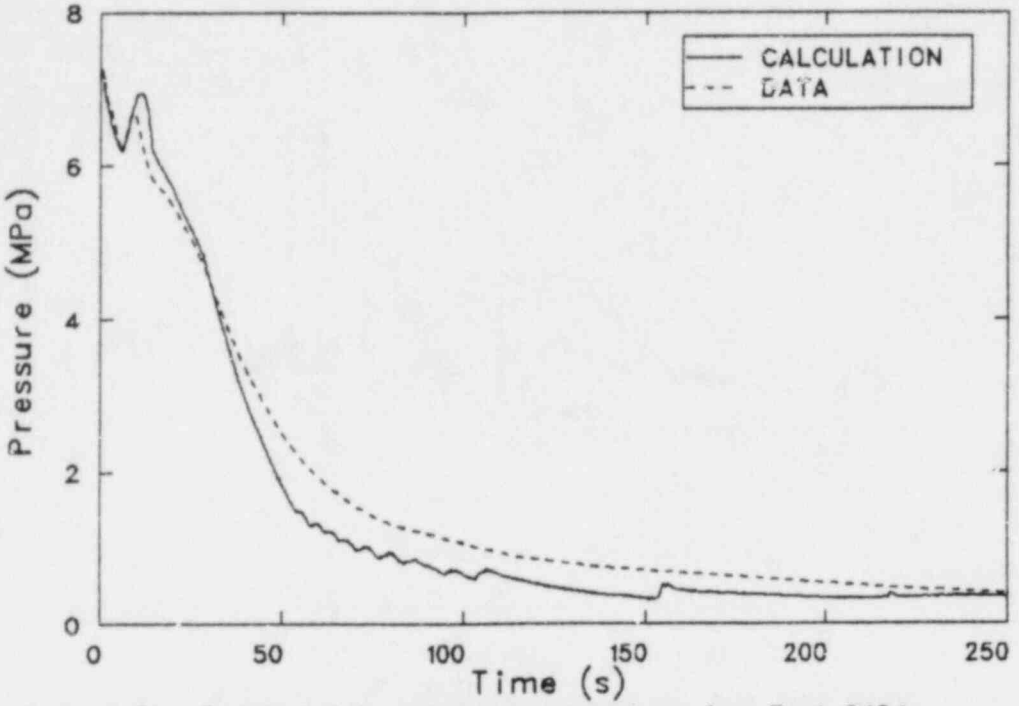

Figure 51. Break inlet pressure comparison for Test 6424.

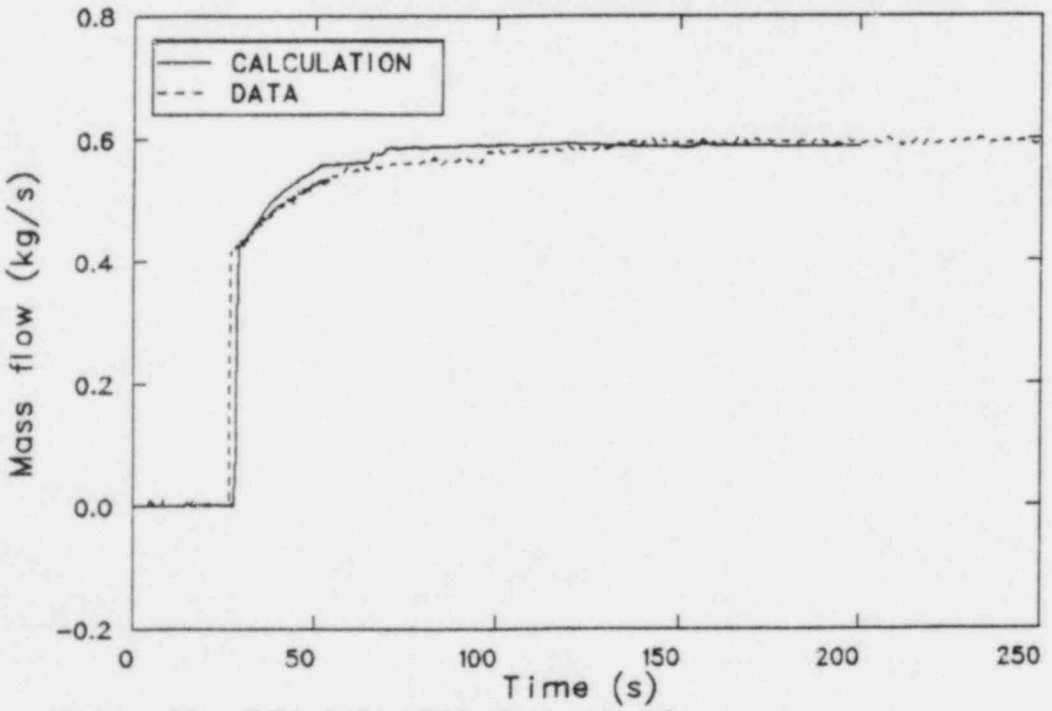

Figure 52. TLTA 6424 HPCS flow comparison.

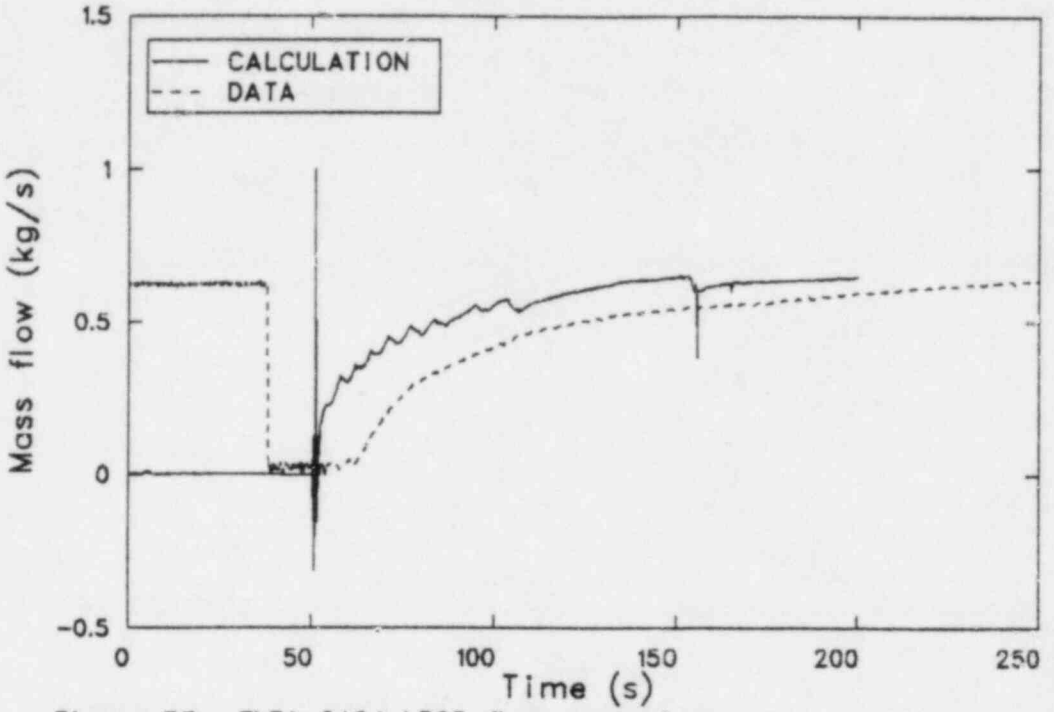

Figure 53. TLTA 6424 LPCS flow comparison.

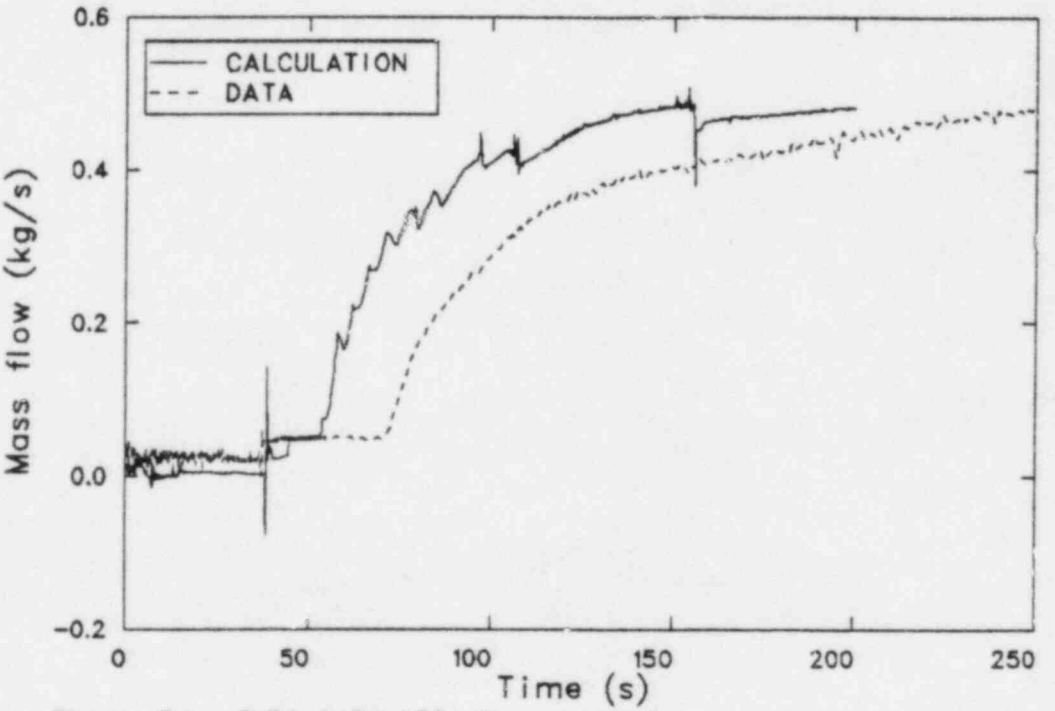

Figure 54. TLTA 6424 LPCI flow comparison.

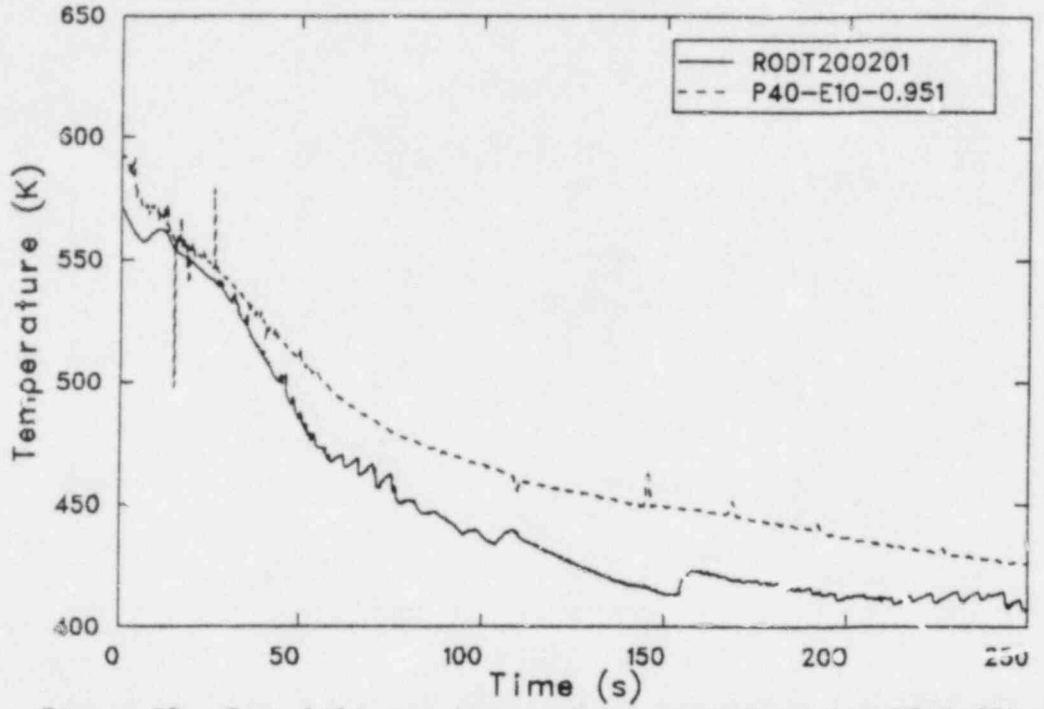

Figure 55. Test 6424 rod temperature comparison for TRAC-BD1 rod group 1 level 1 and rod thermocouple data at .25 m from BHL.

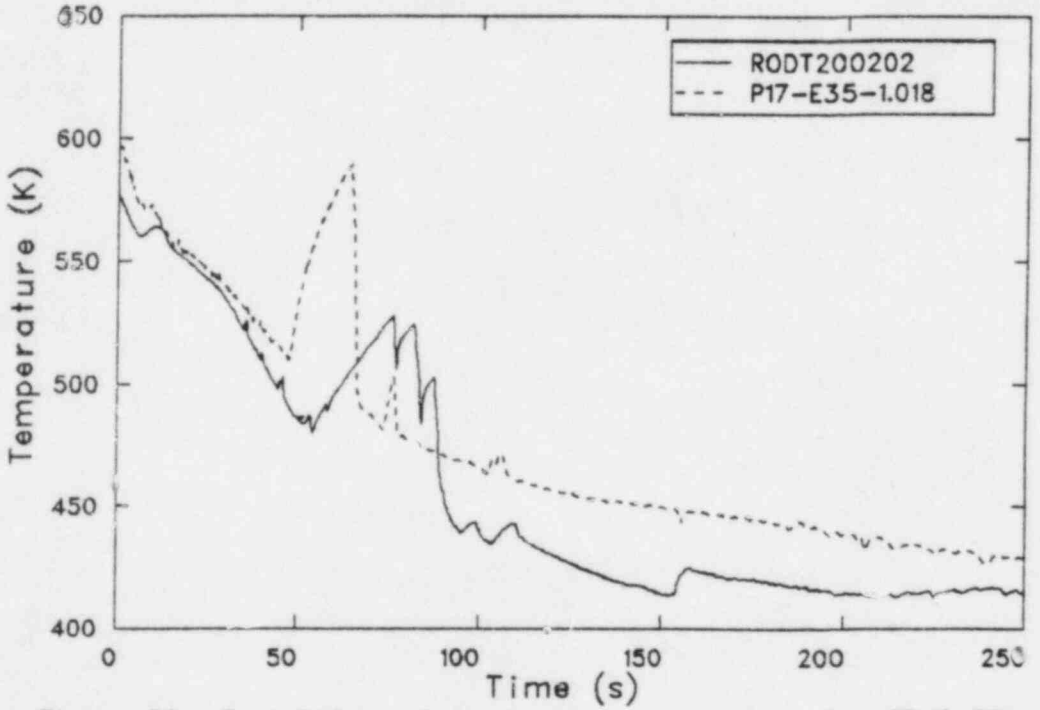

Figure 56. Test 6424 rod temperature comparison for TRAC-BD1 rod group 1 level 2 and rod thermocouple data at .89 m from BHL.

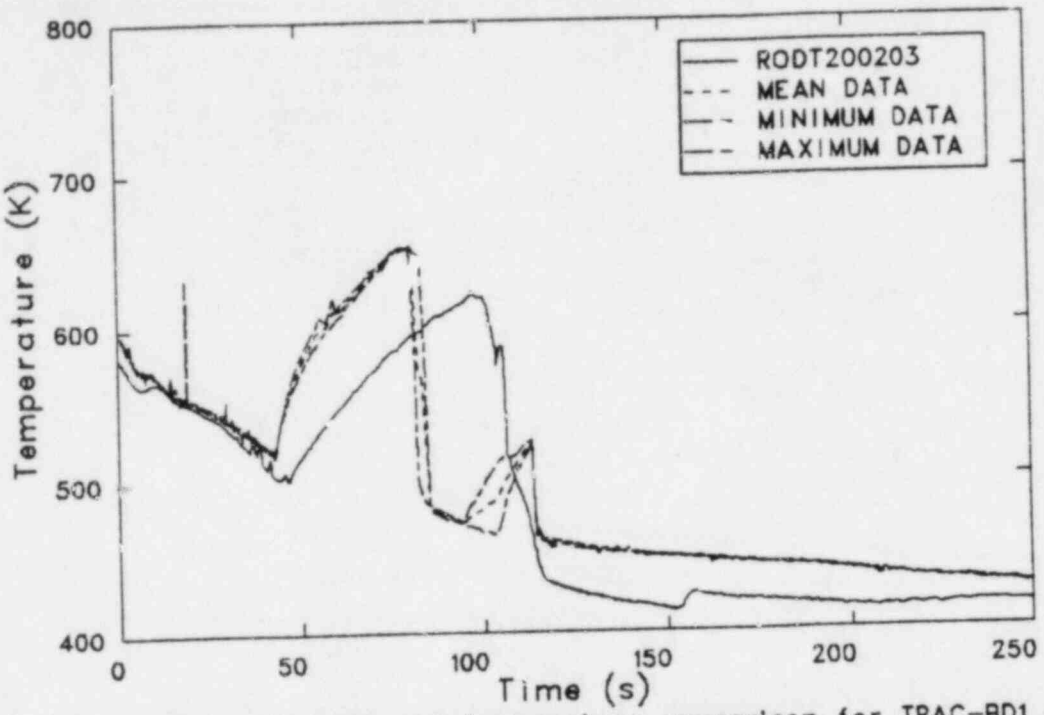

Figure 57. Test 6424 rod temperature comparison for TRAC-BD1 rod group 1 level 3 and rod thermocouple data at 1.27 m from BHL.

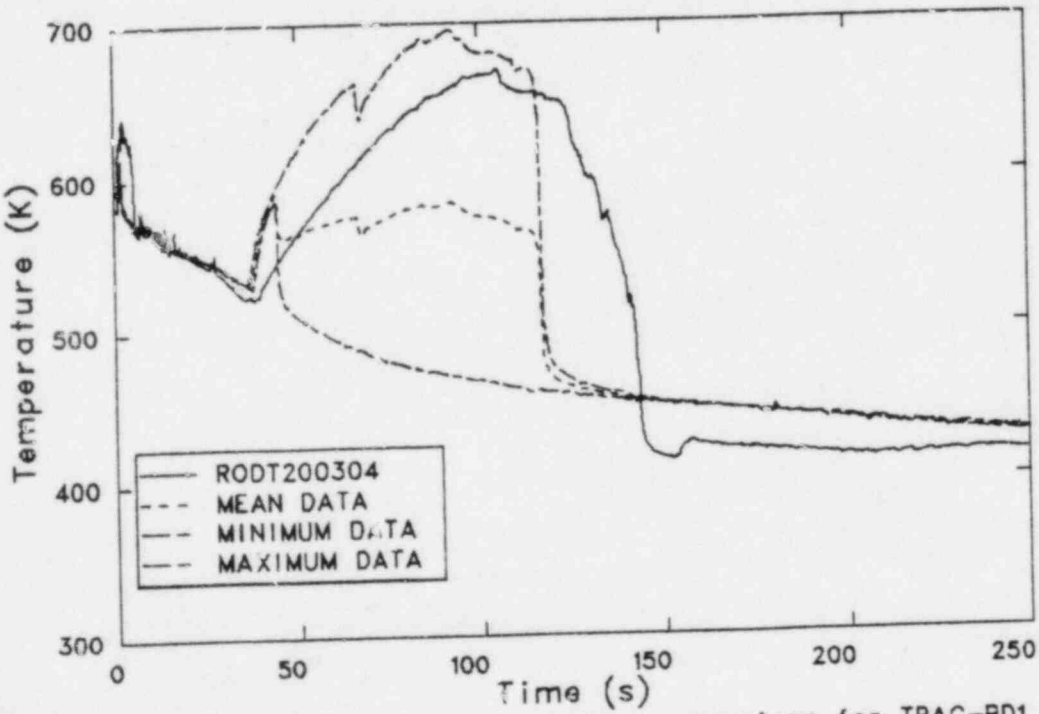

Figure 58. Test 6424 rod temperature comparison for TRAC-BD1 rod group 2 level 4 and rod thermocouple data at 1.80 m from BHL.

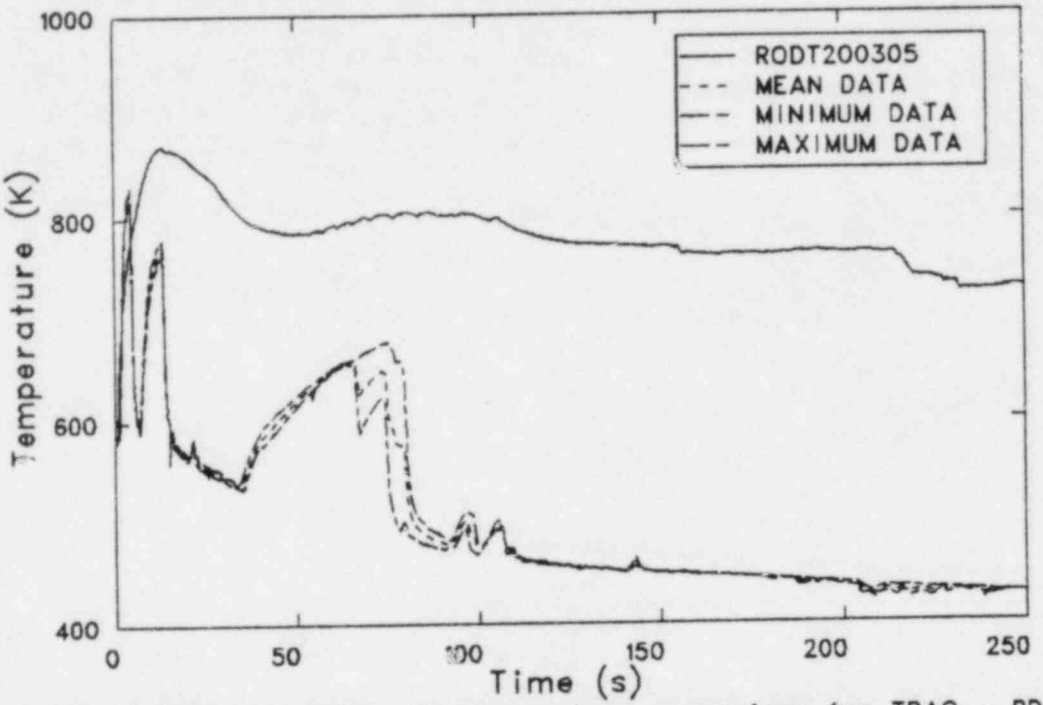

Figure 59. Test 6424 rod temperature comparison for TRAC - BD1 rod group 2 level 5 and rod thermocouple data at 2.54 m from BHL.

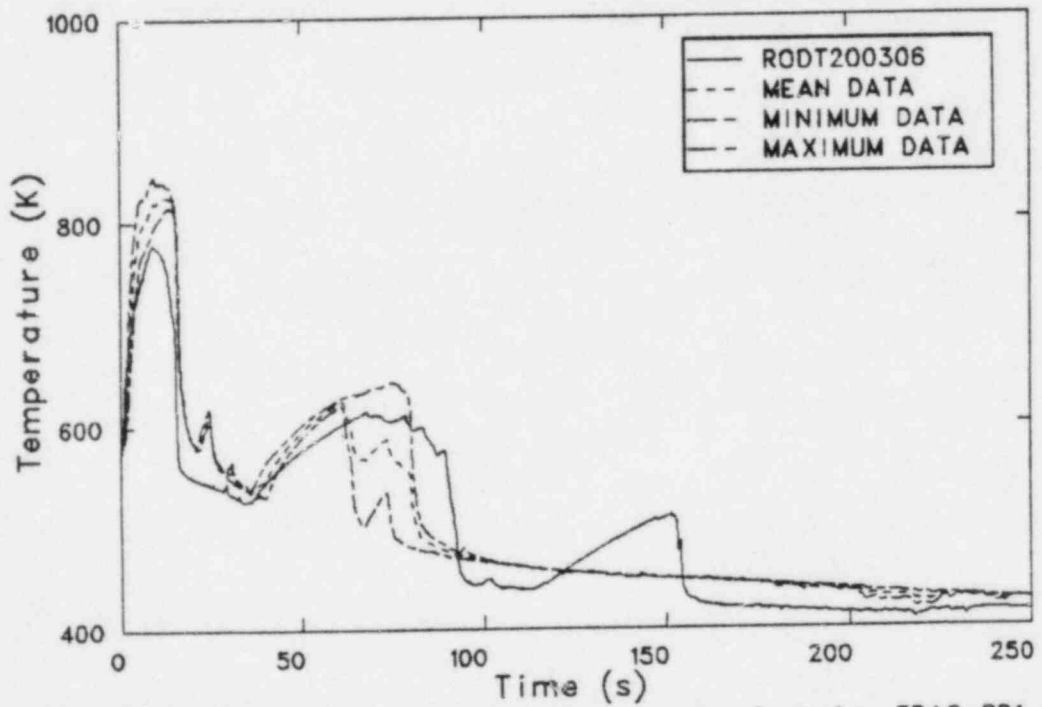

Figure 60. Test 6424 rod temperature comparison for TRAC-BD1 rod group 2 level 6 and rod thermocouple data at 3.05 m from BHL.

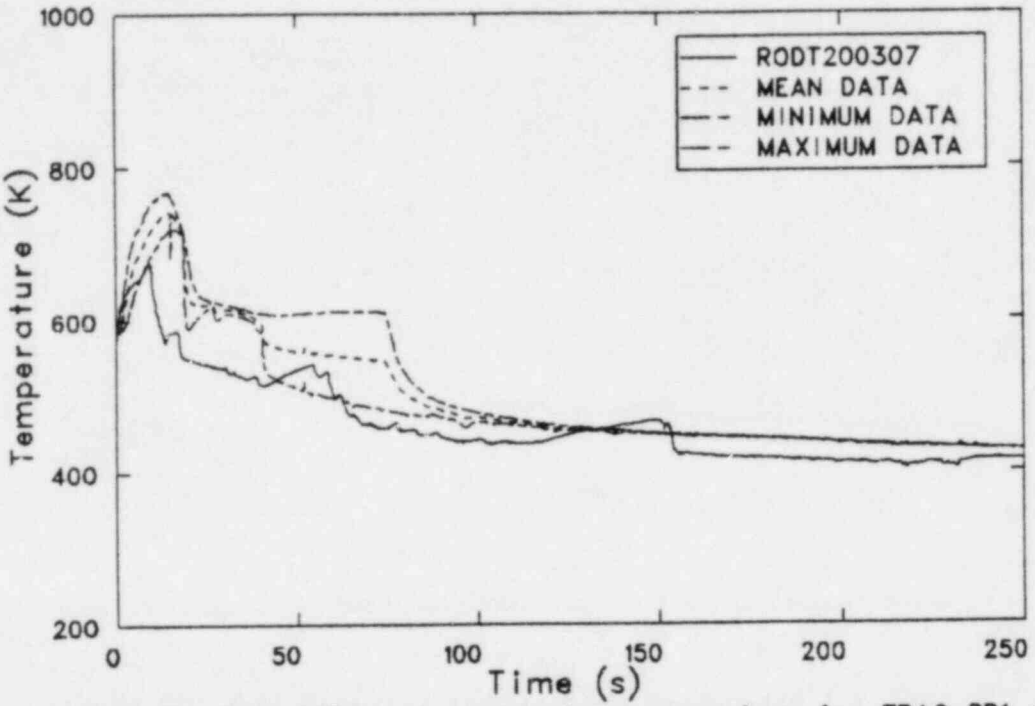

Figure 61. Test 6424 rod temperature comparison for TRAC-BD1 rod group 2 level 7 and rod thermocouple data at 3.56 m from BHL.

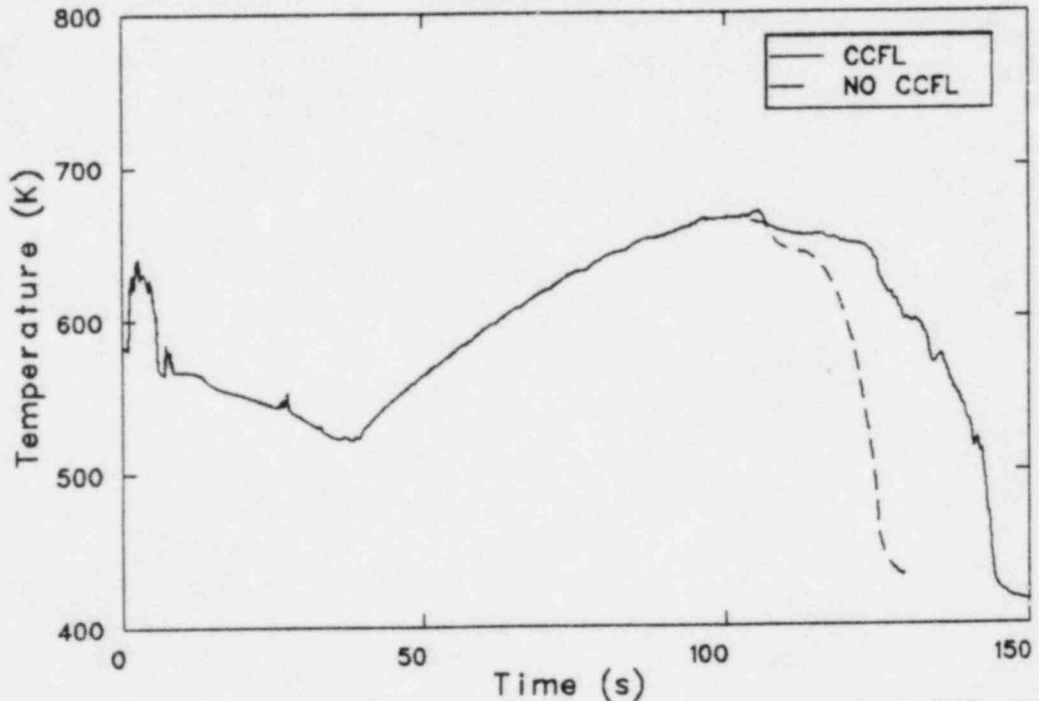

Figure 62. Rod temperature comparison with and without CCFL model at the upper tie plate; rod level 4.

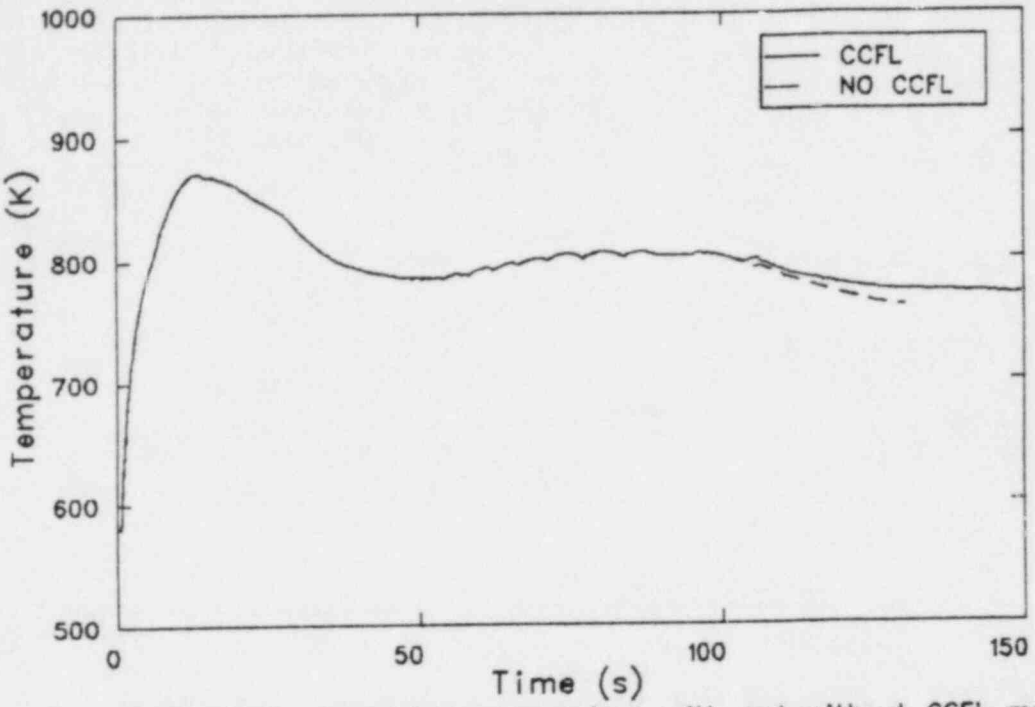

Figure 63. Rod temperature comparison with and without CCFL model at the upper tie plate; rod level 5.

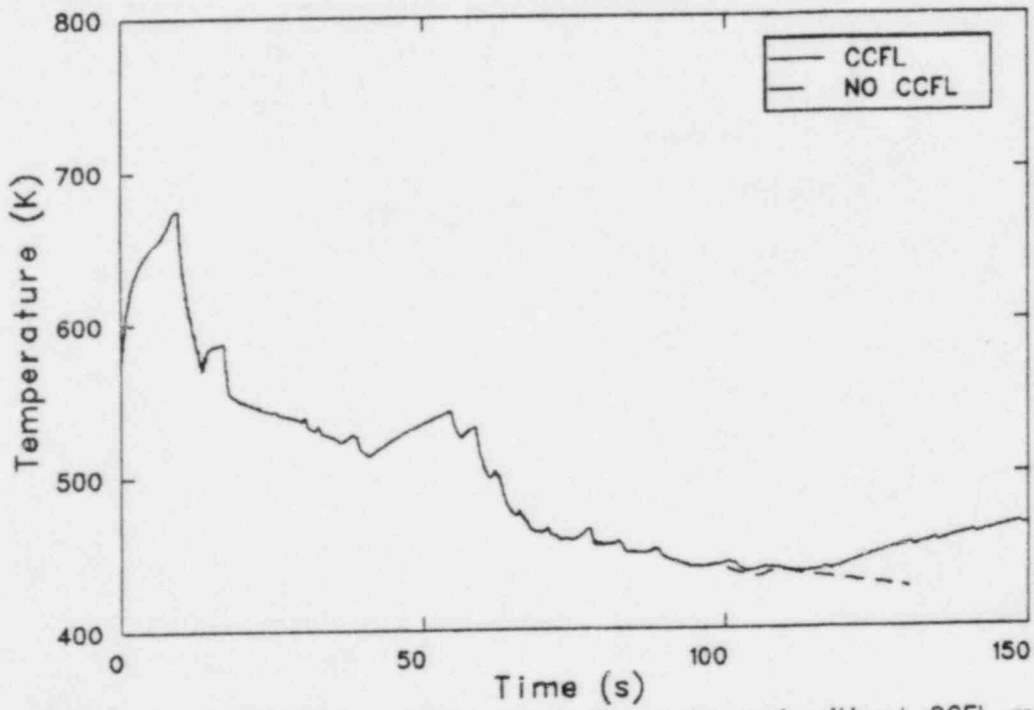

Figure 64. Rod temperature comparison with and without CCFL model at the upper tie plate; rod level 7.

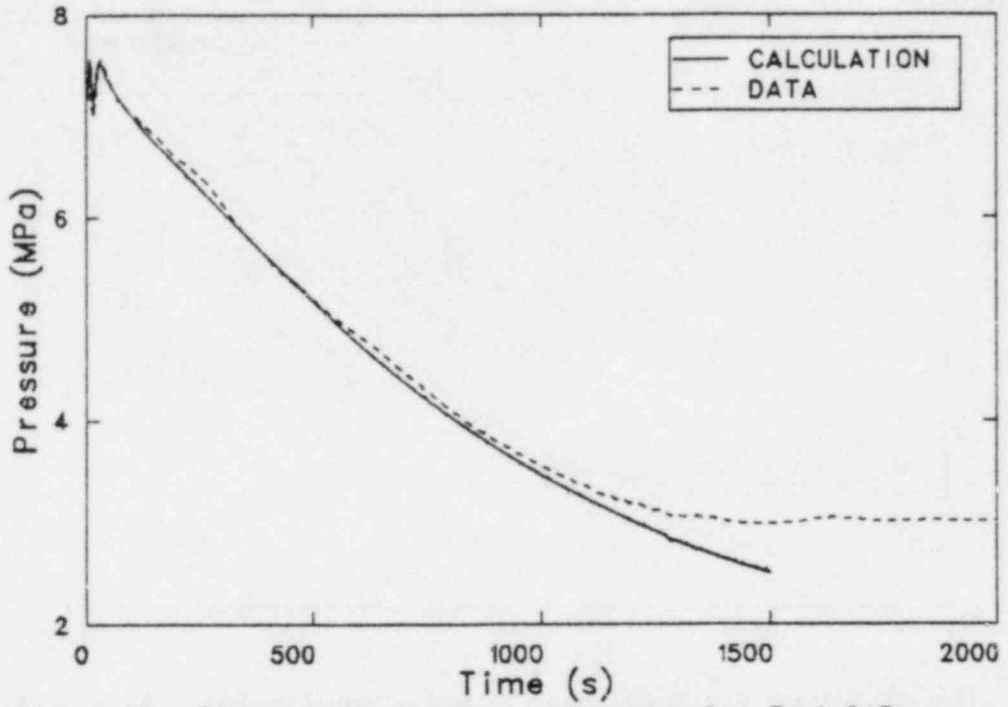

Figure 65. Steam dome pressure comparison for Test 6431.

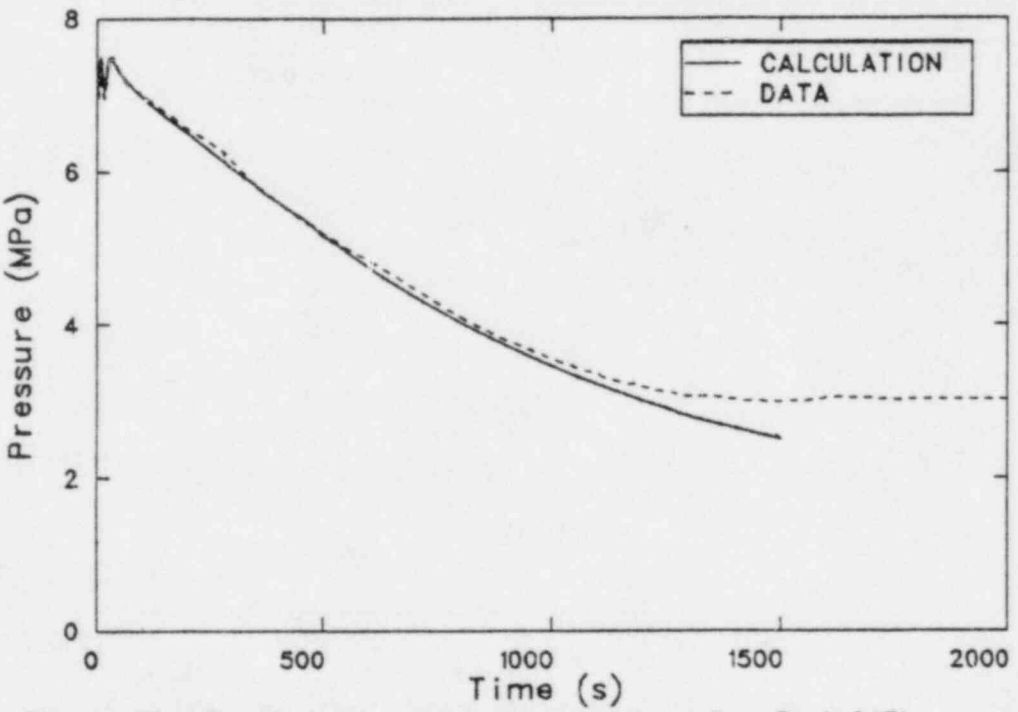

Figure 66. Break inlet pressure comparison for Test 6431.

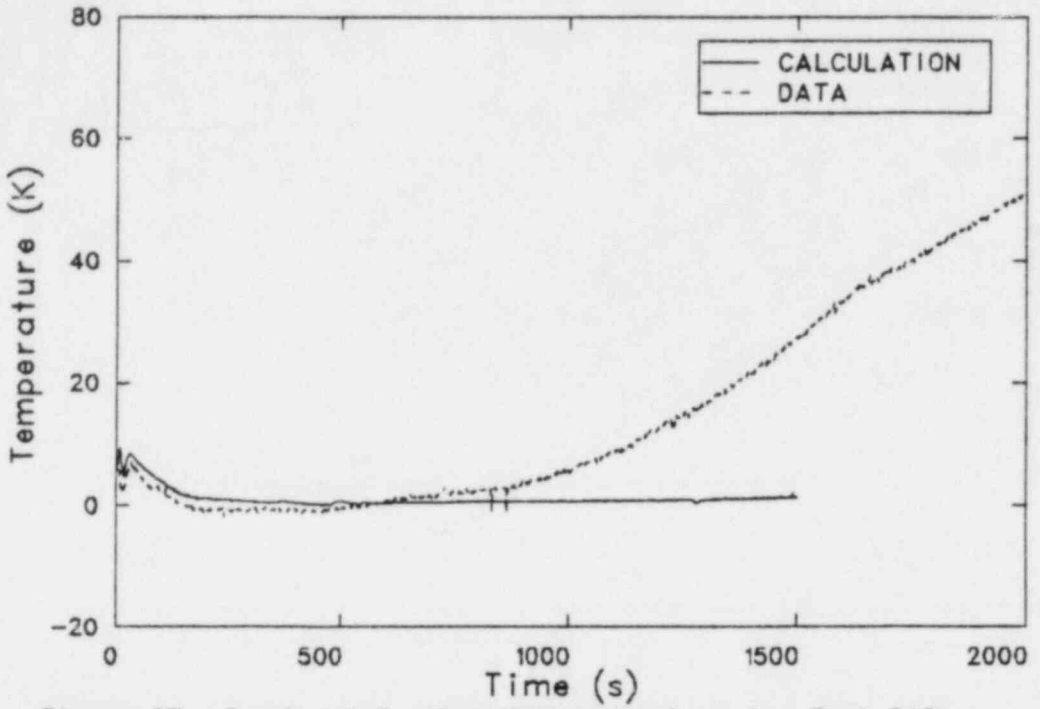

Figure 67. Break inlet subcooling comparison for Test 6431.

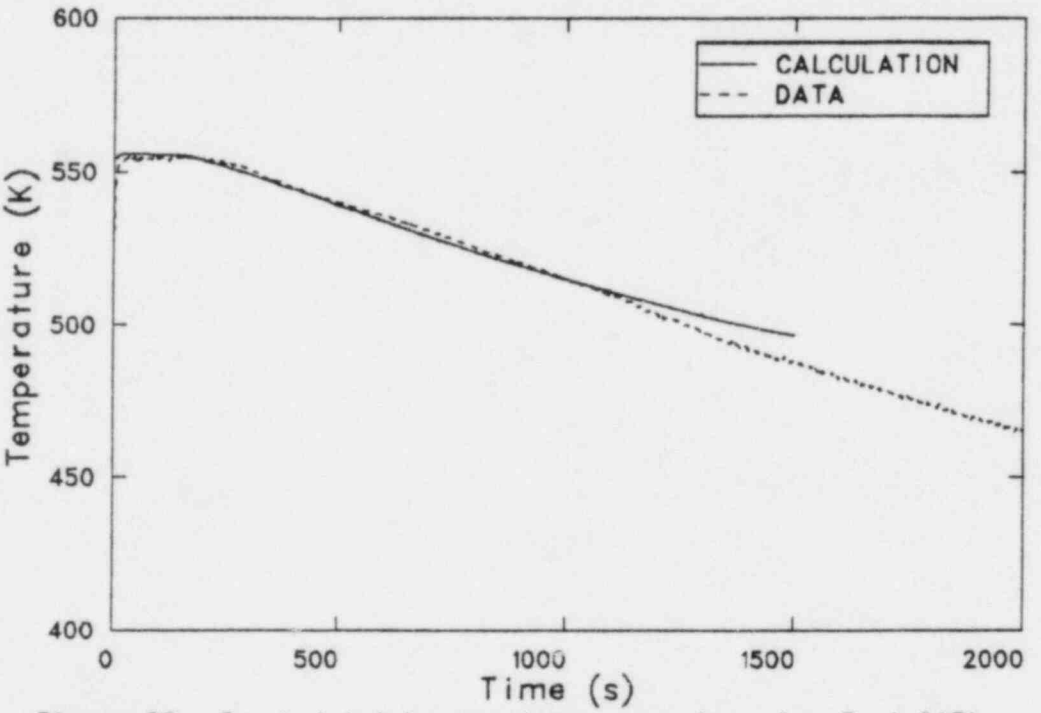

Figure 68. Break inlet temperature comparison for Test 6431.

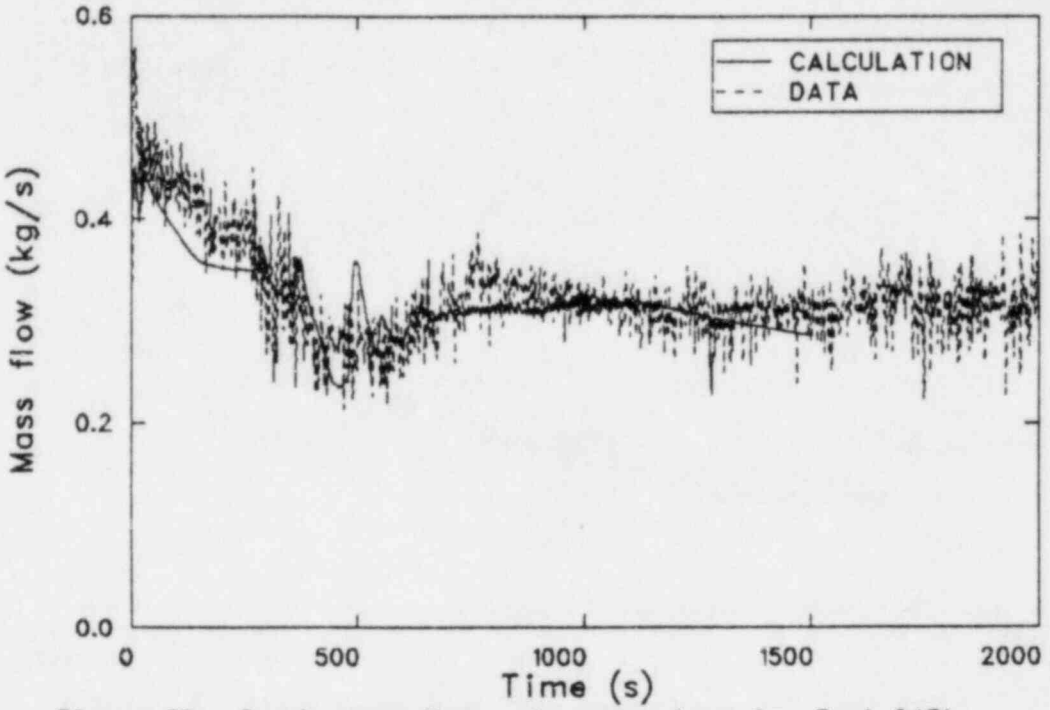

Figure 69. Break mass flow rate comparison for Test 6431.

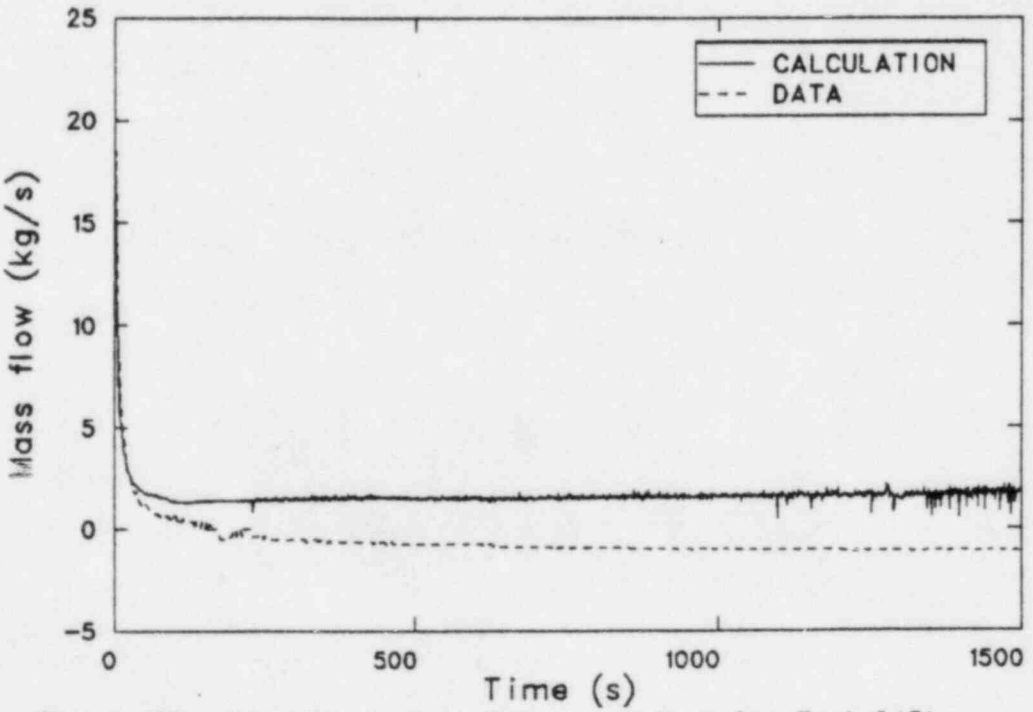

Figure 70. Core inlet mass flow comparison for Test 6431.

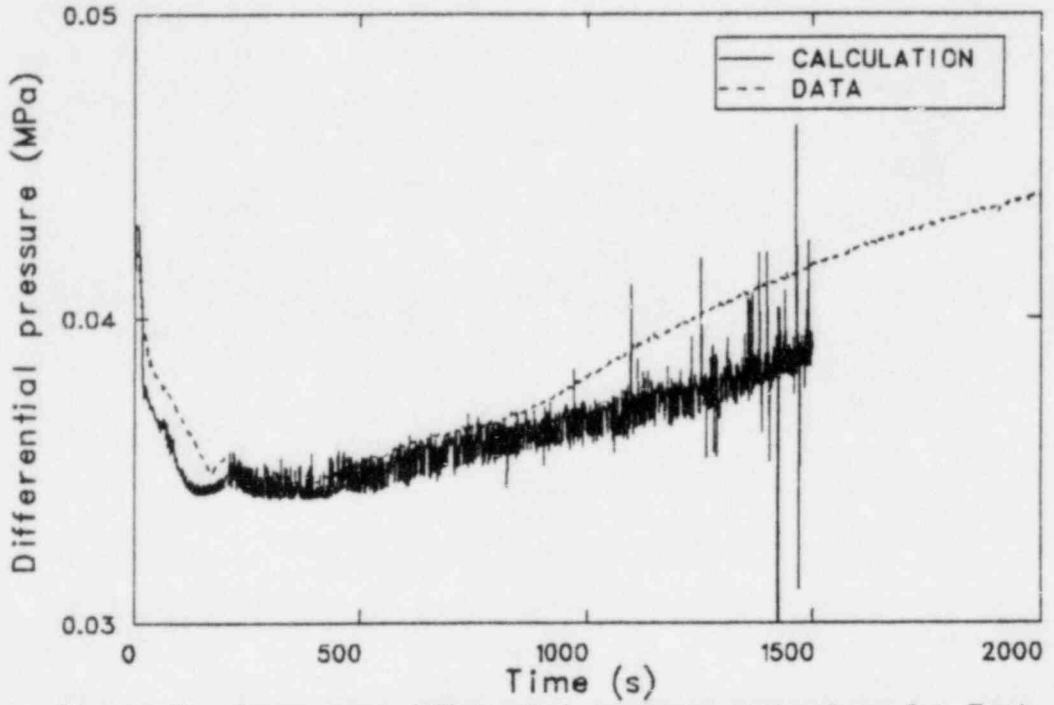

Figure 71. Downcomer differential pressure comparison for Test 6431.

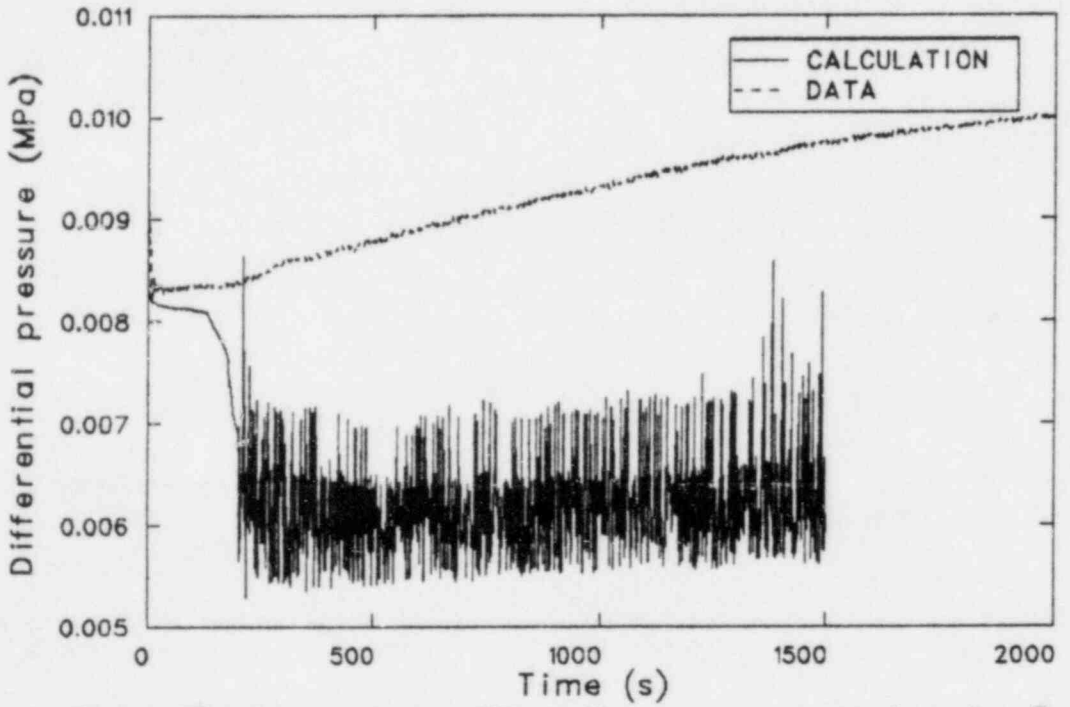

Figure 72. Lower plenum differential pressure comparison for Test 6431.

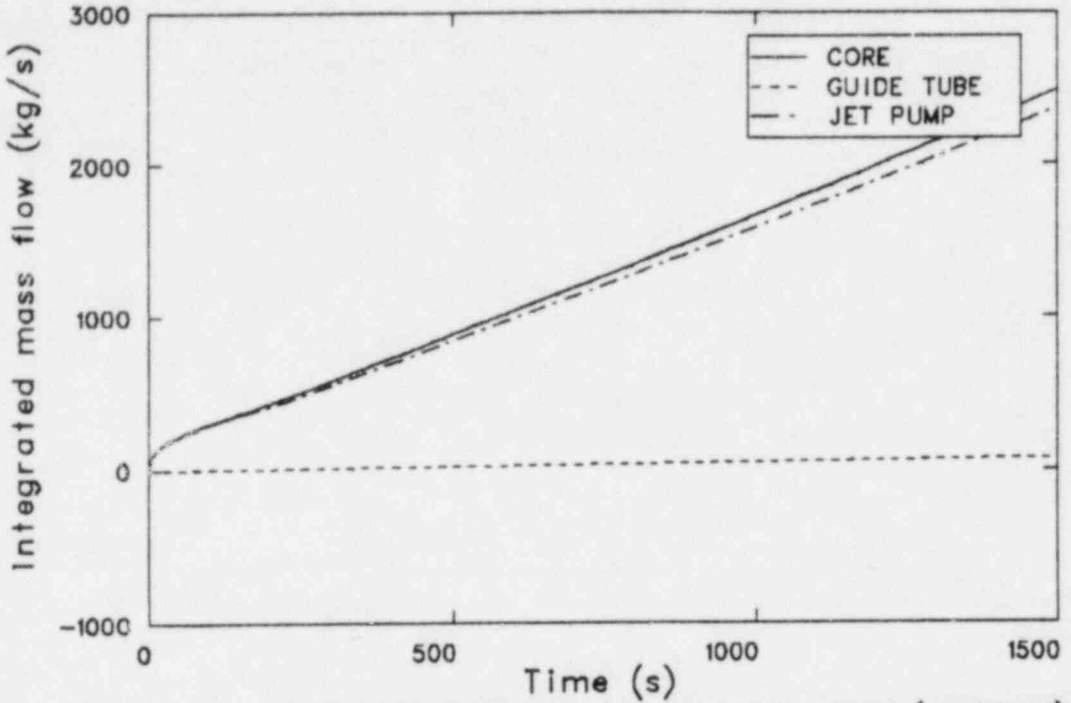

Figure 73. Integrated mass flow for core, jet pumps (combined) and guide tube.

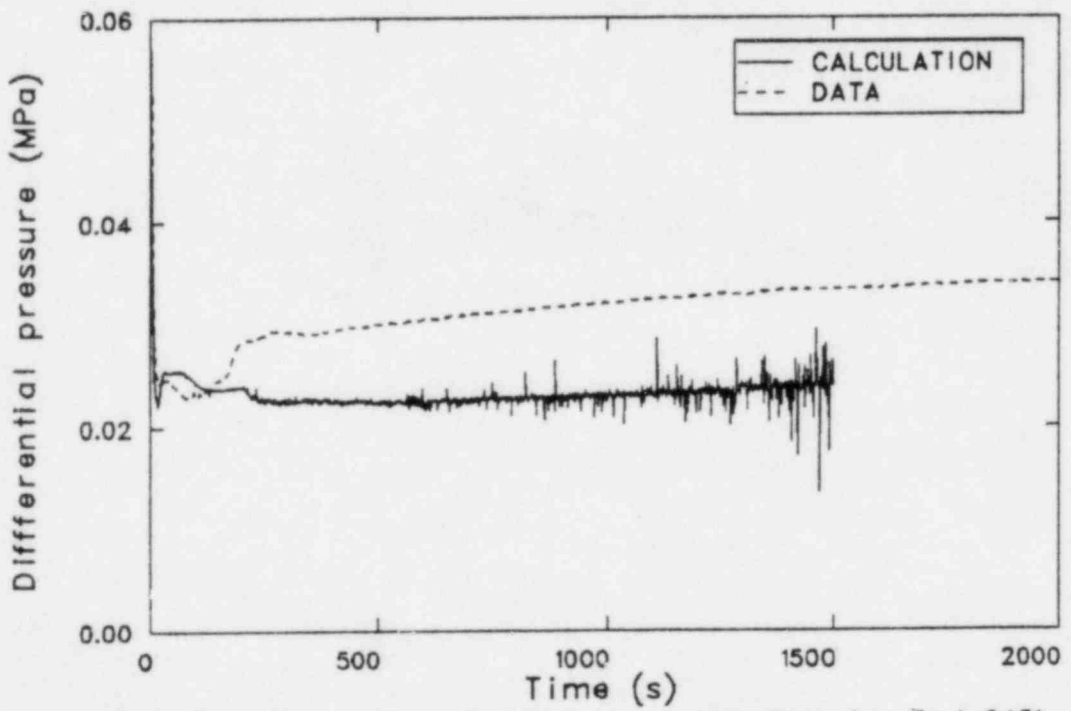

Figure 74. Core differential pressure comparison for Test 6431.

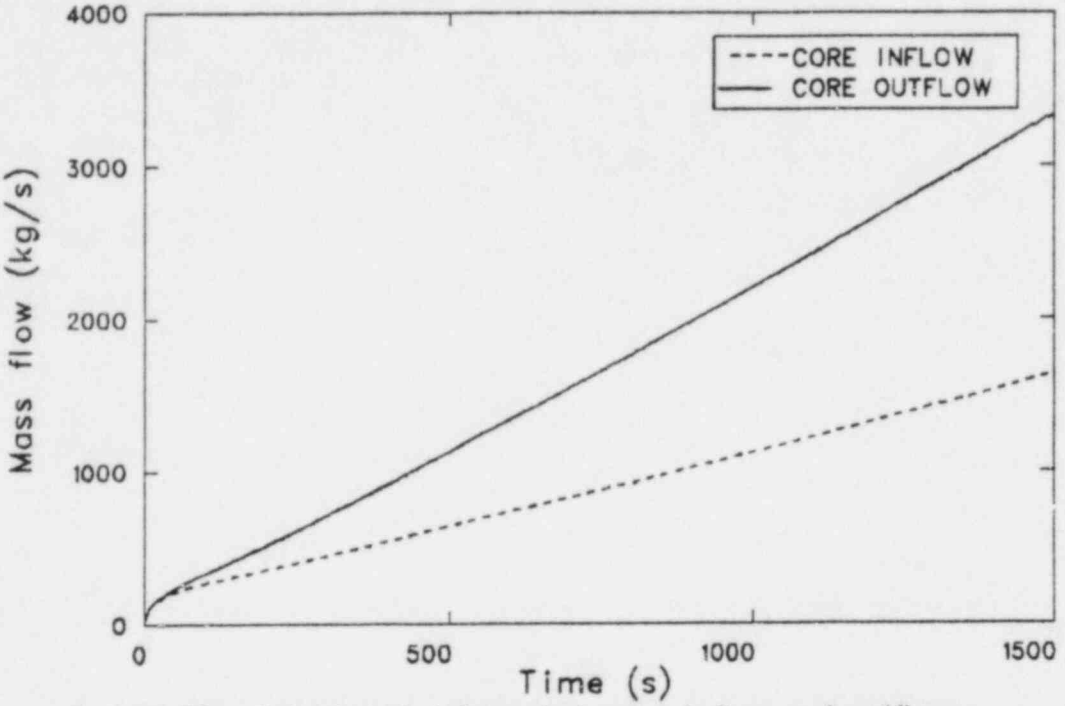

Figure 75. Calculated integrated core inflow and outflow.

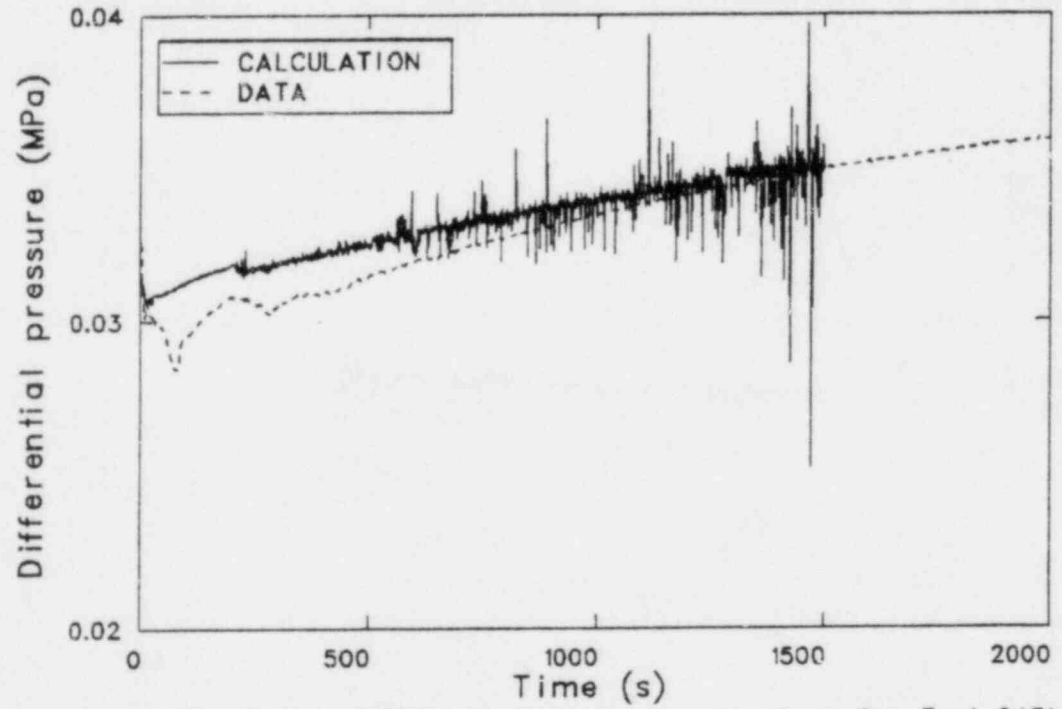

Figure 76. Bypass differential pressure comparison for Test 6431.

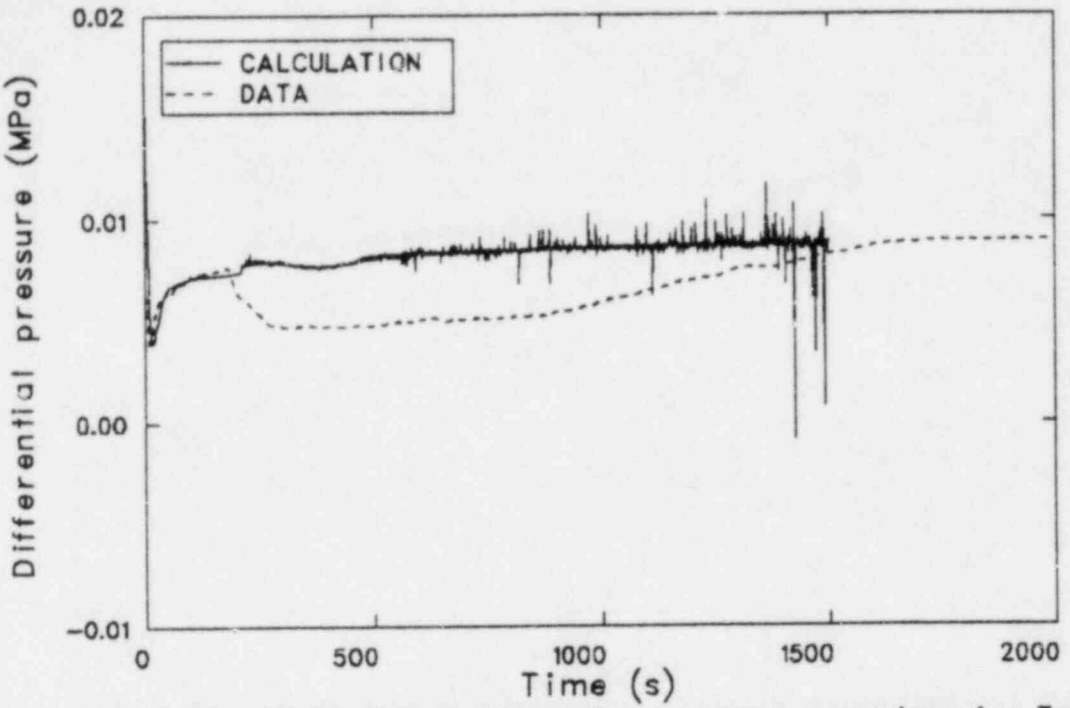

Figure 77. Upper plenum differential pressure comparison for Test 6431.

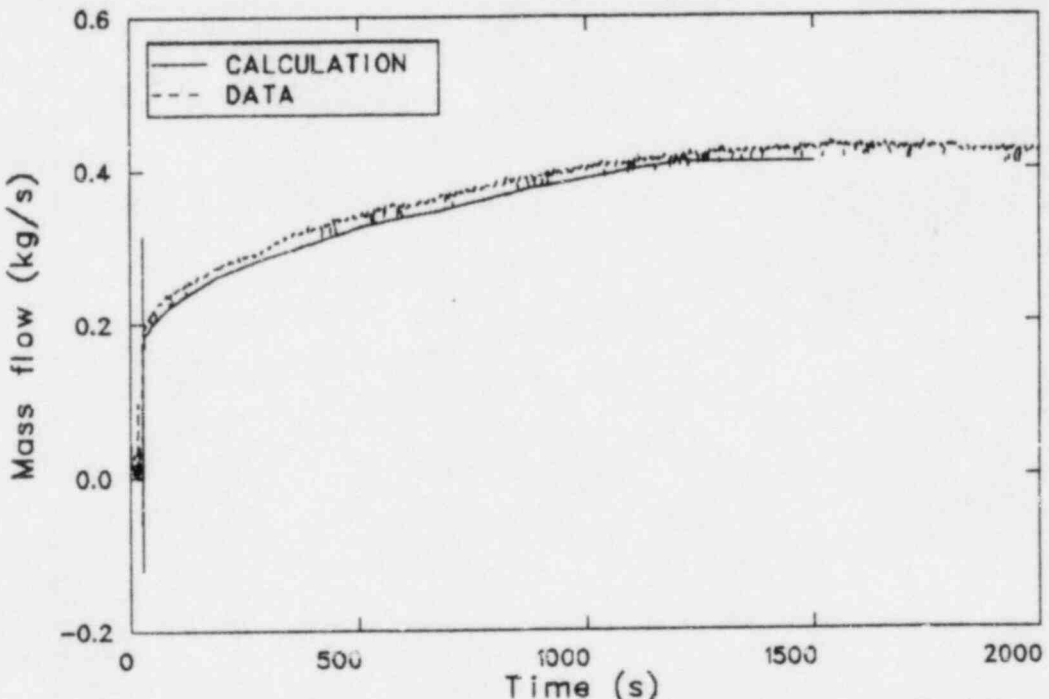

Figure 78. ECCS mass flow rate comparison for Test 6431 (HPCS only).

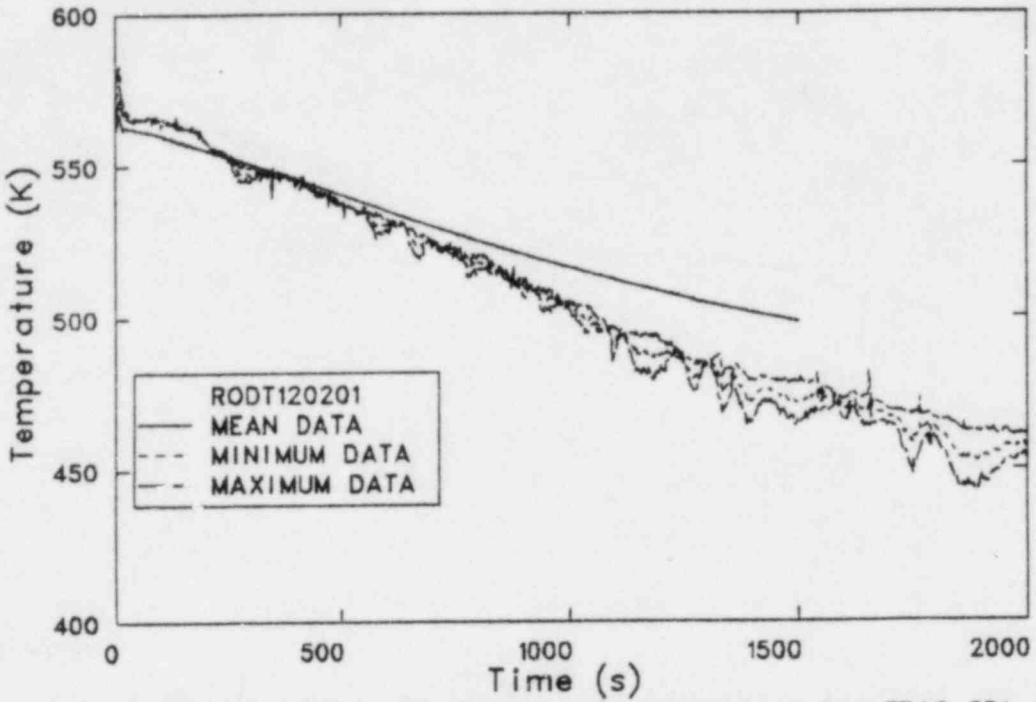

Figure 79. Test 6431 rod temperature comparison for TRAC-BD1 rod group 2 level 1 and rod thermocouple data at .25 m from BHL.

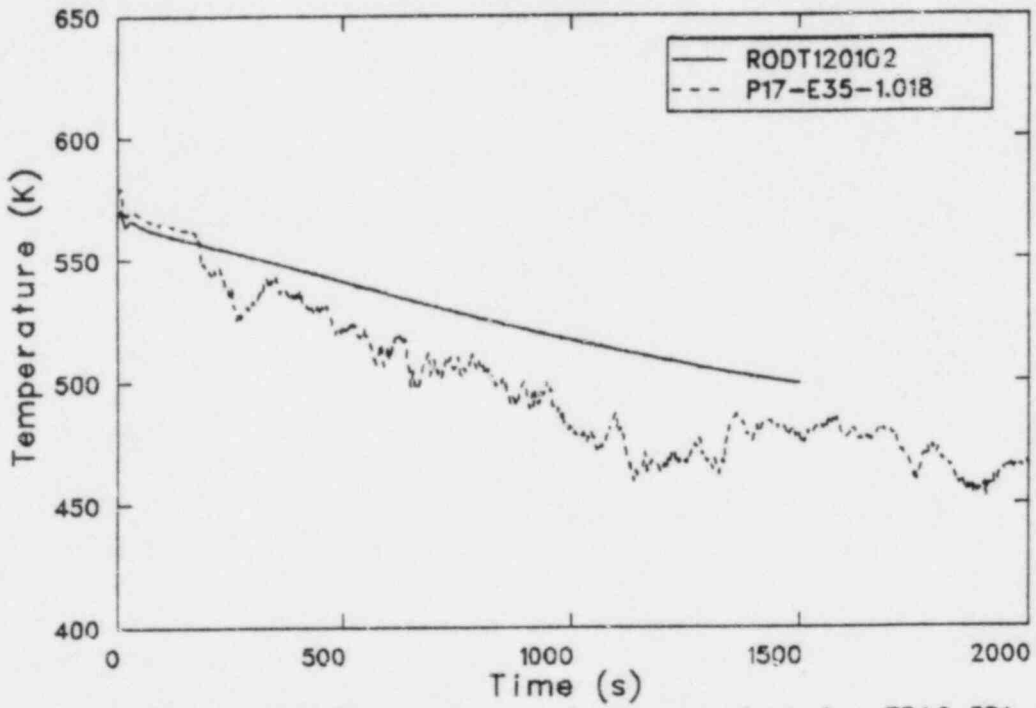

Figure 80. Test 6431 rod temperature comparison for TRAC-BD1 rod group 1 level 2 and rod thermocouple data at .89 m from BHL.

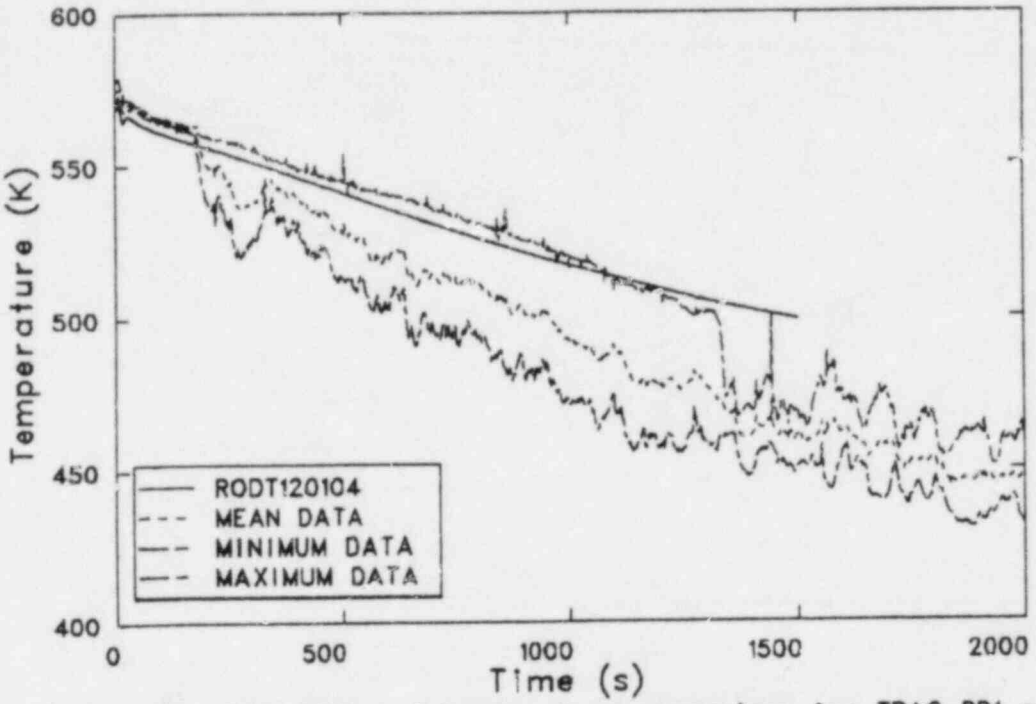

Figure 81. Test 6431 rod temperature comparison for TRAC-BD1 rod group 1 level 4 and rod thermocouple data at 2.01 m from BHL.

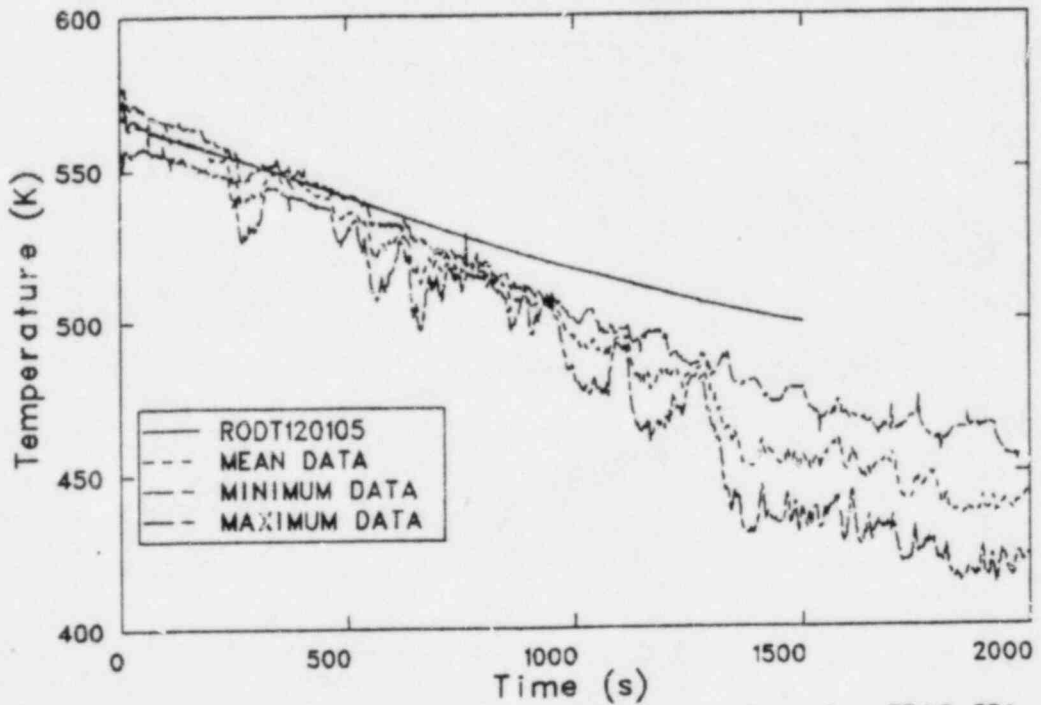

Figure 82. Test 6431 rod temperature comparison for TRAC-BD1 rod group 1 level 5 and rod thermocouple data at 2.29 m from BHL.

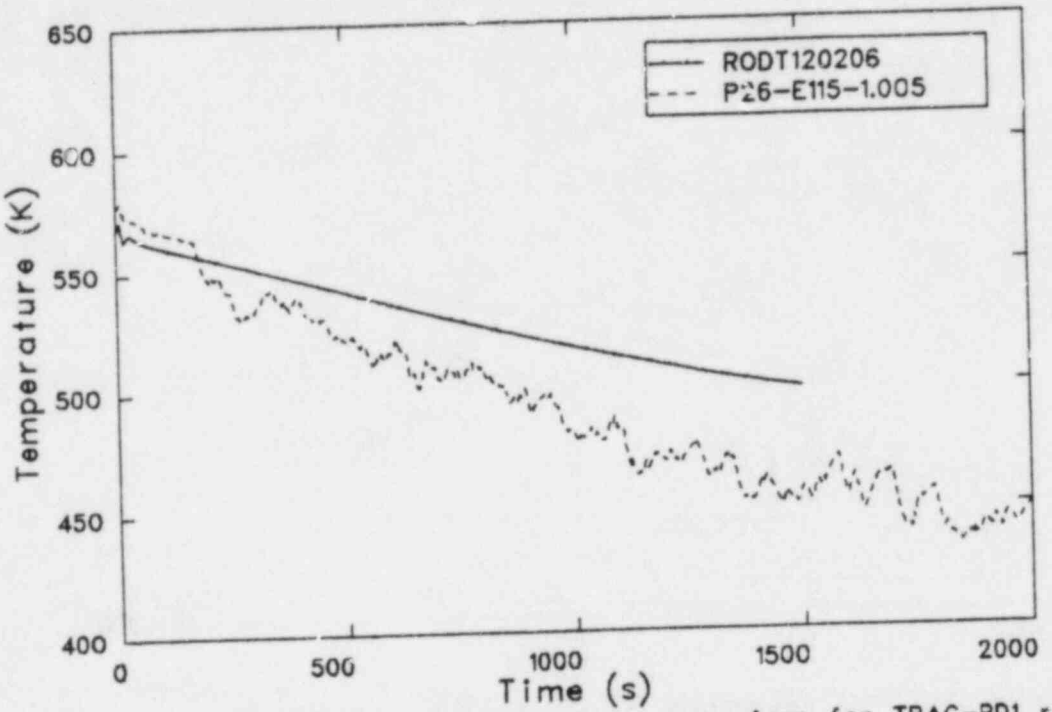

Figure 83. Test 6431 rod temperature comparison for TRAC-BD1 rod group 2 level 6 and rod thermocouple data at 2.92 m from BHL.

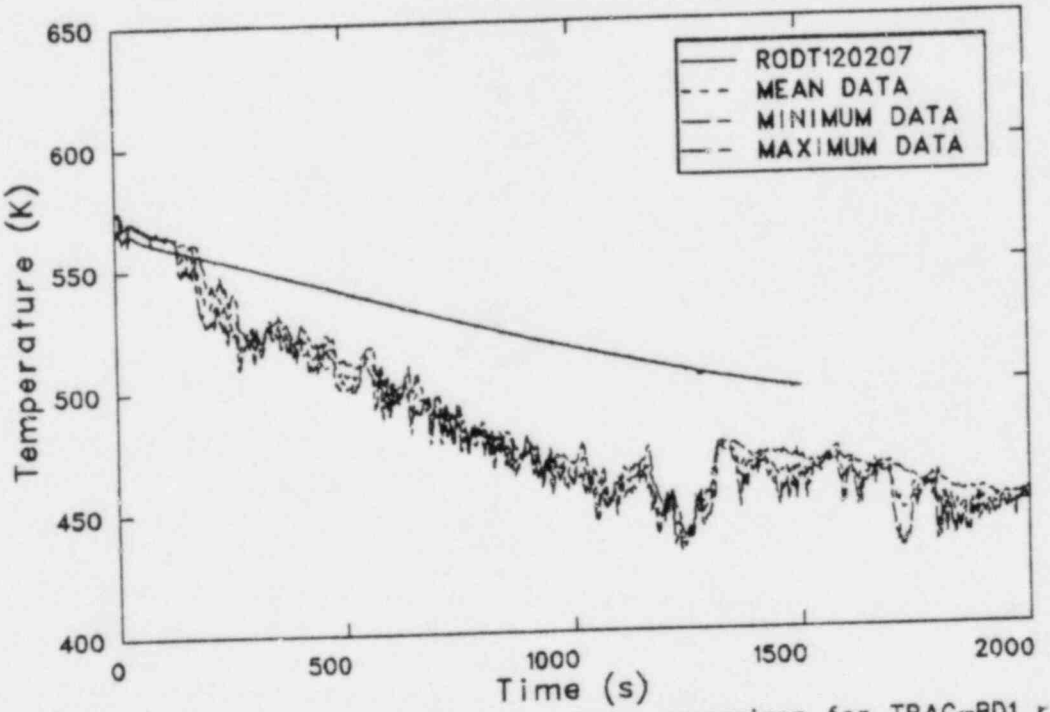

Figure 84. Test 6431 rod temperature comparison for TRAC-BD1 rod group 2 level 7 and rod thermocouple data at 3.56 m from BHL.

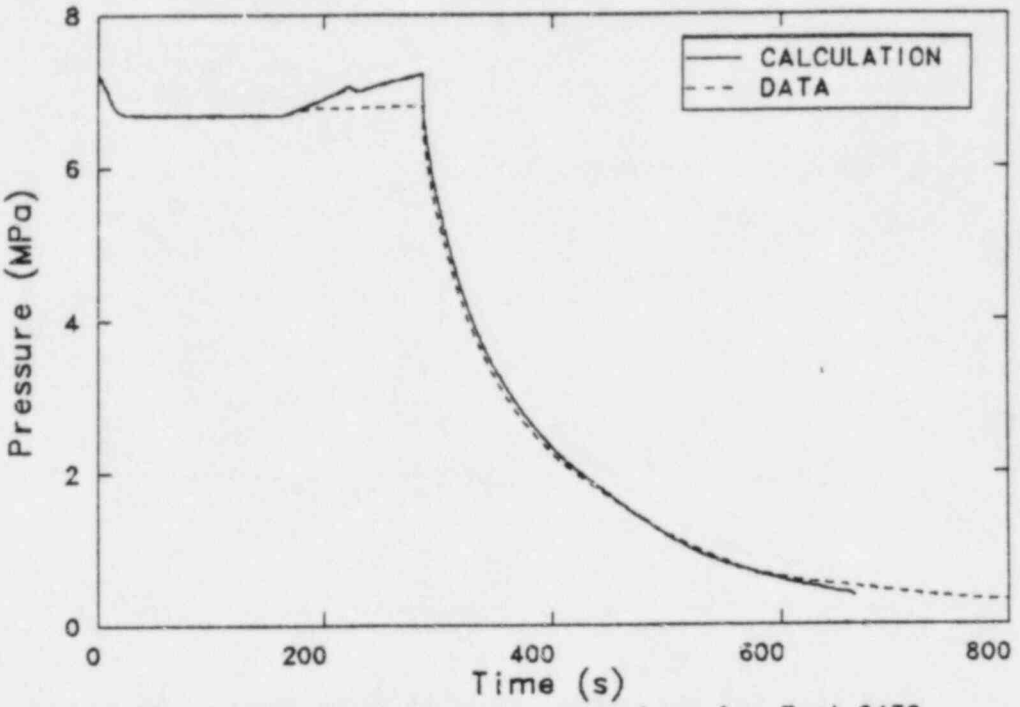

Figure 85. Steam dome pressure comparison for Test 6432.

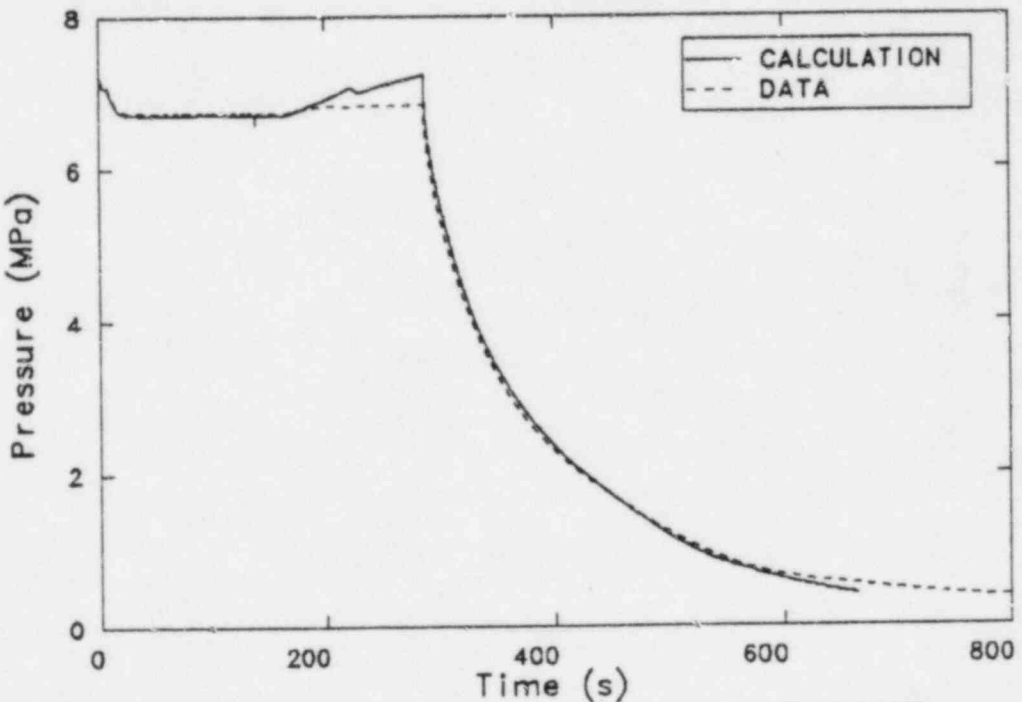

Figure 86. Break inlet pressure comparison for Test 6432.

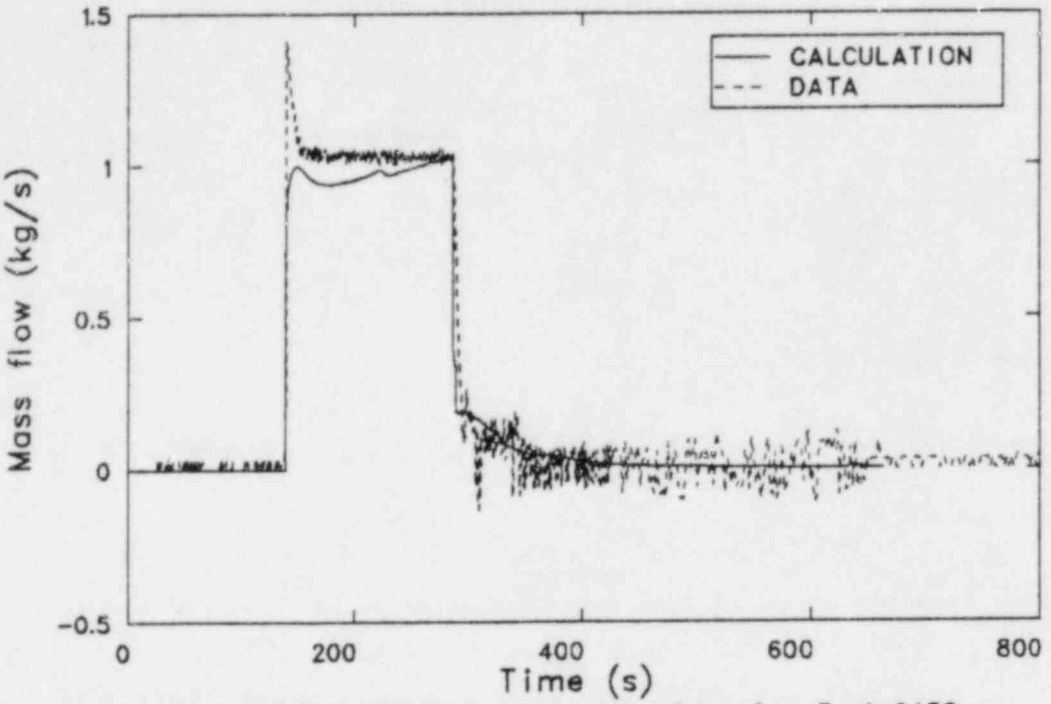

Figure 87. Break mass flow rate comparison for Test 6432.

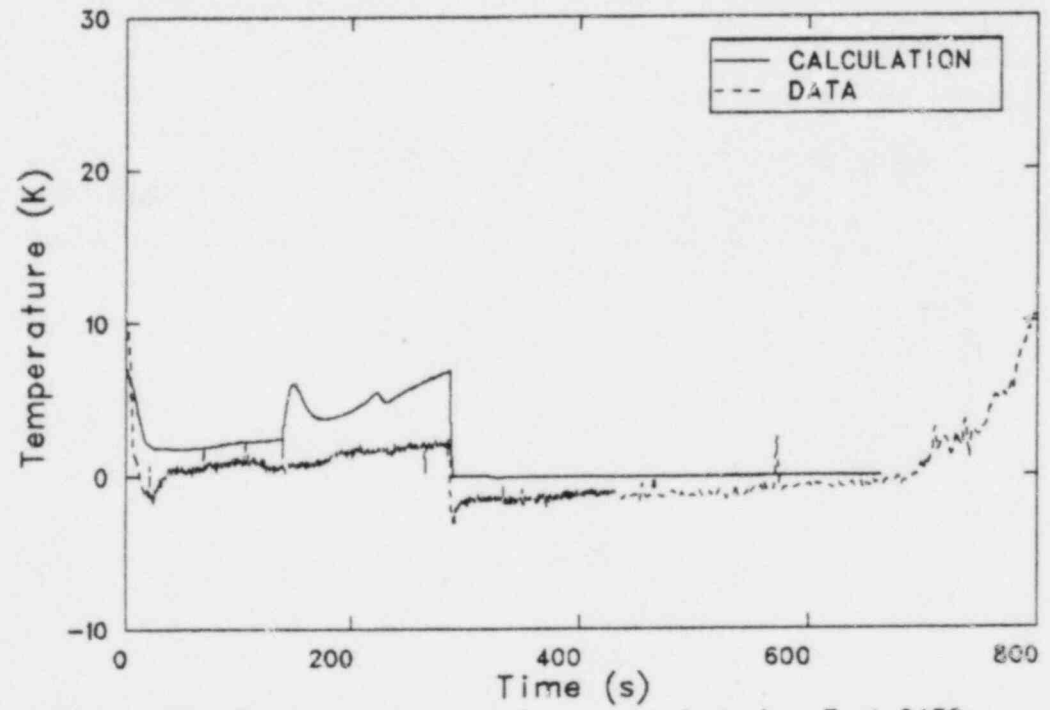

Figure 88. Break inlet subcooling comparison for Test 6432.

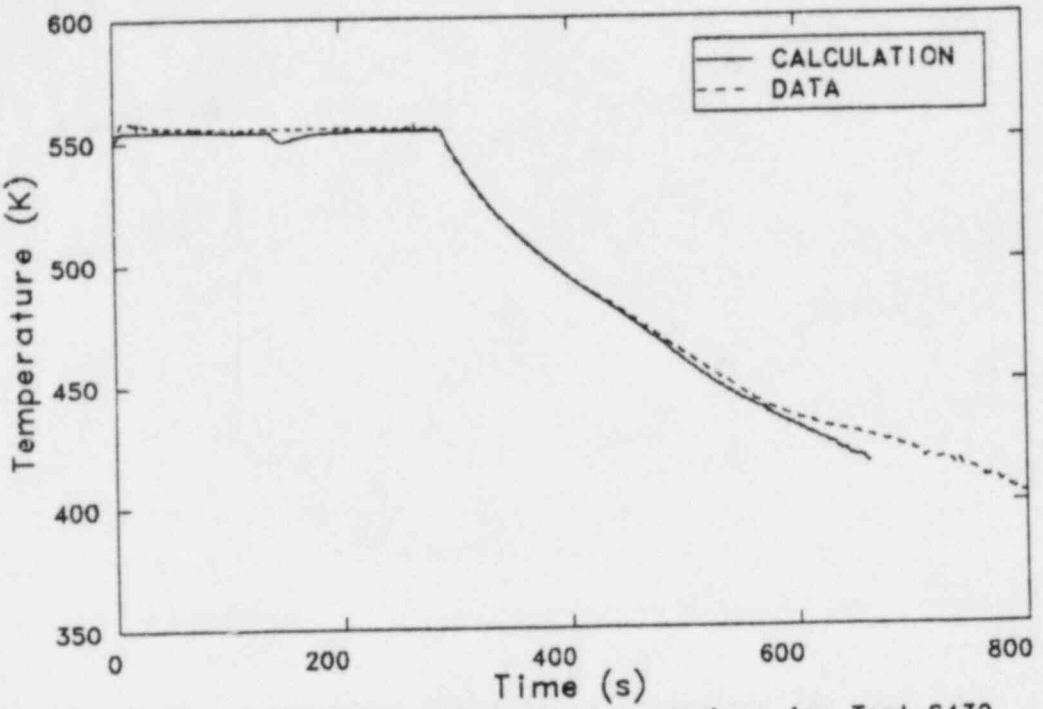

Figure 89. Break inlet temperature comparison for Test 6432.

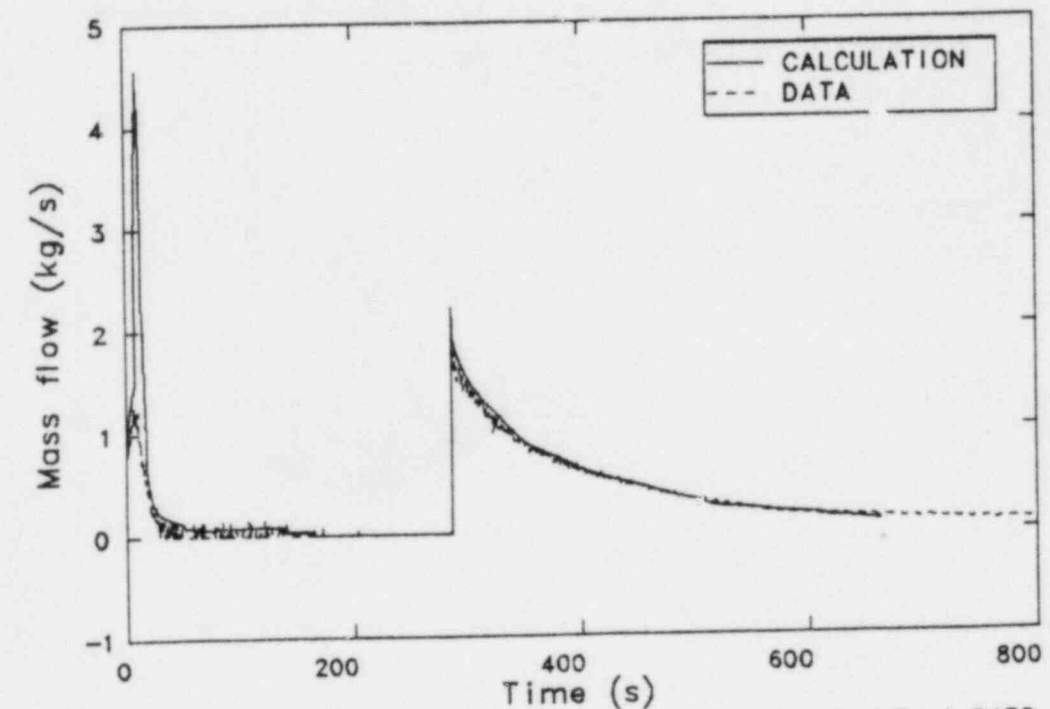

Figure 90. Steam line mass flow rate comparison for Test 6432.

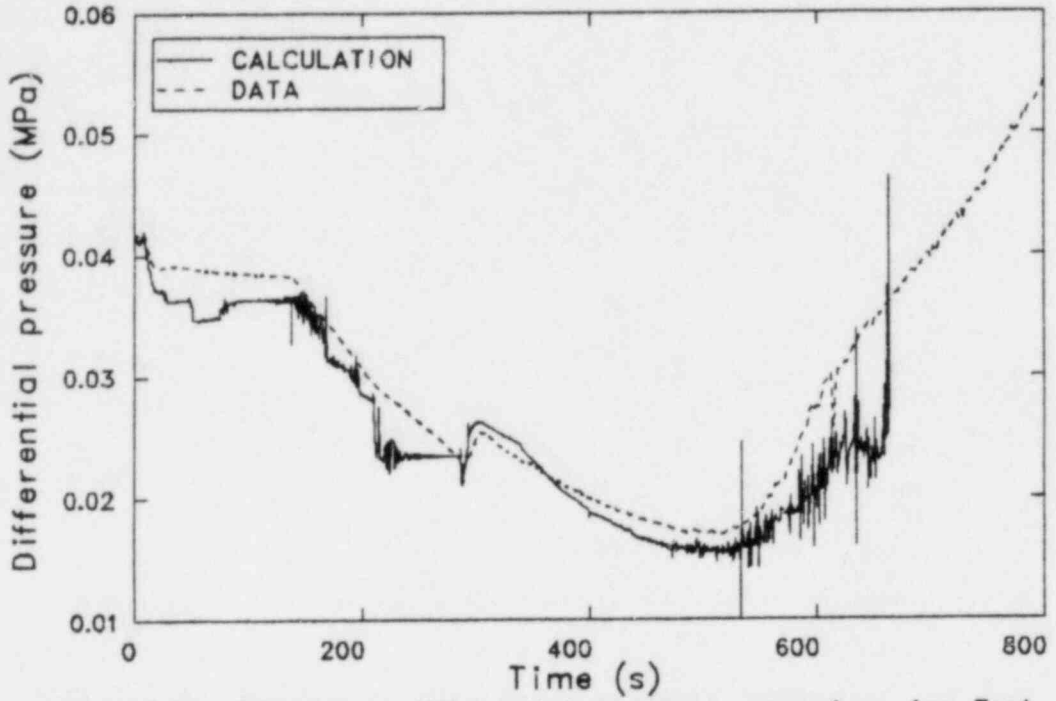

Figure 91. Downcomer differential pressure comparison for Test 6432.

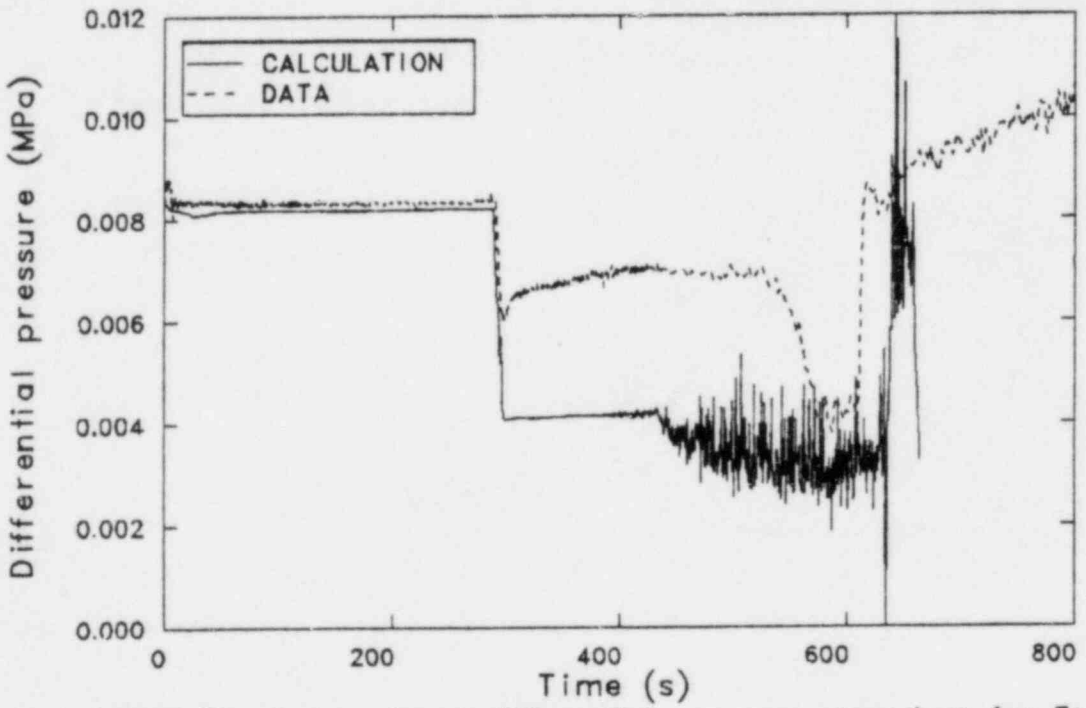

Figure 92. Lower plenum differential pressure comparison for Test 6432.

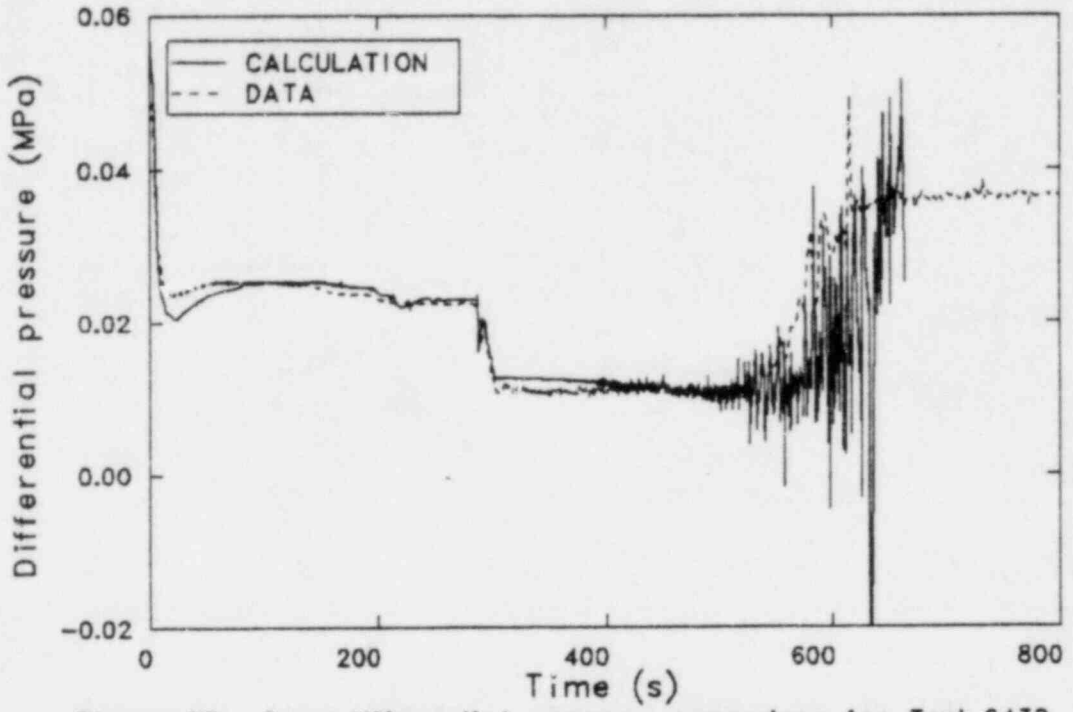

Figure 93. Core differential pressure comparison for Test 6432.

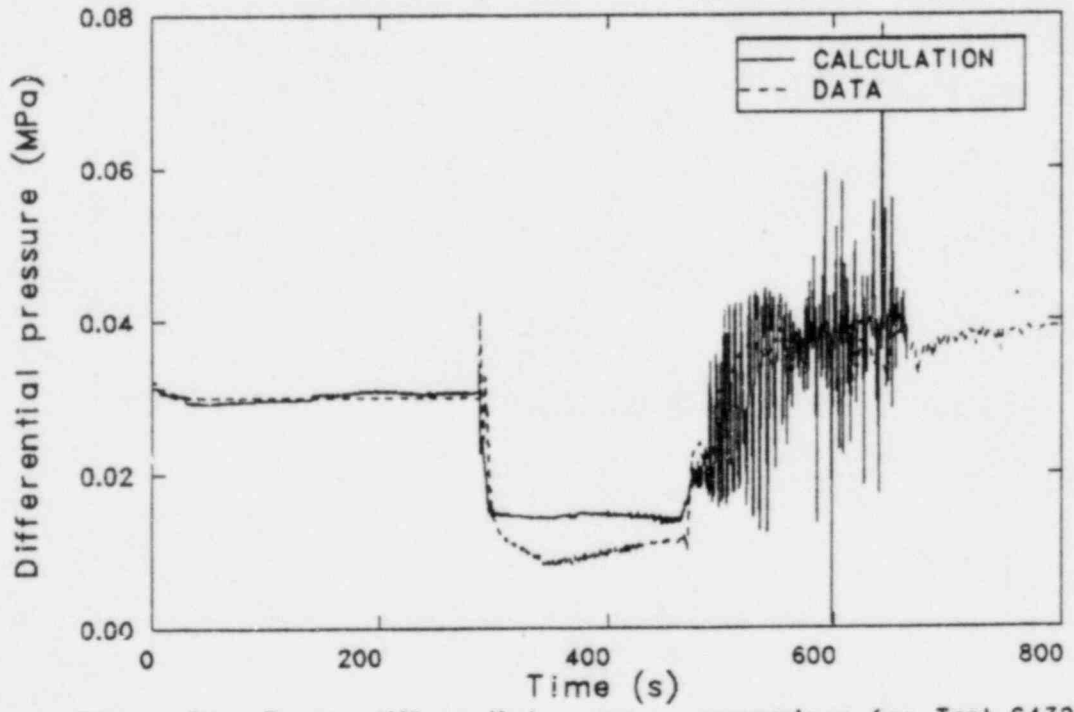

Figure 94. Bypass differential pressure comparison for Test 6432.

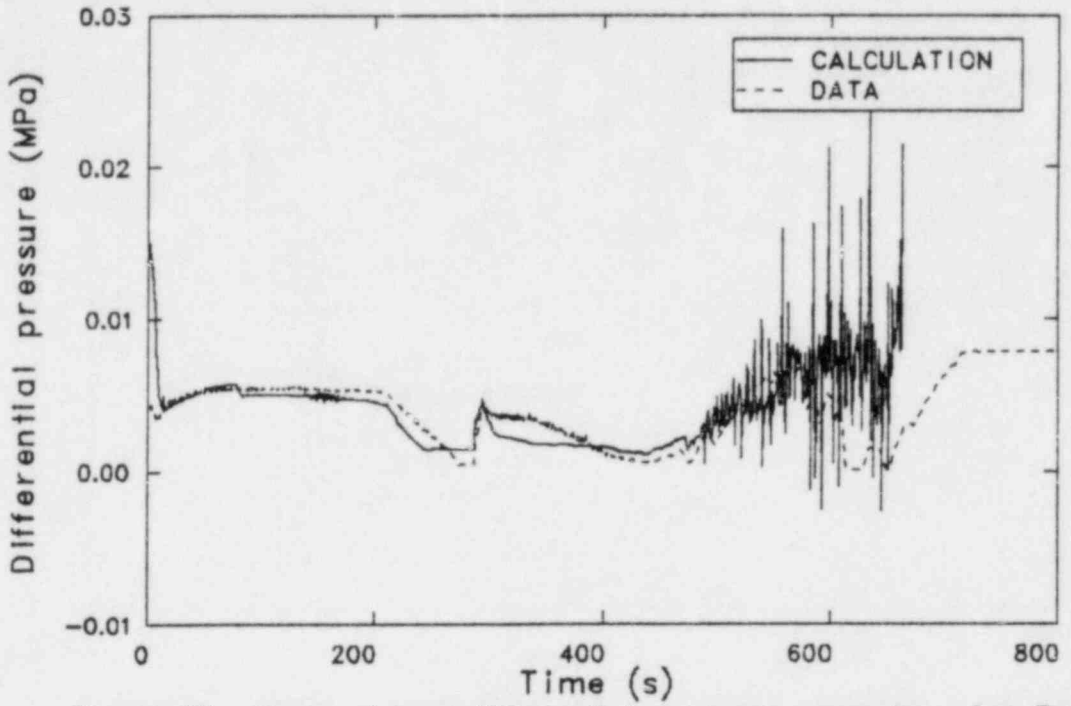

Figure 95. Upper plenum differential pressure comparison for Test 6432.

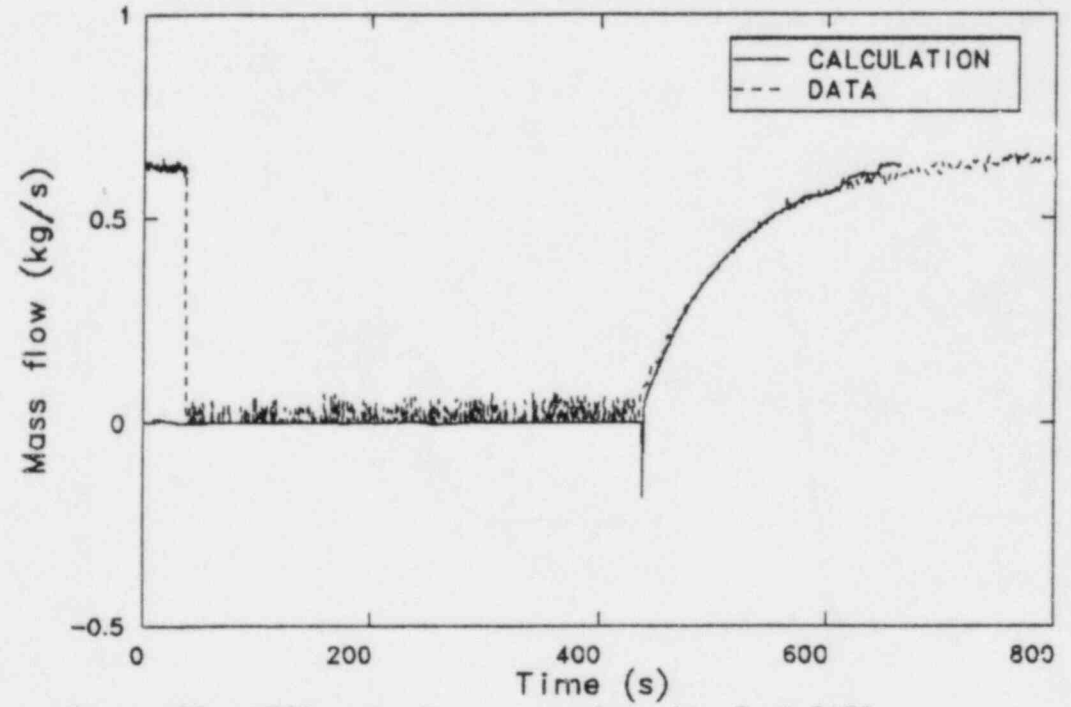

Figure 96. LPCS mass flow comparison for Test 6432.

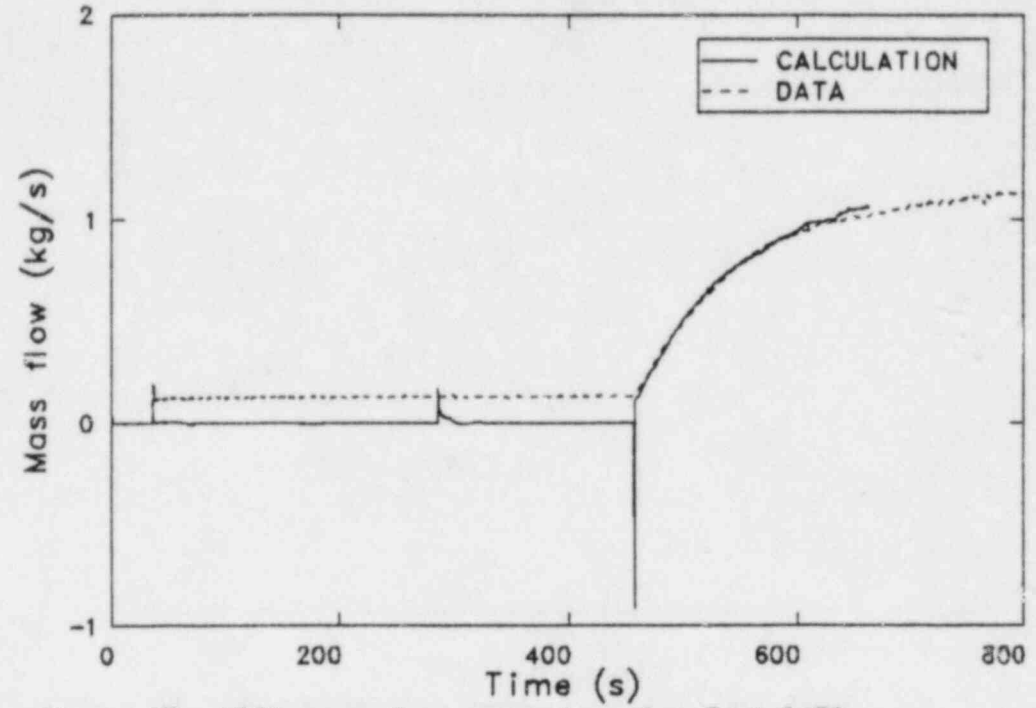

Figure 97. LPCI mass flow comparison for Test 6432.

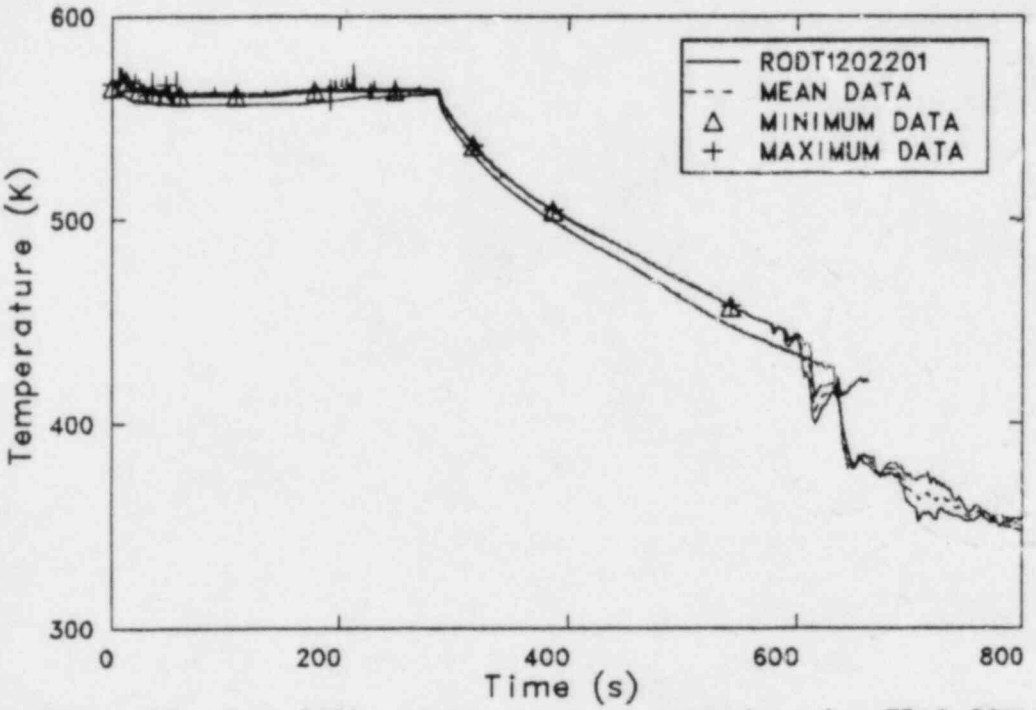

Figure 98. Test 6432 rod temperature comparison for TRAC-B01 rod group 2 level 1 and rod thermocouple data at .25 m from BHL.

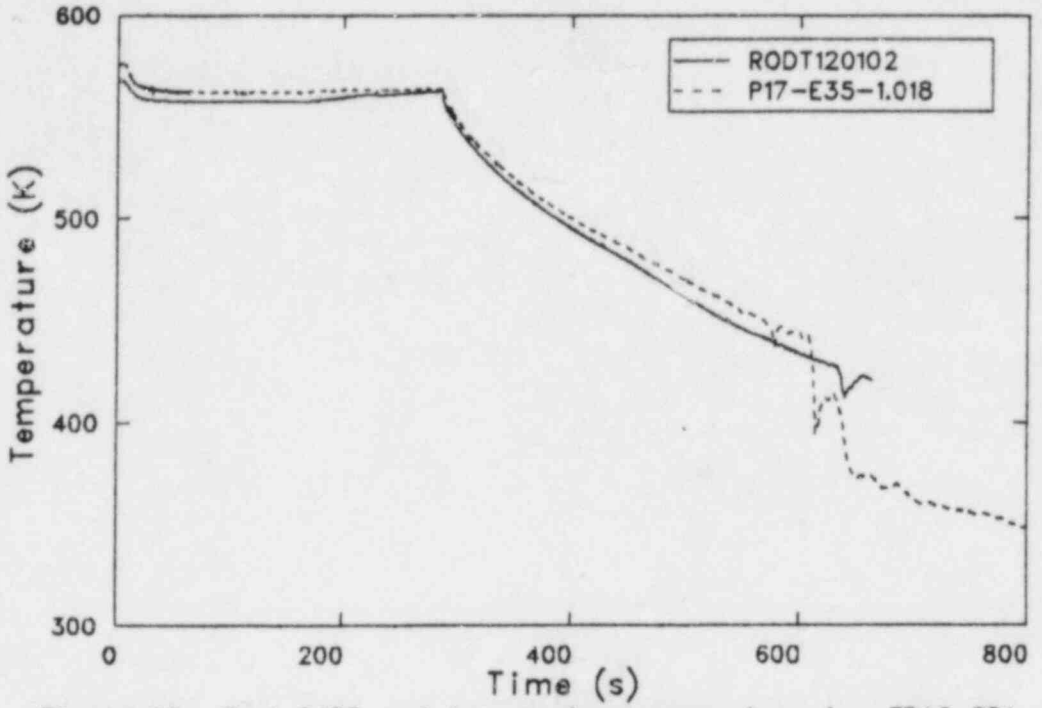

Figure 99. Test 6432 rod temperature comparison for TRAC-BD1 rod group 1 level 2 and rod thermocouple data at .89 m from BHL.

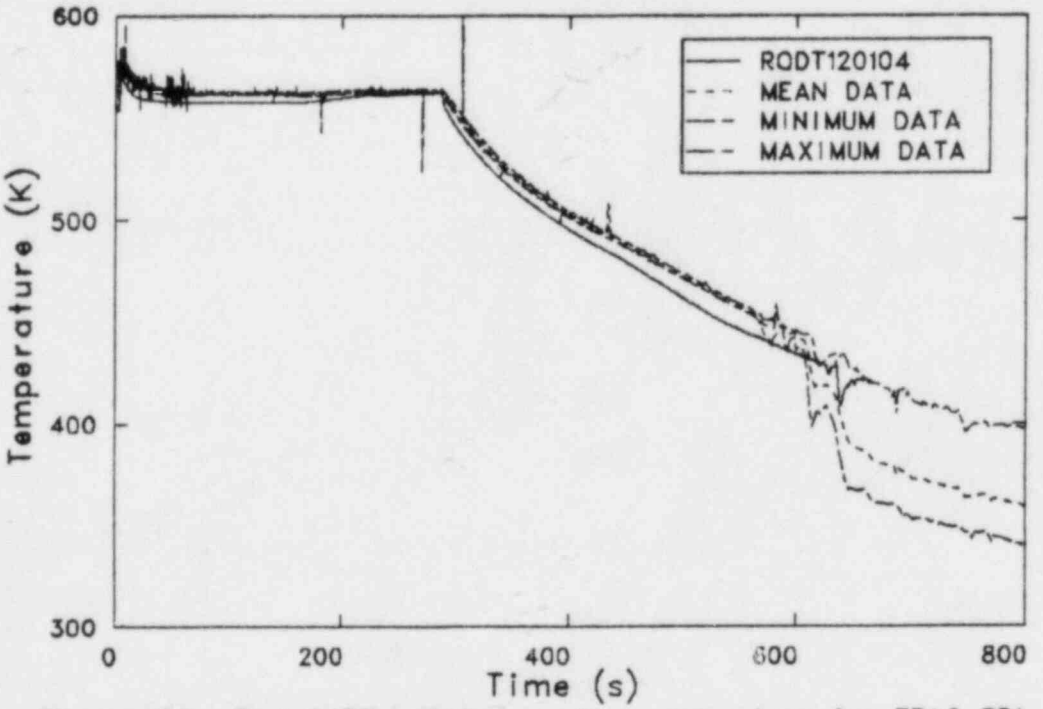

Figure 100. Test 6432 rod temperature comparison for TRAC-BD1 rod group 1 level 4 and rod thermocouple data at 2.01 m from BHL.

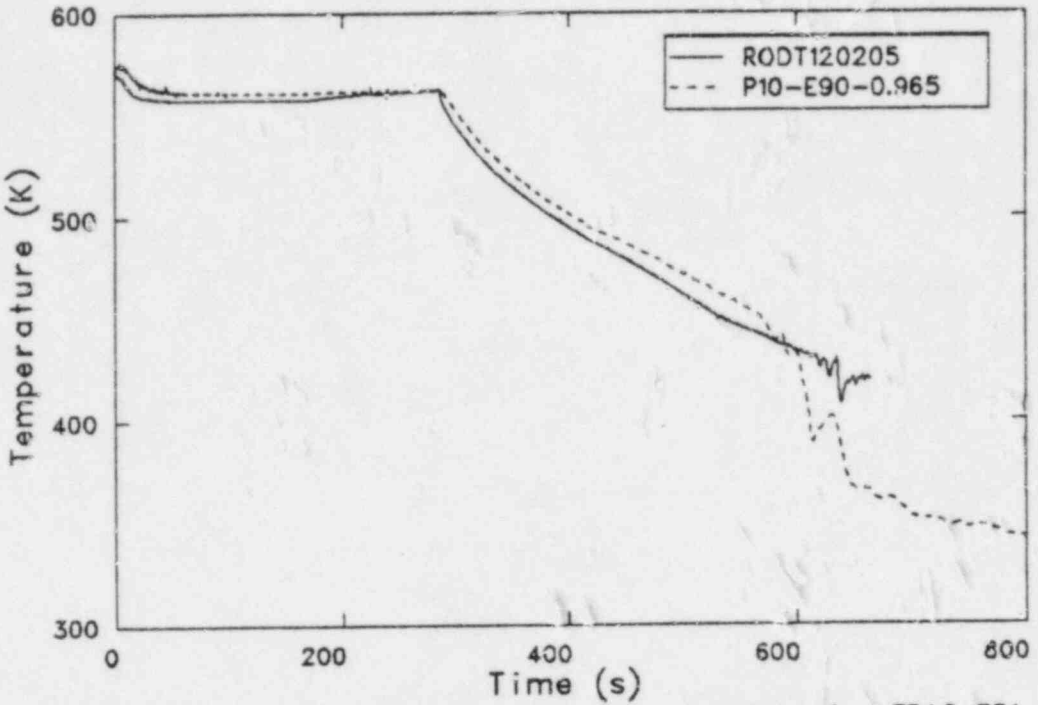

Figure 101. Test 6432 rod temperature comparison for TRAC-BD1 rod group 2 level 5 and rod thermocouple data at 2.29 m from BHL.

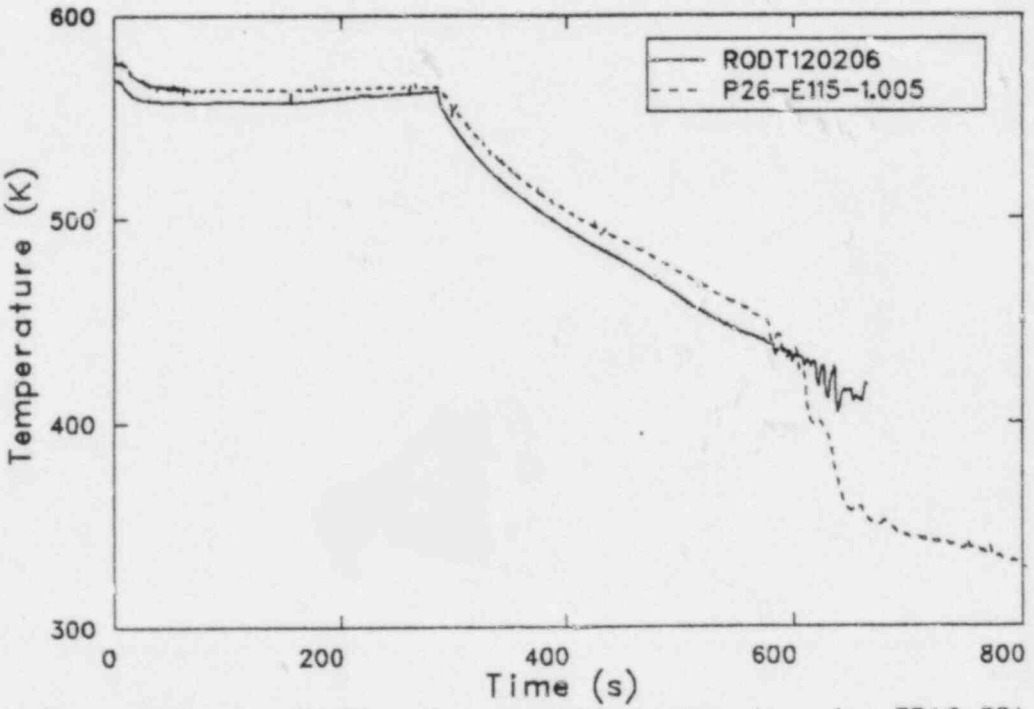

Figure 102. Test 6432 rod temperature comparison for TRAC-BD1 rod group 2 level 6 and rod thermocouple data at 2.92 m from BHL.

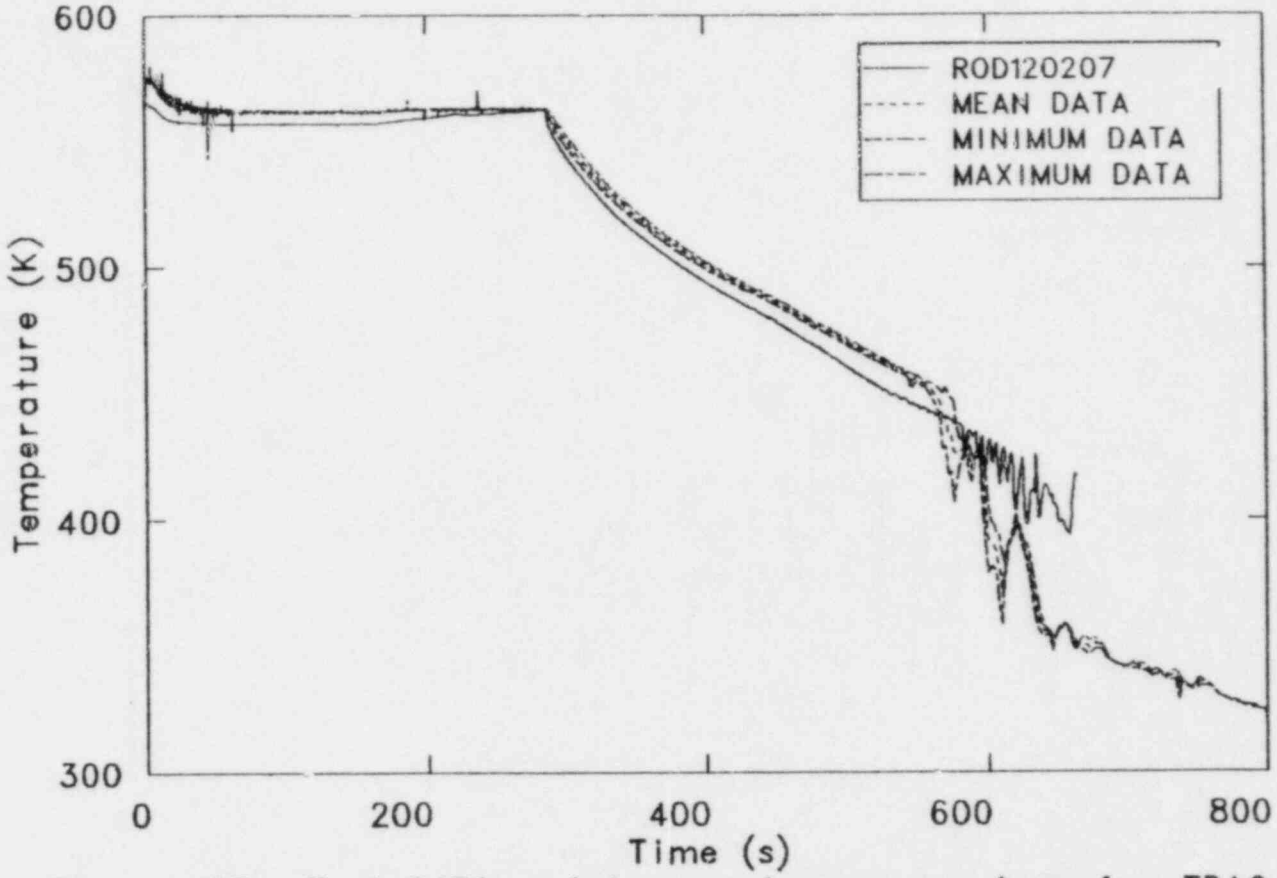

Figure 103. Test 6432 rod temperature comparison for TRAC-BD1 rod group 2 level 7 and rod thermocouple data at 3.56 m from BHL.